January 2014

A Collapsar Model For Bright Linear Type II Supernovae And Numerical Simulations Of Multiple, Interacting Supernova Remnants

Dean D. Smith

A COLLAPSAR MODEL FOR BRIGHT TYPE II LINEAR SUPERNOVAE AND NUMERICAL SIMULATIONS OF MULTIPLE, INTERACTING SUPERNOVA REMNANTS

by

Dean Daniel Smith
Bachelor of Science, University of North Dakota, 1997
Master of Science, University of North Dakota, 2000
Master of Science, University of North Dakota, 2002

A Dissertation

Submitted to the Graduate Faculty

of the

University of North Dakota

in partial fulfillment of the requirements

for the degree of

Doctor of Philosophy

Grand Forks, North Dakota

August

2014

This dissertation, submitted by Dean Smith in partial fulfillment of the requirements for the Degree of Doctor of Philosophy from the University of North Dakota, has been read by the Faculty Advisory Committee under whom the work has been done and is hereby approved.

Dr. Timothy Young

Dr. Wayne Barkhouse

Dr. Ju Kim

Dr. Graeme Dewar

Dr. Ron Marsh

This dissertation is being submitted by the appointed advisory committee as having met all the requirements of the School of Graduate Studies at the University of North Dakota and is hereby approved.

Wayne Swisher
Dean of the School of Graduate Studies

July 23, 2014
Date

PERMISSION

Title A Collapsar Model for Bright Type II Linear Supernovae and Numerical Simulations of Multiple, Interacting Supernova Remnants

Department Physics and Astrophysics

Degree Doctor of Philosophy

In presenting this dissertation in partial fulfillment of the requirements for a graduate degree from the University of North Dakota, I agree that the library of this University shall make it freely available for inspection. I further agree that permission for extensive copying for scholarly purposes may be granted by the professor who supervised my dissertation work or, in his absence, by the Chairperson of the department or the dean of the School of Graduate Studies. It is understood that any copying or publication or other use of this dissertation or part thereof for financial gain shall not be allowed without my written permission. It is also understood that due recognition shall be given to me and to the University of North Dakota in any scholarly use which may be made of any material in my dissertation.

Dean Smith
July 17, 2014

TABLE OF CONTENTS

LIST OF FIGURES vii

LIST OF TABLES ix

ACKNOWLEDGMENTS x

ABSTRACT xi

CHAPTER

I INTRODUCTION 1

Supernova Light Curves 4

Supernovae Remnants 8

II TYPE IIL SUPERNOVA LIGHT CURVES 10

Gamma-Ray Burst History 10

Linear Type II Supernovae 12

Buried Gamma Ray Burst 14

Numerical Fitting 16

Opening Angle and Gamma 21

Black Hole in SN 1979c 23

III SUPERNOVAE REMNANTS 25

Method 27

The ZEUS Code 27

Setup 28

Supernova Initial Conditions 30

Circumstellar Medium 31

Interstellar Medium 32

Post-Processing 33

Setup Results 34

Results 35

Single Supernova Results 35

Double Supernova Results 51

Parameter Study 64

2-D with Instabilities 68

2-D Plots 76

IV CONCLUSION 79

APPENDICES 81

REFERENCES 91

LIST OF FIGURES

Figure Page

1: SN 1969L, a Type II-P (top) and SN 1979c, a Type II-L (bottom) 7

2: Collapsar Model of a Linear Type II Supernova 15

3: SN 1969l data with lines fit. This interpolated function served as msn(t) 17

4: SN 1979C light curve fit to a Type II-P and jet 18

5: SN 1980k light curve fit to a Type II-P and jet 19

6: SN 1985l fit to a combination of a Type II-P and jet emission 19

7: SN 1985l fit to jet emission alone 20

8: SN 1970g fit to a Type II-P and jet 20

9: SN 1990k fit to a Type II-P and jet 21

10: Initial circumstellar setup 34

11: 15 solar mass star with no CSM at 1000 years. 38

12: 15 solar mass star with no CSM at 3000 years. 39

13: 15 solar mass star with no CSM at 30,000 years. 40

14: Single supernova at 200 years. 41

15: Single supernova at 600 years. ISM=0.1/cm^3 42

16: Single supernova at 1000 years. ISM=0.1/cm^3 43

17: Single supernova at 5000 years. ISM = 0.1/cm^3 44

18: Single supernova at 8000 years. ISM = 0.1/cm^3 45

19: Single supernova at 11,000 years. ISM=0.1/cm^3 46

20: Single supernova at 21,000 years. ISM=0.1/cm^3 47

21: Single supernova at 30,000 years. ISM=0.1/cm^3 48

22: Single supernova at 40,000 years. ISM=0.1/cm3 49

23: Single supernova at 30,000 years with an ISM density of 0.2/cm^3 50

24: Double supernova at 11,000 years. ISM=0.1/cm^3 53

25: Double supernova at 14,000 years. ISM=0.1/cm^3 54

26: Double supernova at 15,500 years. ISM=0.1/cm^3 55

27: Double supernova at 16,000 years. ISM=0.1/cm^3 56

28: Double supernova at 16,300 years. ISM=0.1/cm^3 57

29: Double supernova at 17,000 years. ISM=0.1/cm^3 58

30: Double supernova at 18,000 years. ISM=0.1/cm^3 59

31: Double supernova at 22,000 years. ISM=0.1/cm^3 60

32: Double supernova at 27,000 years. ISM=0.1/cm^3 61

33: Double supernova at 35,000 years. ISM=0.1/cm^3 62

34: Double Supernova. The 2nd supernova blast occurs 34,000 years after the first. 63

35: Single 2-d supernova at 1000 years 70

36: Single 2-d supernova at 21,000 years 71

37: Single 2-d supernova at 35,000 years 72

38: Double Supernova at 14,000 years 73

39: Double Supernova at 22,000 years. The second shock has caught up to the first. ... 74

40: Double Supernova at 28,000 years 75

41: SNR with instabilities. The high density shell breaks up due to instabilities. 76

42: Early attempt at modeling a 30 solar mass supernova with high angular resolution. 77

43: Single Supernova from 20 sm star and 10sm CSM at t = 30,000 years 77

44: Double Supernova at 28,000 years 78

LIST OF TABLES

Table Page

1: Best Fit Parameters fitting Type II-L to a jet model 18

2: Jet Angles and Lorentz Factors 22

3: Single Supernova structure with ISM density of 0.1/cm^3 65

4: Double Supernova structure with ISM density of 0.1/cm^3 66

5: Single Supernova structure with ISM density of 0.2/cm^3 66

6: Double Supernova Structure with ISM density of 0.2/cm^3 67

7: Structure of 15 solar mass supernovae at 24,000 years 67

ACKNOWLEDGMENTS

This project took much longer than expected but it's finally finished. I need to thank my advisor, Dr. Timothy Young for sticking with me through the years and being patient and helpful when answering my questions. Dr. Barkhouse provided me with a computer and office space that I used for the final portion of this research. I also wish to thank my committee members for taking time out of their summer to read and comment on this dissertation.

Supernova remnants were simulated using ZEUS-MP from the Laboratory for Computational Astrophysics at the National Center for Supercomputing Applications. ZEUS was run on computer clusters maintained by the Computational Research Center at the University of North Dakota. Aaron Bergstrom provided a lot of help with the Shale and Hodor clusters.

On a personal level, I want to thank my parents for their support and encouragement throughout the years. My friend Jennifer Rogers provided much needed emotional support during the final months as well as the food provided at my presentation (the cookies were very well received).

ABSTRACT

This dissertation includes two projects. Part one applies the collapsar model to Bright Linear Type II supernovae. The collapsar model is commonly used to explain gamma-ray bursts. In this model, a stellar core collapses to a black hole surrounded by an accretion disk. In addition to the supernova caused by the core collapse, the black hole powers a high energy jet. Shocks within the jet create the gamma ray burst while the jet's later interaction with circumstellar material creates an afterglow. In a Type II supernova, the hydrogen envelope of the star results in a lower energy jet that does not result in a gamma-ray burst. However, the jet is still mildly relativistic when it interacts with the circumstellar material and generates an afterglow. I present results that some Type II Linear light curves can be modeled as a Type II Plateau plus a jet-related afterglow.

In part two, I examine the morphology of supernova remnants using two different hydrodynamic codes. In particular, I simulate the evolution of a remnant resulting from the explosion of two massive stars and compare the result to that of a single-explosion remnant. Most supernova remnants are assumed to result from the explosion of a single massive star; however, most massive stars are part of systems involving more than one star. Some of these binaries should contain two stars that are each massive enough to end life as a supernova. Results of supernova remnants resulting from different mass stars and circumstellar environments are presented.

In addition, results from two different hydrodynamic codes using the same initial conditions are presented. One of these included the effects of instabilities resulting in 2-dimensional structures. Not including instabilities resulted in the formation of a high density shell. This shell is very Rayleigh-Taylor unstable and breaks up when it expands into an inhomogeneous environment.

CHAPTER I

INTRODUCTION

Supernovae have been observed for millennia but only recently has their true nature been discovered. One of the most famous occurred in the year 1054, an event that was recorded by Chinese astronomers. The aftermath of this event can be seen in amateur telescopes as the Crab Nebula, a well-known supernova remnant with a pulsar at its center. The last supernova observed in our galaxy was Kepler's supernova in 1604, five years before Galileo began observing the sky with a telescope. All observed supernovae during the era of telescopic astronomy have occurred in other galaxies, with the nearest being SN 1987a in the Large Magellanic Cloud. Until the twentieth century, all appearances of new stars were known as nova (Latin for new). The term was first used by Tycho Brahe when describing SN 1572 in his book "De Stella Nova". In 1934, Walter Baade and Fritz Zwicky recognized that some nova were intrinsically brighter than others and coined the term "super-nova". They proposed that the brightness was due to the very fast expansion of an exploding star (Baade & Zwicky, On super-novae, 1934). They also suggested that supernovae occur during the transition of a star to a neutron star (Baade & Zwicky, Remarks on super-novae and cosmic rays, 1934), although their original idea involved neutrons forming at the surface and raining down toward the center.

Supernovae are indeed the explosions of stars and can involve the creation of neutron stars. These events are important to the structure and composition of galaxies. They are one of the ways in which heavy elements are formed and dispersed. These elements are incorporated into subsequent generations of stars and planets, and are required for the formation of life. The blast wave from a supernova may have been responsible for the collapse of the pre-solar nebula, triggering the formation of our solar system.

There are two main progenitors of a supernova: white dwarfs and core collapse of massive stars. A white dwarf is the leftover core of a star similar in mass to the Sun. It avoids collapse because its gravity is balanced by electron degeneracy pressure. However, Subrahmanyan Chandrasekhar found that this pressure can only support a star with a mass less than 1.4 solar masses. If a white dwarf is in a binary system, it may gain material from its companion star. This can accumulate its mass over the Chandrasekhar limit causing the star to explode. Since these supernovae form from nearly identical progenitors, they have similar luminosities and are used as standard candles to measure distances in the universe.

The supernovae discussed in this dissertation are formed from core collapse. These are formed from stars with initial masses larger than 8 solar masses (Smartt, 2009). A star's life is a struggle against gravity. To avoid gravitational collapse, there needs to be outward pressure. Soon after star formation, the stellar core becomes hot enough to permit nuclear fusion of hydrogen into helium. The energy released by nuclear fusion balances the force of gravity. Once the core extinguishes the fusionable hydrogen, the core contracts and heats up until helium can fuse into carbon. Once a carbon core is

formed, the star is near the end of its life. After only a few thousand years, successive stages of nuclear fusion and contraction create an core of iron group elements. Iron and nickel have the highest binding energy per nucleon. This means they are the most tightly bound and have the lowest potential energy of all nuclei. The core is no longer able to generate energy through fusion and it is only supported by electron degeneracy pressure. However, once the iron core reaches the Chandrasekhar limit of 1.4 solar masses, the core begins to collapse. Electrons and protons combine to form neutrons and neutrinos through beta decay. The collapse produces a shock wave, resulting in a supernova explosion. The core is left behind as a neutron star or, for stars larger than 20-25 solar masses, a black hole (Smartt, 2009) (Heger, 2003).

Supernovae are classified based on whether or not hydrogen appears in their spectra. Hydrogen does not appear in the spectra of Type I supernovae while it does in Type II. Type I includes Type 1a that are believed to be formed from white dwarfs and are not formed through core collapse. Type Ib and Ic supernovae are believed to be core collapse supernovae that have previously lost their hydrogen envelope during the stellar lifetime. This can occur because of a strong stellar wind that blows off the outer layers. This usually occurs in high metallicity stars (larger amounts of elements heavier than helium) that are more opaque to radiation. Another possibility is mass loss to a companion. Type II supernovae are formed from core collapse but the stars have retained their hydrogen envelope.

Supernova Light Curves

The Type II spectral type can be further categorized by their light curves, mainly Type II Plateau (Type II-P) and Type II Linear (Type II-L) (Barbon, Ciatti, & Rosino, Photometric Properties of Type II Supernovae, 1979). Both light curves show a rapid increase in brightness followed by a decline over a period of months. The initial brightness of a supernova can be explained due to rapid expansion and the subsequent very large surface area. The energy driving expansion was deposited by the shock wave that moved through the stellar envelope. The average kinetic energy of supernovae is about 10^{51} ergs (Woosley S. , 2005), resulting in ejecta velocities of 5000-10,000 km/s (Reynolds, 2008).

As the shock front moves through the very inner core of the star, it triggers explosive nucleosynthesis, creating nearly 0.1 solar masses of ^{56}Ni (Patat, 1994) which decays to ^{56}Co with a half-life of 6.1 days (Carroll, 1996).

$$^{56}_{28}\mathrm{Ni} \rightarrow {}^{56}_{27}\mathrm{Co} + e^{+} + \nu_e + \gamma \qquad \textbf{(1)}$$

This decay injects a large amount of additional energy into the star. However, this energy is initially trapped in the opaque interior and the luminosity begins to drop as the gas adiabatically cools. The shock will continue through the outer core and envelope but will not be hot enough to cause any nucleosynthesis reactions.

For Type II supernovae, light curves with plateaus are the most common. In these light curves, after the initial drop the luminosity remains mostly constant for a period of time. The plateau can be explained by the slow release of energy deposited by the shock wave. The energy from ^{56}Ni decay is initially trapped in the star's interior and must make its way to the photosphere before it can be radiated away. The photosphere is the

surface where the star becomes optically thin (transparent) and photons can escape to be seen. Here, it is the boundary between ionized and neutral hydrogen in the star, occurring where the temperature is less than 6000K (Arnett, 1996). As the star expands and cools, recombination of electrons and nuclei moves the photosphere inward in mass (the amount of mass outside the photosphere increases). The actual radius of the photosphere during the plateau is nearly constant. A model of SN 1987a puts this radius at 8×10^{14} cm (Nomoto, 1990), equivalent to 11,500 solar radii or 50AU.

This motion of the photosphere in mass coordinate is known as the recombination wave. As deeper parts of the star are exposed, the previously trapped radiation is allowed to escape. If the progenitor star has a small radius like SN 1987A, the energy of the shock will dissipate faster and most of the energy will be used to increase the volume. In this case, the plateau would appear as a secondary peak rather than a distinctive plateau (Young T. R., A Parameter Study of Type II Supernova Light Curves Using 6 Solar Mass He Cores, 2004). The plateau in the light curve represents light escaping from deeper areas of the hydrogen envelope, maintaining the high temperature. The thicker the envelope, the longer the plateau phase lasts. During the plateau phase, the observed luminosity is due to light being emitted from a sphere the size of the solar system and as hot as the Sun. Given the same temperature, an estimate for the luminosity during the plateau phase compared to the Sun can be found from the ratio of radii squared.

$$L_{plateau} = 11{,}500^2 L_{sun} = 1.32 \times 10^8 L_{sun} \quad \textbf{(2)}$$

Luminosities are usually represented in log scale using absolute magnitude. In the magnitude system, lower numbers are brighter and every five magnitude decrease represents a luminosity that is 100 times greater. Given the absolute magnitude of the

Sun is 4.8, one can find the absolute magnitude of the plateau. This value matches measured light curves such as SN 1969L (see Figure 1).

$$\sqrt[5]{100}^{4.8-M} \approx 2.51^{4.8-M} = 1.32 \times 10^8$$

$$Log_{2.51}(1.32 \times 10^8) = 4.8 - M$$

$$M_{plateau} = -15.5$$

After the plateau phase, there is a linear decline in luminosity seen in all Type II supernovae. This part of the light curve represents energy released from the decay of ^{56}Co into ^{56}Fe with a half-life of 77.7 days (Patat, 1994) (Carroll, 1996). The Cobolt-56 originally comes from the beta decay of Nickel-56 mentioned above. While the energy from that reaction is important in supernova models, only the subsequent Cobolt-56 decay has direct observational evidence in the form of the light curve tail.

$$^{56}_{27}\text{Co} \rightarrow {}^{56}_{26}\text{Fe} + e^+ + \nu_e + \gamma \quad \textbf{(3)}$$

In radioactive decay, the number of parent element atoms, *N*, drops exponentially with a half-life τ.

$$\boldsymbol{N(t) = N_0\, e^{-\lambda t}} \text{ where } \boldsymbol{\lambda = \ln(2)\,/\tau} \quad \textbf{(4)}$$

The rate of energy released (luminosity) is proportional to the decay rate.

$$\frac{d\ Log(L)}{dt} \propto \frac{d\ Log(N)}{dt}$$

$$\frac{d\ Log(N)}{dt} = \frac{d}{dt}[Log(N_0) - \lambda t Log(e)] = -\lambda Log(e) = -.434\lambda$$

$$\frac{d\ Log(L)}{dt} \propto -.434\lambda \quad \textbf{(5)}$$

On a log-scale light curve plot, radioactive decay therefore results in a linear decline. This is seen as the radioactive tail after 150-200 days.

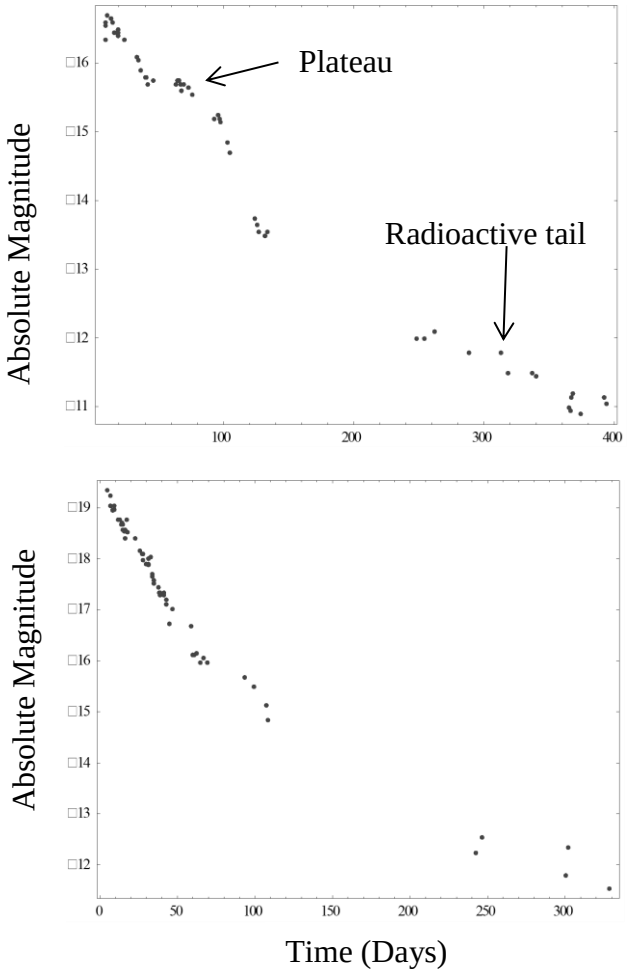

Figure 1: SN 1969L, a Type II-P (top) and SN 1979c, a Type II-L (bottom)

Less common are the Type II Linears. These show a steep drop off in luminosity after peak luminosity and lasting 100-150 days. Further, while Type II-P show a broad range of maximum luminosities, most Type II-L supernovae have similar maximum luminosities. There are a small number of high-luminosity outliers (Young & Branch, 1989) (Gaskell, 1992) that have prompted a further subdivision for Bright Type II-L (Patat, 1994).

Part one of this dissertation proposes that this class of bright Type II-L supernovae are the result of a jet and represent a buried gamma ray burst. Gamma-ray bursts are commonly explained by the collapsar model, in which a jet forms during a Type Ic core collapse supernova. Collisions within a relativistic jet (internal shocks) create the observed gamma rays. Soon afterwards, the jet interacts with the circumstellar medium and creates an afterglow (external shocks). In the model presented here, a jet forms in a Type II supernova, as it would in a Type Ic. The hydrogen envelope effectively buries the gamma ray burst caused by internally generated shocks, but a lower energy jet is able to break out of the surface layers and cause external shocks that produce the observed afterglow.

Supernovae Remnants

After the initial supernovae explosion, the material from the star continues to expand outward as a supernova remnant. The leading edge is a shockwave that travels first through the circumstellar material and then the interstellar medium. Analytic solutions for simple blast waves suggest multiple phases for a supernova remnant. For the first couple hundred years, the remnant is in a "free expansion" phase where the blast wave expands at nearly constant velocity. This is followed by the Sedov-Taylor stage, where the blast wave is nearly adiabatic. The amount of energy lost through thermal radiation is small compared to the kinetic energy of the gas. Together, these two stages make up the "non-radiative" stage of the remnant (Truelove & McKee, 1999). This term shouldn't be taken literally. While radiation occurs, the energy loss is small compared to the kinetic energy and is assumed to be dynamically insignificant. Eventually, the temperature cools enough that bound electrons result in line emission, which accelerates

the cooling. This decreases the pressure pushing the shock forward but it still expands due to momentum. The leading edge of the remnant becomes a dense shell pushing out against the interstellar medium and is often referred to as the snowplow phase.

Part two of this dissertation presents results of using ZEUS hydrodynamic code to model supernova remnants. The motivation for this research was to investigate the outcome of a double supernova. Since most massive stars occur in binary systems (Preibisch, 2000), it is likely that some systems would contain two massive stars that end as supernovae. In the case of a double supernova, the simulation is modified to investigate a single remnant followed by another supernova several thousand years later. The simulation calculates the density, velocity, and temperature of the remnants. Features of the remnants are discussed as well as differences between the remnants that result from a single or double supernova.

CHAPTER II

TYPE IIL SUPERNOVA LIGHT CURVES

This chapter explores a model for Linear Type II supernovae. The two-component model developed here combines the collapsar model for gamma ray bursts (without hydrogen) and applies it to an iron core collapse supernova of a red supergiant that still has a hydrogen envelope. The iron core collapses into a black hole and the resulting accretion disk produces a jet. The resulting model light curve is a combination of a typical Type II-P supernova and emission from the interaction of the jet with circumstellar material.

Gamma-Ray Burst History

Between 1969 and 1972, a search through archived data showed that sixteen bursts of high energy photons were recorded by detectors on four Vela spacecraft (Klebesadel, Strong, & Olson, 1973). The main purpose of these spacecraft was to detect nuclear explosions. Due to the wide spacing of the spacecraft, the Earth and Sun were ruled out as possible sources. A likely cosmic source would be supernovae but none coincided with the location or timing of the any burst. The source of these bursts remained a mystery for decades.

The orbiting Compton Gamma Ray Observatory included an all-sky detector call the Burst and Transient Source Experiment. It observed thousands of these bursts

between 1991 and 2000. The bursts were found to be uniformly distributed across the sky and didn't correspond to sources in other wavelengths. Uniformly distributed sources place restrictions on the distance and energy of these sources. If they are galactic in origin, they would be expected to be clumped along the galactic disk. There are two possibilities that would allow galactic sources to be uniformly distributed. They could be weak, meaning only very close (within the 1000 light year thickness of the disk of the Milky Way) sources are detected. These would have a distribution similar to the nearby stars visible to the eye. The other possibility is that they reside in the galactic halo. To be extragalactic and uniformly distributed, they must be very distant and therefore very energetic. Sources within 100 million light years would show clumping in the nearby Virgo cluster of galaxies.

The breakthrough arrived from observations using Bepposax, an Italian-Dutch satellite launched in 1996. This satellite included X-Ray detectors that could pinpoint positions within 1 arc minute. This allowed follow-up observations by optical observatories. On February 28, 1997, a fading optical afterglow was observed at the same position of a GRB. This afterglow was observed within a galaxy, providing evidence that GRBs are galactic in nature. On May 8 of that same year, spectra were obtained of another optical afterglow using the Keck II 10 meter telescope. A redshift of $z = 0.835$ was measured for some absorption lines (Metzger, Djorgovski, & Kulkarni, 1997), showing that GRBs could be observed from distances of billions of light years and exhibiting energies greater than supernovae.

Another clue to the nature of gamma-ray bursts came with the detection of GRB 980425. This burst occurred in the same location as the Type Ic supernova, SN1998bw

(Galama, 1998) (Iwamoto, 1998). Since then, other gamma-ray bursts have been associated with Type Ic supernovae, i.e. those that are formed by core collapse in stars that have lost their hydrogen envelope.

Observations have shown that there are two types of gamma-ray bursts based on their duration. Short GRBs that last less than two seconds are likely not connected to supernovae due to their occurrence in elliptical galaxies which rarely produce core collapse supernovae. These are possibly caused by the merging of two neutron stars. This dissertation focuses on long GRB's that can last minutes and have been connected to core collapse supernovae. The commonly accepted explanation for long gamma-ray bursts is the collapsar model (Macfadyen, Woosley, & Heger, 2001). In this model, a stellar core collapses into a black hole, resulting in the formation of an accretion disk and two relativistic jets. Hydrodynamic simulations suggest these jets have Lorentz factors near 200 (Woosley, Zhang, & Heger, 2002). High energy internal shocks within these jets create gamma-rays. Relativistic beaming causes the emission to be highly directional so that bursts are only seen if a jet is pointing toward Earth. Since the radiation isn't isotropic, it requires less energy to produce the observed luminosity. The jet's interaction with the circumstellar medium results in the observed afterglow.

Linear Type II Supernovae

Type II supernovae are identified by the existence of hydrogen in their spectra and an extended hydrogen envelope is believed to play a role in the plateau observed in most Type II light curves. These supernovae are further classified by their light curves. Early attempts at sorting out Type II light curves include those by (Pskovskii, 1978), who made note that there was no universal shape; some contained plateaus while others didn't.

Rather than depending on subjective shapes, many studies classify light curves with the simple parameter β_{100}, the average decline rate for 100 days after maximum brightness. This shows that some light curves show a faster drop than others. Barbon et al. introduced the modern classification of splitting light curves into Plateau and Linear subclasses. He noted that about 2/3 of Type II supernova exhibited a plateau (Barbon, Photometric properties of type II supernovae, 1979). Further studies showed that most of the Linear subclass have maximum absolute magnitudes of about -16.5 with the exception of a handful of high luminosity outliers (Young & Branch, 1989) (Gaskell, 1992). This prompted the introduction of a further subclass: bright Type II Linear supernovae (Patat, 1994).

The most common explanation for the lack of a plateau in Linear Type II supernovae is that the star has lost most of its hydrogen envelope. A low mass hydrogen envelope still shows up in the spectra, but it is not massive enough for the long recombination stage that would create a plateau (Barbon, Photometric properties of type II supernovae, 1979) (Smartt, 2009). There has been some success in recreating the linear decline with this model at the expense of not fitting the tail (Swartz, 1991). Reducing the ejected mass also reduces the amount of radioactive ^{56}Co that powers the tail. Modeling bright Type II Linears such as SN 1979c has been a challenge. One proposal suggests a carbon deflagration model, similar to the cause of Type Ia supernova (Swartz, 1991). Another model, (Blinnikov & Bartunov, 1993) requires a very dilute star: a stellar radius 6000 times the sun but with only 1.84 solar masses of hydrogen. In comparison, this is more than three times the size of the largest known stars (Arroyo-

Torres, 2013). None of the papers above provide a satisfactory explanation for the Bright Type II-L supernovae.

Buried Gamma Ray Burst

The problems explaining the light curves of Bright Type II Linear supernovae provided the motivation for a new model. While gamma-ray bursts have been associated with Type Ic supernova, there is no reason why a black hole and corresponding jets should not also form in a Type II supernova. In addition, bright Type II-L supernovae light curves contain features similar to gamma-ray burst afterglows.

The afterglow observed after a gamma-ray burst is believed to be due to the collision of the jet with circumstellar material. Shock-accelerated electrons result in synchrotron radiation and a broken power law light curve (Rhoads, 1999) (Sari, Piran, & Halpern, 1999). Another feature of some afterglow light curves is a "bump" that has been interpreted as light from an underlying supernova (Bloom, 1999). These two features show that afterglow light curves are a combination of a supernova and a jet. The model of Linear Type II supernovae presented here suggests that at least some Bright Type II-L supernova light curves show these same features and share a similar origin.

Since a Type II supernova forms from a star that has retained much of its hydrogen envelope, the jet should lose much of its energy by the time it emerged into view. Models of jets in red supergiants suggest that the most powerful jets would be limited to a Lorentz factor of $\gamma = 2.5$ (Macfadyen, Woosley, & Heger, 2001). This jet would not produce a gamma ray burst, but interaction with circumstellar material could produce an "orphan afterglow". Macfadyan et al. suggest that these afterglows have yet to be discovered. This part of the dissertation presents evidence that these afterglows

have already been observed and the light curves of some Bright Type II-L supernovae can be produced by a mildly relativistic jet. Specifically, the observed light curve is shown to be a combination of the more common Type II-P light curve plus an afterglow due to a jet that has pierced the envelope and interacted with the surrounding circumstellar medium.

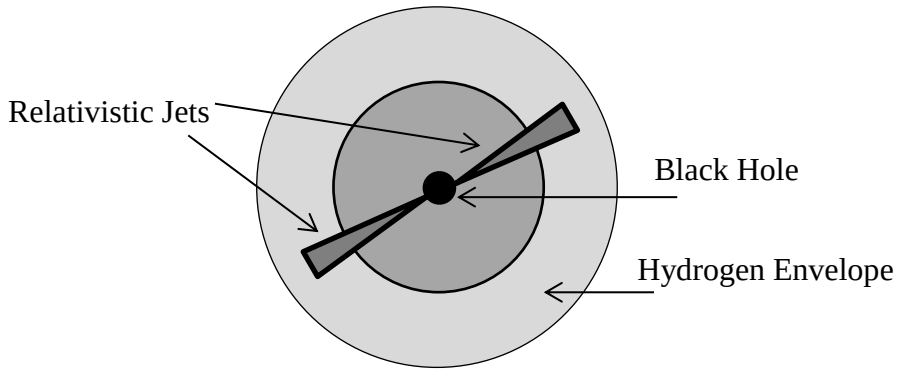

Figure 2: Collapsar Model of a Linear Type II Supernova

The flux of synchrotron emission resulting from the interaction of the jet with the circumstellar medium can be modeled as a broken power law. When the Lorentz factor, $\gamma = \frac{1}{\sqrt{\left(1-\frac{v^2}{c^2}\right)}}$, drops below 1/θ (θ being the opening angle of the jet), there is a break in the light curve (Sari 1999). The flux of the afterglow is given by (Zeh, Klose, & Hartmann, 2004):

$$F_{afterglow} = 10^{-0.4m_c}\left[\left(\frac{t}{t_b}\right)^{\alpha_1 n} + \left(\frac{t}{t_b}\right)^{\alpha_2 n}\right]^{-\frac{1}{n}} \quad \textbf{(6)}$$

Here t_b is the break time when the decay slope transitions from α_1 to α_2, and m_c is the magnitude at the break time. The supernova component is based on data from an observed Type II-P supernova, SN1969l. Since supernovae are not identical, parameters are introduced that can change the shape of the light curve to achieve a best fit.

$$F_{supernova} = k\ 10^{-0.4msn\left(\frac{t}{s}\right)} \quad \textbf{(7)}$$

The function *msn(t)* is an empirical fit to data from SN1969l. The parameter *k* allows the light curve of the underlying supernova to be made brighter or dimmer while *s* stretches the light curve in time. Putting these together and converting to magnitude, we get the composite light curve function.

$$m = -2.5 \times \log\left\{10^{-0.4m_c}\left[\left(\frac{t}{t_b}\right)^{\alpha_1 n} + \left(\frac{t}{t_b}\right)^{\alpha_2 n}\right]^{-\frac{1}{n}} + k\ 10^{-0.4msn\left(\frac{t}{s}\right)}\right\} \quad \textbf{(8)}$$

Numerical Fitting

Mathematica was used for all light curve fitting. SN 1969l was used as a template Type II Plateau supernova. The function *msn(t)* was found by fitting lines to portions of the SN1969l light curve. The data was broken up into pieces, with linear fits performed for each piece. The intersection of each line was found and used to create an interpolated function that could be used in the above equation. The first data point for SN 1969l was set to day 10. Data from bright Type II-L supernovae were then fit to the composite light curve function with m_c, t_b, α_1, α_2, *s*, and *k* as free parameters. The parameter *n* was fixed manually since the success of a fit was sensitive to this value. Allowing it to vary often led to a failure in the fitting function. Supernovae are usually not first observed on day 0. The date of first observation was changed manually to achieve a good fit.

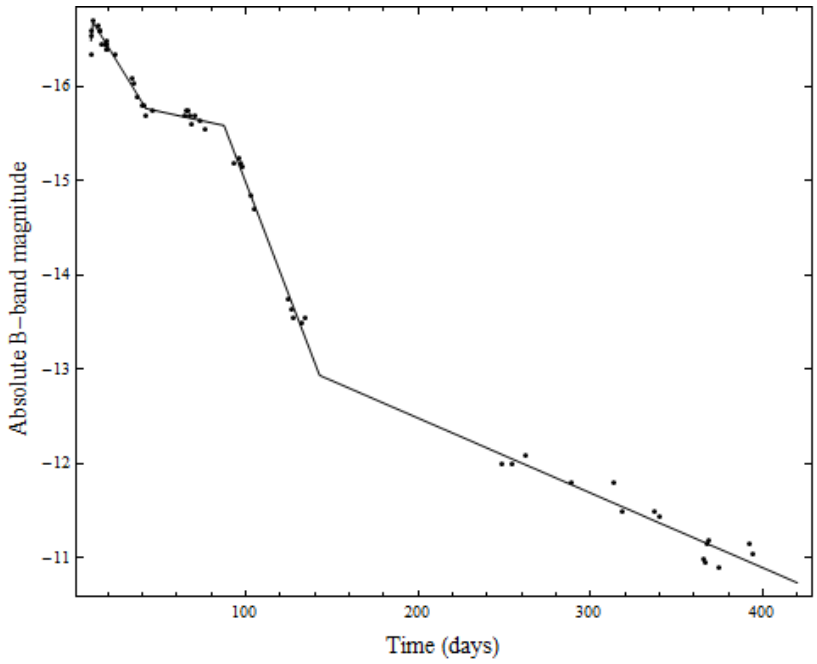

Figure 3: SN 1969l data with lines fit. This interpolated function served as msn(t).

Five bright Type II-L supernovae were fit to this composite light curve using Mathematica: SN 1979c, SN 1970g, SN 1980k, SN 1985l, and SN 1990k. The Mathematica code used to fit the light curves is presented in Appendix I. The light curves and best fit parameters are summarized in the table below. Errors represent 95% confidence levels. Of the five supernovae, SN 1979c best fit the model. The parameter *k* was left fixed at one. While *s* was allowed to vary, its value had little effect on the underlying supernova template. The first data point of SN 1979c was set to day 5. SN 1980k also successfully fit the two-component model. The first data point of SN 1980k was set to day 10. SN 1970g was fit to a modified version of SN 1969L. To achieve a fit, the last three data points from SN 1970g were removed because the tail had a different slope than SN 1969l. The resulting fit shows a rapidly dropping afterglow. The first data point was set to day 18 after the supernova. For SN 1985l, there is little contribution from the underlying supernova. The data is fit well by the afterglow model

alone. The first data point for SN 1985l was set to day 10. SN 1990k showed no break in the power law and the resulting fit is not very good. The first data point was set to day 20.

Table 1: Best Fit Parameters fitting Type II-L to a jet model

	SN 1979c	SN 1970g	SN 1980k	SN 1985l (jet only)	SN 1985l	SN 1990k
mc	-17.8 ±0.2	-15.8 ±3.5	-16.3 ±0.3	-17.3 ±0.5	-17.1 ±1.4	-17.1 ±1E7
α1	0.785 ±0.123	2.08 ±15.37	.845 ±0.330	0.296 ±.390	0.279 ±0.505	1.74 ±1223.63
α2	3.41 ±0.40	4.69 ±1.75	5.14 ±1.73	2.24 ±0.12	2.24 ±0.16	1.75 ±1529.5
t_b	31.0 ±2.3	29.3 ±33.4	29.5 ±4.1	30.3 ±5.9	32.3 ±15.1	7.7 ±4.1E7
n	10	10	10	20	20	10
k	1	1.40 ±0.74	0.57 ±0.09	NA	0.838 ±5.297	0.41 ±0.36
s	1.05 ±.04	0.693 ±0.033	0.67 ± 0.02	NA	0.30 ±0.17	0.52 ±0.12

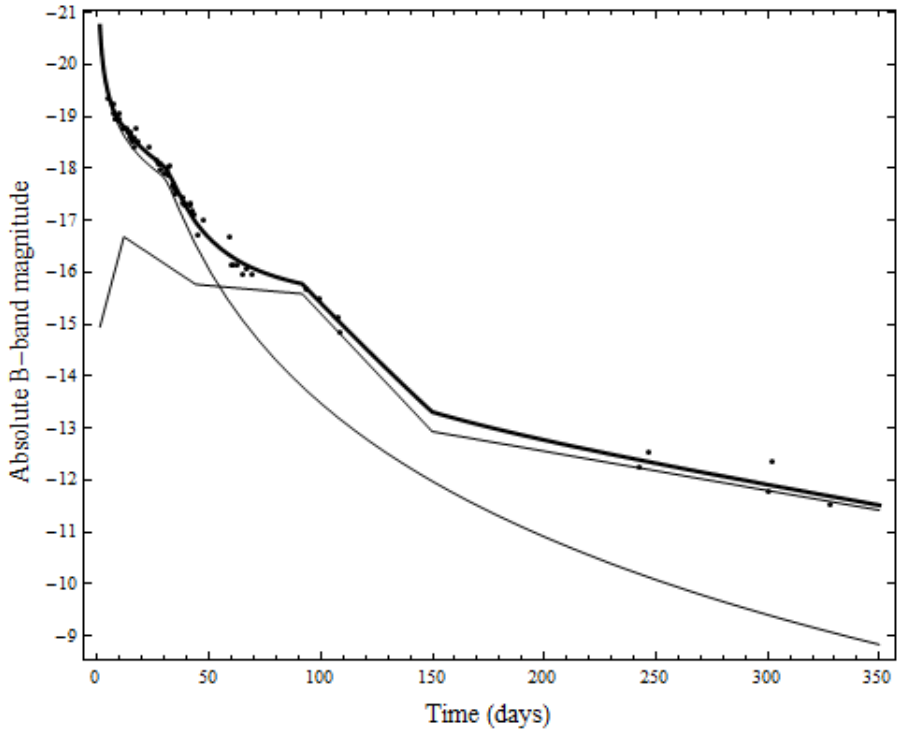

Figure 4: SN 1979C light curve fit to a Type II-P and jet

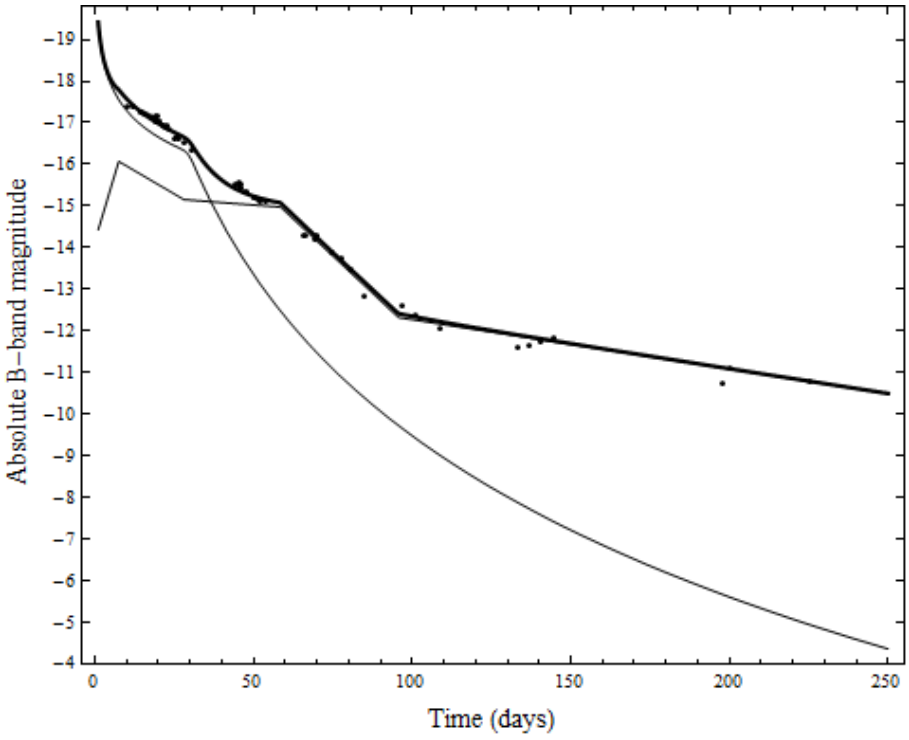

Figure 5: SN 1980k light curve fit to a Type II-P and jet

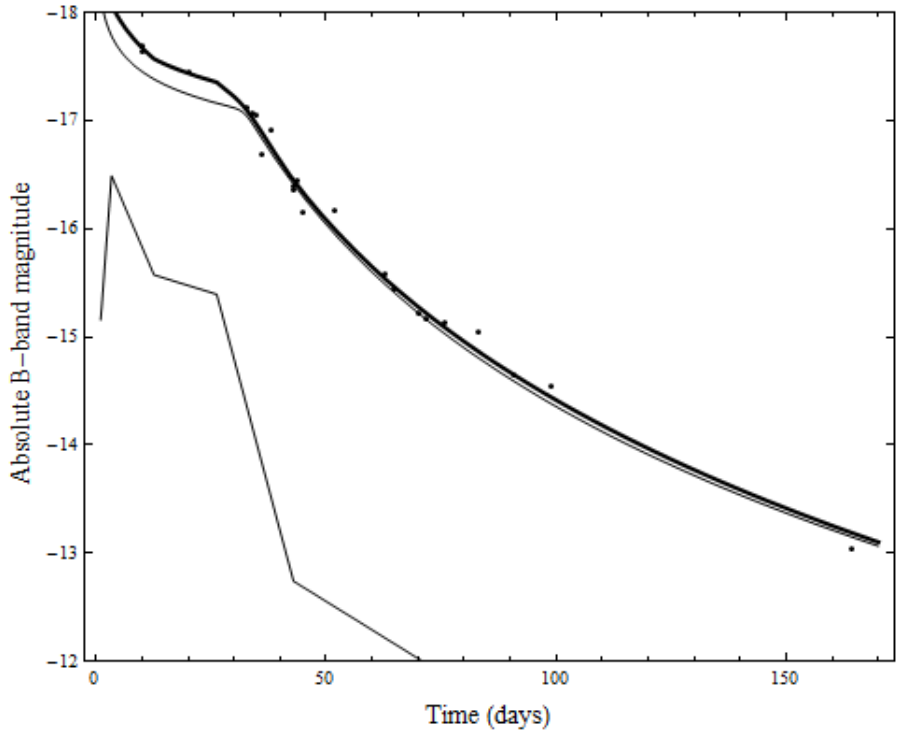

Figure 6: SN 1985l fit to a combination of a Type II-P and jet emission

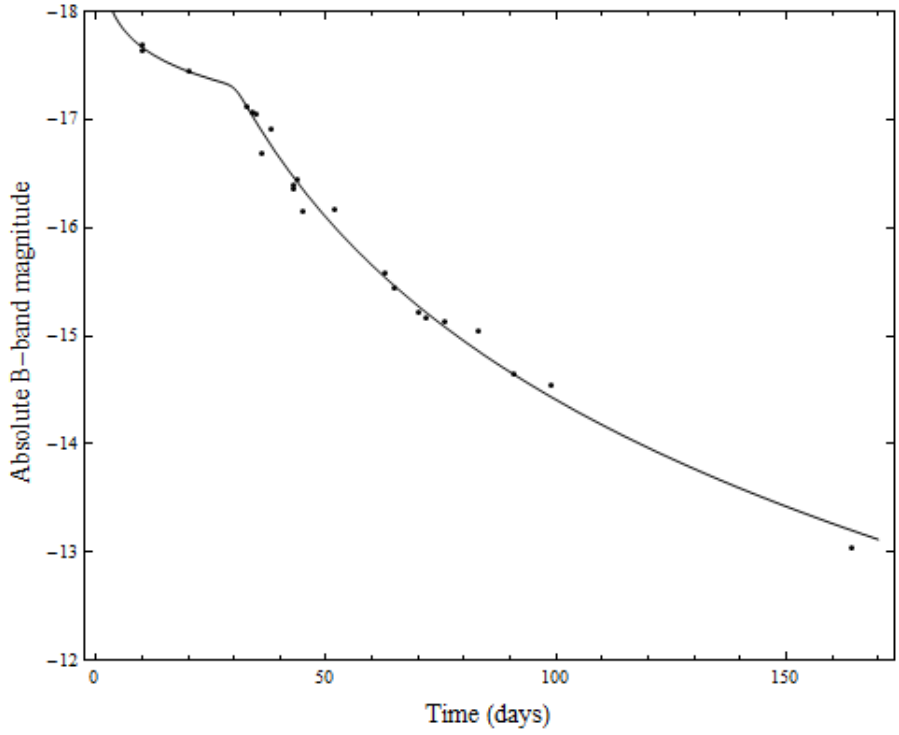

Figure 7: SN 1985l fit to jet emission alone

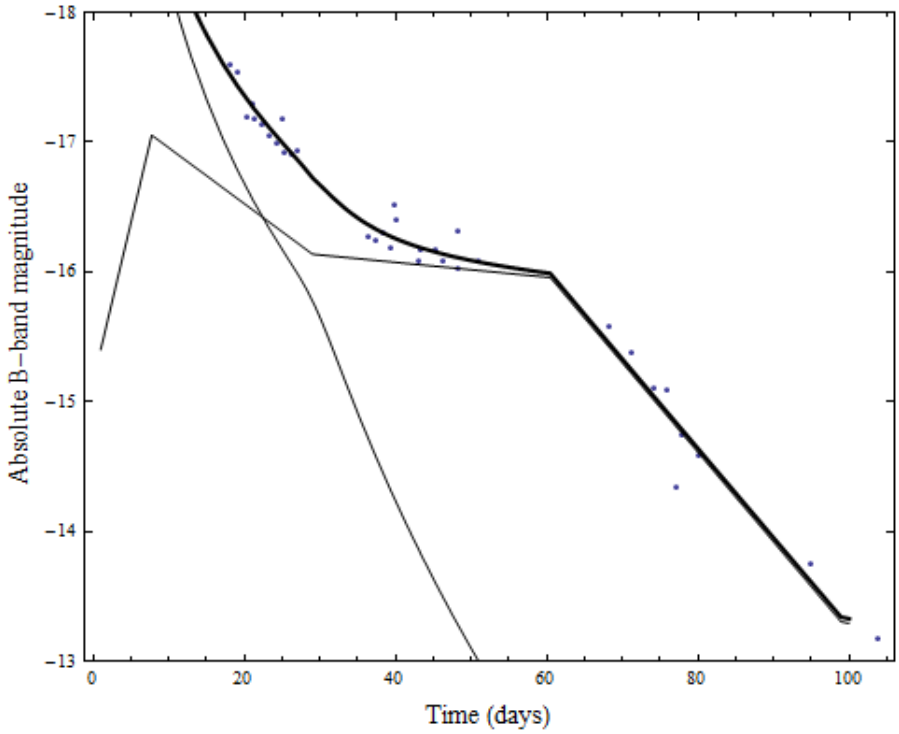

Figure 8: SN 1970g fit to a Type II-P and jet

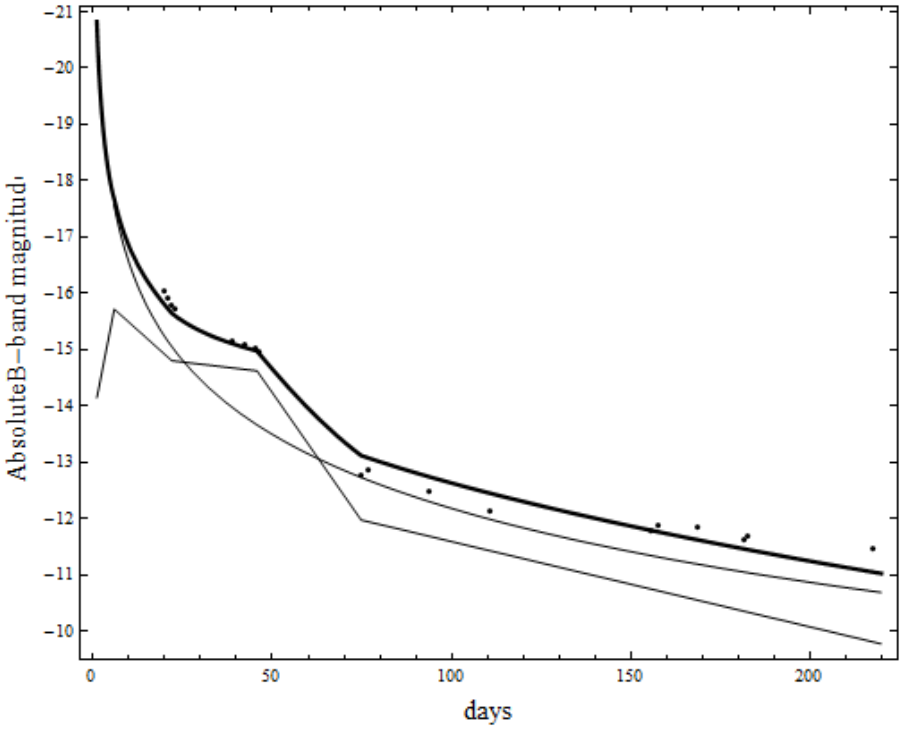

Figure 9: SN 1990k fit to a Type II-P and jet

Opening Angle and Gamma

The slope of the afterglow power law emission changes at the break time, t_b. This occurs when the Lorentz factor drops below 1/θ where θ is the jet opening angle in radians of the conical blast wave that is interacting with the circumstellar medium. At this point, sideways expansion of material in the jet becomes significant (Sari, Piran, & Halpern, 1999) and the luminosity drops faster. This break in the light curve is a signature of a conical jet rather than spherical isotropic emission. The jet opening angle can be found from (Frail, 2001).

$$\theta = 0.057 \times \left(\frac{t_b}{1day}\right)^{\frac{3}{8}} \left(\frac{1+z}{2}\right)^{-\frac{3}{8}} \left(\frac{E_{iso}}{10^{53}erg}\right)^{-\frac{1}{8}} \left(\frac{\eta}{0.2}\right)^{\frac{1}{8}} \left(\frac{n}{0.1cm^{-3}}\right)^{1/8} \quad \textbf{(9)}$$

The redshift, *z*, was found from NED (NASA/IPAC Extragalactic Database). E_{iso} is an equivalent isotropic energy, *n* is the number density of the circumstellar material, and η is the efficiency for converting ejecta energy to gamma rays. I used common GRB values of η=0.2 (Frail, 2001) (Guetta, 2001) and $E_{iso}=10^{51}$ erg. I also used *n* = 0.1 hydrogen atoms /cm^3, a typical value for the interstellar medium. These values make the last two terms equal to one. This simplifies the equation:

$$\theta = .101 \times \left(\frac{t_b}{1day}\right)^{\frac{3}{8}} \left(\frac{1+z}{2}\right)^{-\frac{3}{8}} \quad \textbf{(10)}$$

The Lorentz factors in Table 2 agree with the predictions of jets in a red supergiant. Jets in gamma-ray bursts vary from 1° to 25° but are more common at the low end of that range (Frail 2001). The two-component model used here predicts jet opening angles for Type II-L supernovae of 27°, which is at the high end of this range. This is expected since, unlike gamma-ray bursts, the jets here must first pass through a hydrogen envelope and will lose collimation before interacting with the circumstellar medium and creating the observed power-law emission. This still results in a mildly relativistic jet so that beaming will prevent the observed emission from being seen unless the jet is pointed toward Earth.

Table 2: Jet Angles and Lorentz Factors

	t_b (days)	z	θ (degrees)	Lorentz factor
SN 1979c	31.0 ±2.27	0.00529	27.3 +0.732/-0.766	2.10 +0.061/-0.055
SN 1970g	29.3 ±33.34	0.0008039	26.7 +8.81/-inf	2.14 +inf/-0.53
SN 1985l	30.3 ±5.9	0.002919	27.0 +1.87/-2.1	2.12 +0.18/-0.14
SN 1980k	29.5 ±4.1	.000133	26.8 +1.34/-1.46	2.14 +0.12/-0.10

Black Hole in SN 1979c

The results of this analysis for SN 1979c were presented at the 2005 American Astronomical Society meeting and published in the Astrophysical Journal (Young, Smith, & Johnson, An Optical Afterglow Model for Bright Linear Type II Supernovae, 2005). Based on the mechanism involved, this paper predicted the formation of a black hole in SN 1979c from a star with an initial mass of 20 solar masses.

In 2010, archival X-Ray observations from 1995-2007 showed that SN 1979c has had a constant X-Ray luminosity of 6.5×10^{38} erg/s over this period (Patnaude, 2011). While X-Ray emission is expected when the supernova blast wave collides with the circumstellar medium, the luminosity should decrease with time as the density of circumstellar material decreases with distance. This is what has been observed in the aftermath of other supernovae such as SN 1993J (Immler 2002). However, the constant X-Ray luminosity can be explained by the presence of a black hole with an accretion disk. As matter accumulates around a black hole, it forms a high temperature disk. The radiation from this disk exerts a pressure and is limited in the same way as luminosity from a star. This maximum luminosity is known as the Eddington limit and represents an optimal luminosity that maintains material in the disk. A higher luminosity would drive material from the accretion disk while less would result in material falling into the black hole at a rate faster than it is supplied from the environment. The Eddington limit is directly related to the mass of the black hole.

$$L_{Edd} = 1.4 \times 10^{38} \left(\frac{M}{M_{sun}}\right) \text{erg/s} \quad \textbf{(11)}$$

Given the observed X-ray luminosity of 6.5×10^{38} erg, this predicts an object with a mass of

$$M = \frac{6.5 \times 10^{38}}{1.4 \times 10^{38}} M_{sun} = 4.6 \text{ Solar Masses} \quad \textbf{(12)}$$

.

Patnaude et al. were also able to fit the X-ray spectrum to a 2-component model composed of a thermal plasma and relativistic accretion disk around a black hole. Their spectral fit predicted a black hole mass of 5.2 solar masses, close to the mass predicted by the Eddington limit.

CHAPTER III

SUPERNOVAE REMNANTS

This chapter details the portion of my research regarding supernova remnant simulations. Simulations were run with two different codes, one of which included initial fluctuations that resulted in instabilities. I present results of these simulations and discuss the resulting structures. Simulations were run for single supernova as well as for binary systems in which a second supernova expands into the environment formed by the first. Most supernova remnants are assumed to result from the explosion of a single massive star; however, many stars exist in binary systems. This is especially true for massive stars, the type destined to end life as a supernova. Observations have shown that massive stars are more likely than not to have companions and they tend to be more equal in mass as the mass of the binary increases (Preibisch, 2000). Massive stars that have survived a nearby supernova explosion have been observed. There is evidence for surviving companion stars to SN 1993J (Maund, 2004) and in the young remnant of Tycho's supernova (Lu, 2011). More relevantly, binary systems containing two neutron stars have been found (Taylor, Fowler, & McCulloch, 1979). As supernovae are the only known source of neutron stars, this requires two supernovae within a single system. A double supernova has been proposed to explain observations of the Vela supernova remnant. ROSAT and ASCA observations show slow moving fragments and 1.2×10^6 K X-ray emission outside the blast wave. These features could have been caused by an

earlier supernova that occurred 100,000 years before a second one which is responsible for the main remnant now observed (Young, Shigeyama, & Suzuki, 1996).

For the time span studied here, the remnant is considered to be in a non-radiative stage. This means the energy loss through radiation is small compared to its kinetic energy. However, this does not mean there is no radiation. As can be seen in the graphs below, temperatures inside the remnant are over 10^6 K, which will result in the X-ray emission commonly observed. Interactions between the shock front with pre-shock atoms in the ISM can stimulate line emission, which has been observed in Tycho's supernova (Chevalier, Kirshner, & Raymond, 1980) and the Cygnus Loop (Levenson, 2002). As the remnant adiabatically cools to ~10^4 K, the shocks began to radiate through line emission, commonly Hα, OIII, and SII. This accelerates the cooling which also decreases the pressure driving the shock. The shock continues to expand due to momentum and the leading edge of the remnant becomes a dense shell in what is often referred to as the snowplow phase. An approximate age for the transition to the radiative stage is given by (Blondin, 1998):

$$t_{rad} \approx 2.9 \times 10^4 E_{51}^{\left(\frac{4}{17}\right)} n_0^{-\frac{9}{17}} \text{ years} = 98{,}000 \text{ years} \quad \textbf{(13)}$$

Here E_{51}, the explosion energy in units of 10^{51} ergs, is one and n_0, the number density in hydrogen atoms/cm^3, is 0.1. This can happen much sooner in high density environments. The Cygnus Loop is in a very inhomogeneous environment and exhibits both radiating and non-radiating shocks (Levenson, 2002).

The time-span of the supernova remnant between a few hundred years and the onset of the snowplow phase is often described as a Sedov-Taylor blast wave, named after an analytical solution for a blast wave from a point explosion into a low-pressure,

uniform medium (Sedov, 1959). Although different than the simulations given here, this solution serves as a test for the results of the simulation. An estimate of the radius of the blast wave as a function of time is (Blondin, 1998):

$$R = 12.5 \times \left(\frac{E_{51}}{n_0}\right)^{\frac{1}{5}} t_4^{\frac{2}{5}} \text{ parsecs} \quad \textbf{(14)}$$

Here, t_4 is the time in units of 10,000 years.

Method

The ZEUS Code

For much of this research, supernova remnants were modeled in two dimensions on the Shale cluster and then the Hodor cluster operated by the Computational Research Center at UND. I used ZEUS-MP, a multi-processor, massively parallel version of ZEUS. ZEUS is an open source FORTRAN program designed to solve astrophysical hydrodynamics problems (Stone & Norman, 1992) (Norman, 2000) maintained by the Laboratory for Computational Astrophysics at the National Center for Supercomputing Applications. It solves the equations of hydrodynamics on an Eulerian grid, meaning the grid is fixed and does not move with the fluid as in a Lagrangian method. The equations express conservation of mass, momentum, and energy for a fluid.

$$\frac{d\rho}{dt} + \rho \vec{\nabla} \cdot \vec{v} = 0 \quad \textbf{(15)}$$

$$\rho \frac{d\vec{v}}{dt} + \nabla p = 0 \quad \textbf{(16)}$$

$$\rho \frac{d}{dt}\left(\frac{e}{\rho}\right) + p\vec{\nabla} \cdot \vec{v} = 0 \quad \textbf{(17)}$$

The code employs finite difference methods to express these as approximate algebraic equations. These are time-explicit, meaning the spatial derivatives are evaluated from the previous time step so properties at a grid point can be found independently. In implicit methods, all values are found simultaneously, requiring linear algebra libraries. The simpler explicit method puts limitations on the time step as expressed by the Courant number, $C = \frac{v}{\left(\frac{\Delta x}{\Delta t}\right)} < 1$. Essentially, matter cannot move more than one grid spacing during a time step. The codes used here set C = 0.5.

ZEUS is compiled with a user-supplied code that sets up the initial conditions of a particular problem. This allows the user to create code to solve a variety of problems. This code in turn can read an input file at run time that specifies the physical parameters. At the start of the simulation, the progenitor star is barely resolved on the grid so it has no internal structure. It is basically an injection of mass and energy into the system. It was modeled as a sphere of gas with a constant mass density and a high pressure that would cause it to expand. For these simulations, the ambient medium was composed of two parts: a circumstellar region, which contained material lost by the star before core collapse, and the interstellar medium.

Setup

The ZEUS code consists of a separate function used to set up the specific physical problem. ZEUS is subsequently compiled with this function. In this way, it can be used to study a wide variety of problems by compiling it with different problem generators. Specific numbers for a simulation are provided by an input file. The input file provides data to the main ZEUS code, such as the coordinate system, run time, and the number of

nodes to use in a multi-processor system. It also supplies physical parameters such as density and pressure to the problem generator. These later inputs depend on the specific problem being solved.

The input file passed parameters to the main code describing the grid on which the simulation would be run. For these simulations, a 2-dimensional polar grid was used. The grid does not adjust with simulation time so the grid needed to be big enough to encompass the entire simulation while also providing adequate resolution. Since smaller structures are expected near the center of the grid, I set the grid up so that it had higher resolution near r = 0. This can be done in ZEUS by setting a ratio by which the next grid interval will be larger than the previous. I did this in two parts. The first 103 blocks represented a total distance of 10^{18} cm, with each grid space 10% larger than the previous. The size of the smallest, central blocks was 2.7×10^{12}cm. The remaining 2169 blocks maintained a constant interval size of 9.17×10^{16}cm. The polar angle went from 0 to $\pi/2$ and was divided into 90 sections. Time limitations prevented introduction of instabilities in the ZEUS code so angular effects were not seen. The results are essentially the same as 1-d simulations. Before working with ZEUS, 2-d structures were simulated using a different code, which are presented later for comparison. Despite access to other code that already includes instabilities, the greater flexibility of ZEUS will allow a larger variety of environments to be explored in the future.

Other parameters in the input file set the total time of the run, the times that output would be written to disk, boundary conditions, and how many processors to use. Another important option is whether or not to use a restart file. This allows the simulation to start where a previous one stopped. For simulations including a second

supernova, a restart was used. The simulation was first allowed to run for a set amount of time, usually 10,000 years. Then, the simulation was run again, continuing from where it left off. When it restarted, a second supernova was created. To do this, another over pressured region representing a star was placed at the origin that then expanded into the environment created by the first blast wave. In reality, the stars would be offset although this distance is small compared to the large structures being studied. By default, ZEUS continues using the same time step before and after the restart. This causes major problems because the time step had become too large to simulate a young remnant. A new time step appropriate for a new supernova was calculated by calling the function "nudt" at the end of restart.f.

Supernova Initial Conditions

To model a supernova, a sphere of constant mass density and pressure was placed at the origin of the coordinate system. This sphere had a larger pressure than its surroundings, causing it to expand. A radius of 2×10^{13}cm (1.3 Astronomical Units) was used, which is about the size of a red supergiant that is generally expected to produce a Type II supernova. For this project, remnants from stars with masses between 15 and 30 solar masses were examined. This range was implemented by changing the initial density of the sphere that represents the star. For example, a 20 solar mass (4×10^{34} gram) star has a density of

$$\rho = \frac{4 \times 10^{34} grams}{\frac{4}{3}\pi(2 \times 10^{13} cm)^3} = 1.187 \times 10^{-6}\text{g/cm}^3 \quad \textbf{(18)}$$

Supernovae typically explode with a 10^{51} ergs kinetic energy (Woosley S. , 2005). This was input into the code as a pressure. Pressure does work on the gas which provides the kinetic energy, similar to a piston.

$$Work = PV = \Delta KE \tag{19}$$

$$P = \frac{KE}{V} = \frac{10^{51} erg}{\frac{4}{3}\pi(2 \times 10^{13} cm)^3} = 3 \times 10^{10} \text{dyne/cm}^2 \tag{20}$$

Circumstellar Medium

Outside this mass lies the circumstellar medium. During their lifetime, massive stars lose a large amount of mass through a stellar wind. A wind with a constant mass loss rate and velocity results in an inverse square density profile. This agrees with models used in the literature, (Chevalier R. , Are young supernova remnants interacting with circumstellar gas?, 1982) (Truelove & McKee, 1999) as well as direct imaging of the nebula around VY Canis Majoris using the Hubble Space Telescope (Smith, 2001).

$$\rho(r) = \frac{dM}{dV} = \frac{dM}{4\pi r^2\, dr} = \frac{\frac{dM}{dt}}{4\pi r^2 \left(\frac{dr}{dt}\right)} = \frac{\dot{M}}{4\pi r^2 v} \tag{21}$$

Here, $\dot{M}$ is the mass loss rate and *v* is the wind velocity. These values can be inferred from radio and X-Ray emission generated by a supernova's interaction with the CSM. Measurements from multiple supernovae have found $\dot{M}$ to be typically 10^{-5} - 10^{-4} solar masses/year and *v* is about 10^6 cm/s (Chevalier R. , The radio and X-ray emission from type II supernovae, 1982) (Chevalier & Oishi, Cassiopeia A and its clumpy presupernova wind, 2003).

The radius of the circumstellar medium is related to the total amount of expelled mass given a constant wind velocity and mass loss rate. The total mass enclosed in a certain radius is:

$$M = \int_0^{r_{csm}} \rho(r) \times 4\pi r^2 dr = \int_0^{r_{csm}} (\dot{M}/v) dr = (\dot{M}/v)\, r_{csm} \quad \textbf{(22)}$$

If a star is expected to expel 10 solar masses during its lifetime, with a mass loss rate of 10^{-4} solar masses/year and a velocity of 10^6 cm/s, then the radius of the circumstellar medium due to mass loss would be.

$$r_{csm} = \frac{M}{\dot{M}} \times v = \frac{10\, SM}{\frac{0.0001\, SM}{3.16 \times 10^7 s}} \times 10^6 \frac{\text{cm}}{\text{s}} = 3.16 \times 10^{18}\text{cm} \approx 1\text{pc} \quad \textbf{(23)}$$

As observational consistency, a disk of this size has been observed around the red giant Betelgeuse (Decin, 2012). Even larger structures are seen around massive stars, such as the Crescent Nebula extending 3 pc from the Wolf Rayet star WR 136.

Interstellar Medium

Beyond the circumstellar medium is the interstellar medium (ISM). The ISM is composed of multiple regions. There are cold, high density clouds separated by a warm diffuse gas that fills most of the galaxy's volume. This warm component has a temperature of about 10,000K (McKee & Ostriker, A theory of the interstellar medium - Three components regulated by supernova explosions in an inhomogeneous substrate, 1977) and a hydrogen number density between 0.1-0.2/cm^3 (Slavin & Cox, 1992). This component was used to set the properties for the interstellar medium into which the star's material expanded. The thermal pressure of this gas that is input into the code was found

from the ideal gas law where *n* is the hydrogen number density and *k* is the Boltzmann constant.

$$P = nkT = 1.38 \times 10^{-13} \text{dynes/cm}^2 \quad \textbf{(24)}$$

Post-Processing

Results from the simulation are recorded as HDF files. These files contain 2-d arrays of velocity, mass density, and energy density. I wrote an IDL script to read the data from these files and output log scale graphs of density, velocity, pressure, and temperature. Pressure was found from the internal energy density, *e*, assuming a monatomic ideal gas where $e = 3/2\ n\ k\ T$ and $P = n\ k\ T$. Relating these equations results in the simple equation of state:

$$P = 2/3\ e \quad \textbf{(25)}$$

Temperature was derived from the values of pressure and density.

$$P = \frac{N}{V} kT \rightarrow T = \frac{P}{\frac{N}{V} k}$$

$$\frac{N}{V} = \frac{N}{V} \times \frac{m}{m} = \frac{\rho}{m} \text{ where the density } \rho = \frac{N \times m}{V}$$

$$T = \frac{m}{k} \times \frac{P}{\rho}$$

$$Log(T) = Log\left(\frac{m}{k}\right) + Log(P) - Log(\rho) \quad \textbf{(26)}$$

Since velocities could initially be zero and later be negative, using a log of the velocity isn't possible. To avoid log(0), I added one to all velocity values. On a scale of millions of cm/s, this isn't noticeable. I then added the proper sign to the absolute value of the velocity.

$$\log(v)_{graphed} = \frac{v}{abs(v)} \times \log[\text{abs(v)}] \quad \textbf{(27)}$$

Setup Results

Figure 10 shows the CSM and ISM at the beginning of a simulation. It shows the mass density, velocity, pressure, and temperature for 5 solar masses of circumstellar medium resulting from stellar mass loss and a small portion of the interstellar medium.

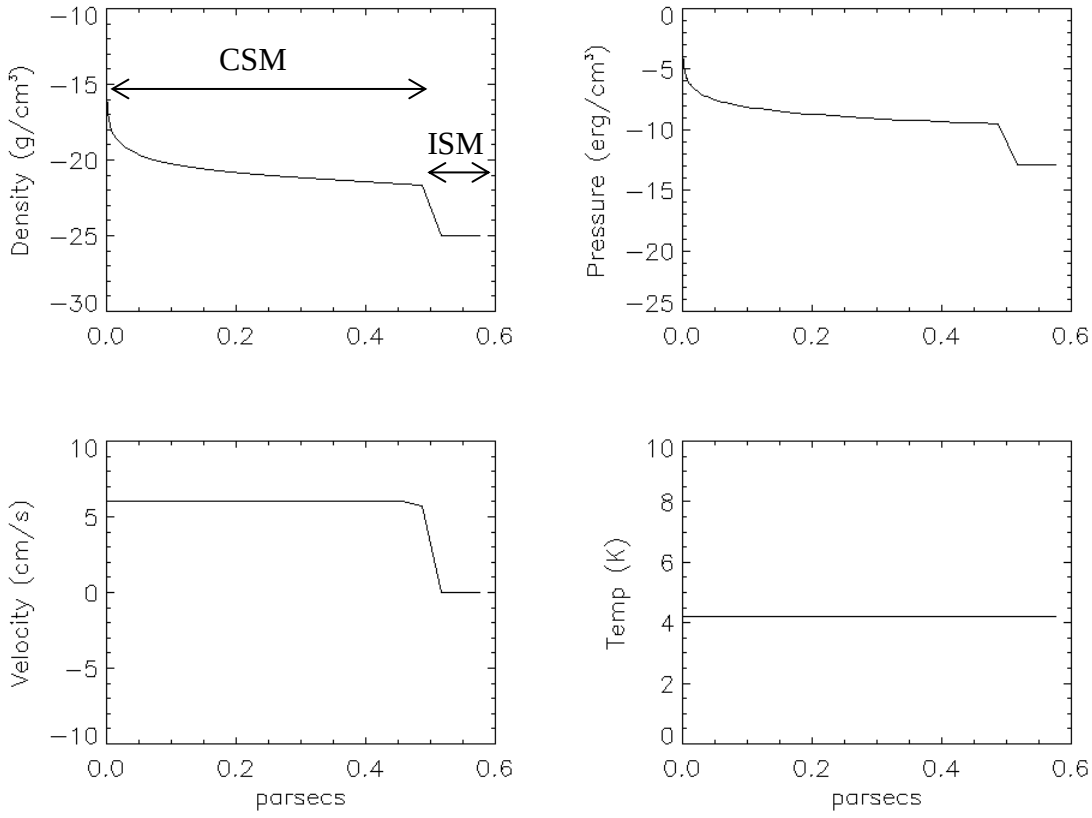

Figure 10: Initial circumstellar setup

Results

Simulations were run for both single and double supernova with varying initial masses and mass loss. For double supernovae, the time between explosions was kept at a constant 10,000 years. In a double supernova, I found that the shock front produced by the second supernova eventually caught up to and passed the first shockwave produced by the initial supernova explosion.

Single Supernova Results

First, I will present results from a single 15 solar mass supernova expanding into the interstellar medium with no additional circumstellar material. Figure 11 shows the remnant after 1000 years when a single shock feature is seen. The shock heats and compresses the ISM which pushes back on the ejecta behind the shock. This creates a reverse shock that impedes the flow of material, as seen in Figure 12. By 30,000 years (Figure 13), material behind the shock has slowed and reversed direction, creating a reverse shock that moves toward the origin, heating the interior of the remnant.

After the circumstellar medium was added, simulations using various combinations of expanding mass (supernova ejecta) and circumstellar mass were run to investigate the positions of the forward shock, reverse shock, and dense shell. To demonstrate results of a single supernova blast simulation, I will use as an example a 20 solar mass star with 10 solar masses of circumstellar material. The density, pressure, velocity, and temperature line profiles start with Figure 14.

Initially, a single shock front travels through the circumstellar material that had been lost by the star before the supernova. After it crosses into the interstellar material, a second shock front forms. There is a large temperature increase in the shocked

interstellar material. This material expands and pushes back on the ejecta, creating a reverse shock seen later. Reverse shocks are a common feature of supernova remnant models (McKee, X-ray emission from an inward-propagating shock in young supernova remnants, 1974) (Truelove & McKee, 1999).

After 1000 years (Figure 16), there are three notable features. The original large shell (3) is still most prominent but there are also two smaller ones in front; the forward shock (1) and reverse shock (2). Looking closely, there is a small decrease in velocity at the location of the reverse shock due to the hot interstellar material pushing back on it. The forward shock has traveled about 3.5 pc. For comparison, this is about the age of the Crab Nebula, a remnant from a supernova that was observed in 1054. Given a distance of 1930 parsecs (Trimble, 1973), and an angular size of 6 arc minutes (Green, 2009), the Crab Nebula currently has a radius of about 3.4pc. Its expansion speed is slower than the simulation, currently about 1500 km/s (Bietenholz, 1991) vs 3000 km/s in the simulation.

After 5000 years (Figure 17), the smaller forward shells have become denser while the larger rear one has a density similar to the others. It is also catching up to the central shell. After 8000 years (Figure 18), the rear density shell has merged with central one. After 11,000 years (Figure 19), a reflected shock starts to form and a small discontinuity can be seen in the velocity profile. The forward shock has traveled about 18 pc. Comparing this with equation (14), the predicted radius of a Sedov-Taylor blast wave, and setting $E_{51} = t_4 = 1$,

$$R = 12.5 \times 0.1^{-.2} = 19.8 \text{ parsecs}$$

The simulated result is close but not exact. The simulated shock has not traveled as far as the ideal analytical solution, likely due to its initial passage through a dense circumstellar

medium and the existence of non-negligible pressure from the interstellar medium. As will be seen later, the radius of the remnant also appears to depend on the mass of the expanding star, which is not included in the Sedov-Taylor relation.

After 21,000 (Figure 20) years the high density central shell has impeded the outward flow behind it and some of the supernova ejecta now has a negative velocity, moving back toward the origin. At this time, there is a forward shock, a reflected shock, and a noticeable high density shell between them. The reflected shock heats previously unshocked ejecta, resulting in X-Ray emission from the interior of the remnant (McKee, X-ray emission from an inward-propagating shock in young supernova remnants, 1974). The overall structure looks similar to a textbook example of forward and reverse shocks, with the high density shell forming just behind a contact discontinuity, defined as a separation between shocked ISM and shocked ejecta (Truelove & McKee, 1999). This region should be Rayleigh-Taylor unstable (Dopita & Sutherland, 2004). This will be shown to be true when the shell breaks up in a different 2-D simulation computer code that includes Rayleigh-Taylor instabilities.

At the end of the simulation, 40,000 (Figure 22) years after the supernovae, there are three notable features: a forward shock (1) that has traveled almost 40 parsecs, a reflected shock (3) traveling toward the origin at about the same speed, and a central, nearly stationary high density shell. Because of the reflected shock, the interior of the remnant is hotter than the outer edge. Despite initially being more complex, the overall structure is similar to the remnant that resulted without a CSM.

Simulations were also run with an ISM density of 0.2 hydrogen atoms/cm^3. A sample plot is shown in Figure 23 showing the remnant at 30,000 years. The structure is

similar but the main shock has not moved as far and the reflected shock is closer to the origin.

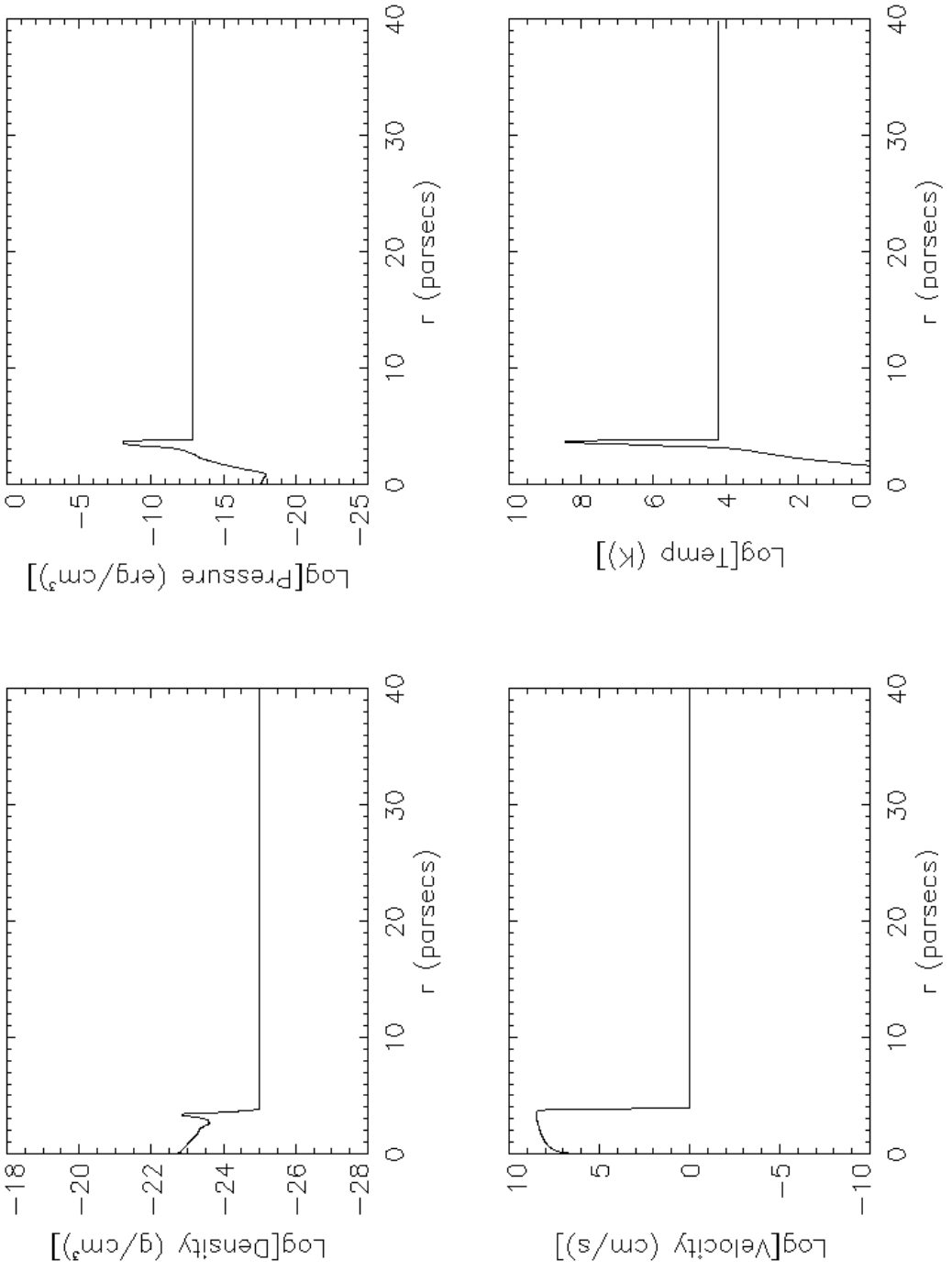

Figure 11: 15 solar mass star with no CSM at 1000 years.

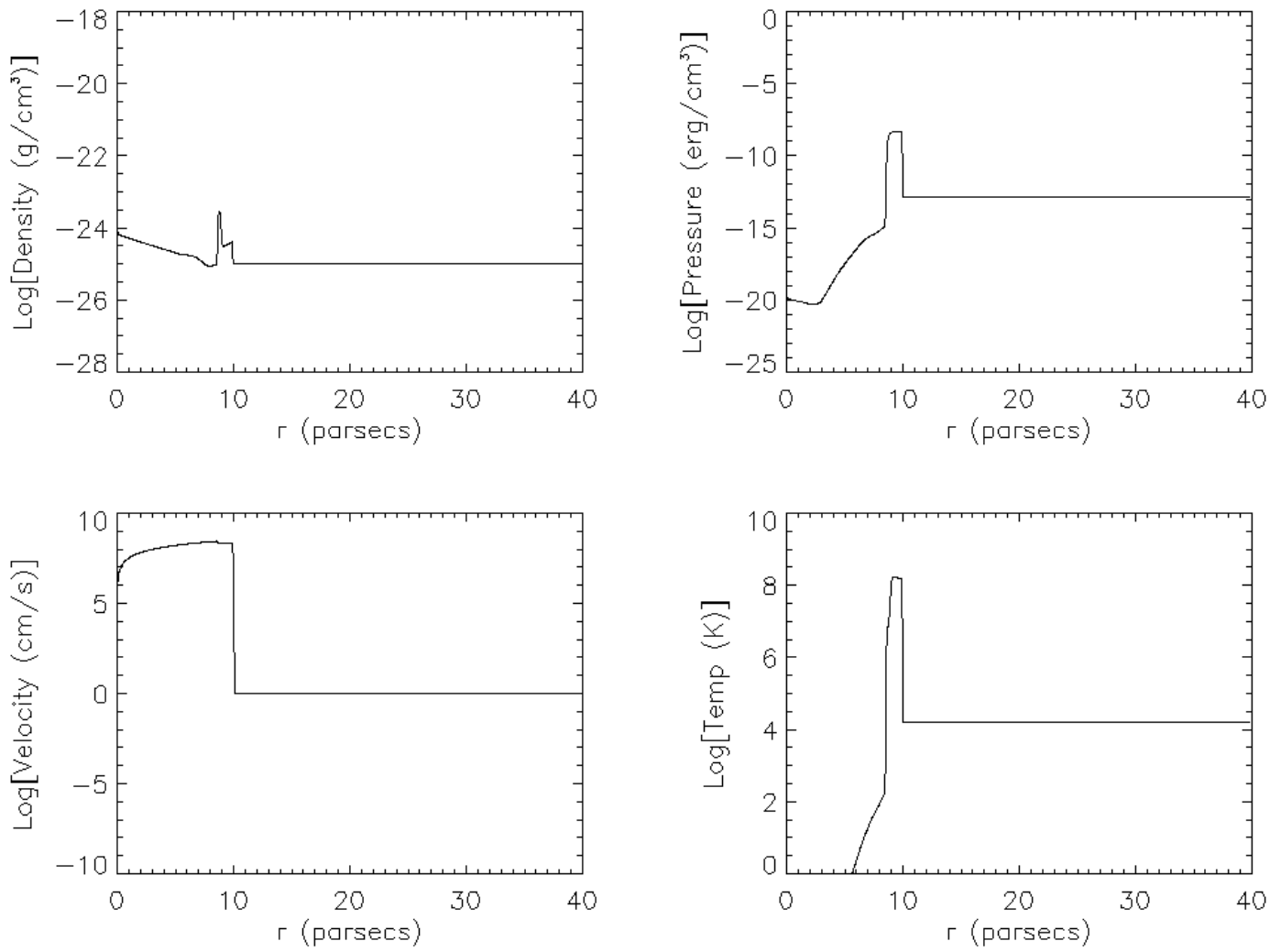

Figure 12: 15 solar mass star with no CSM at 3000 years.

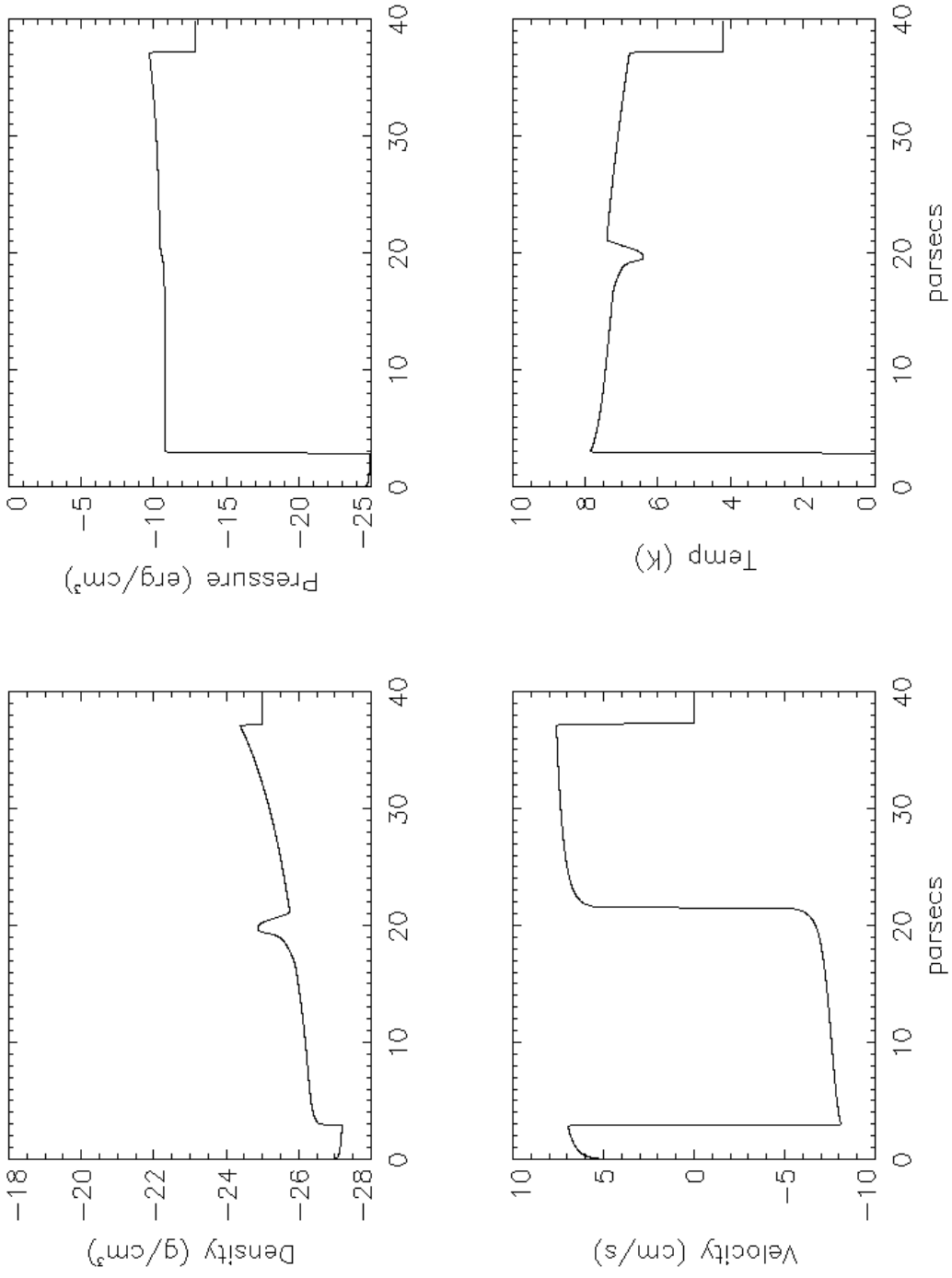

Figure 13: 15 solar mass star with no CSM at 30,000 years.

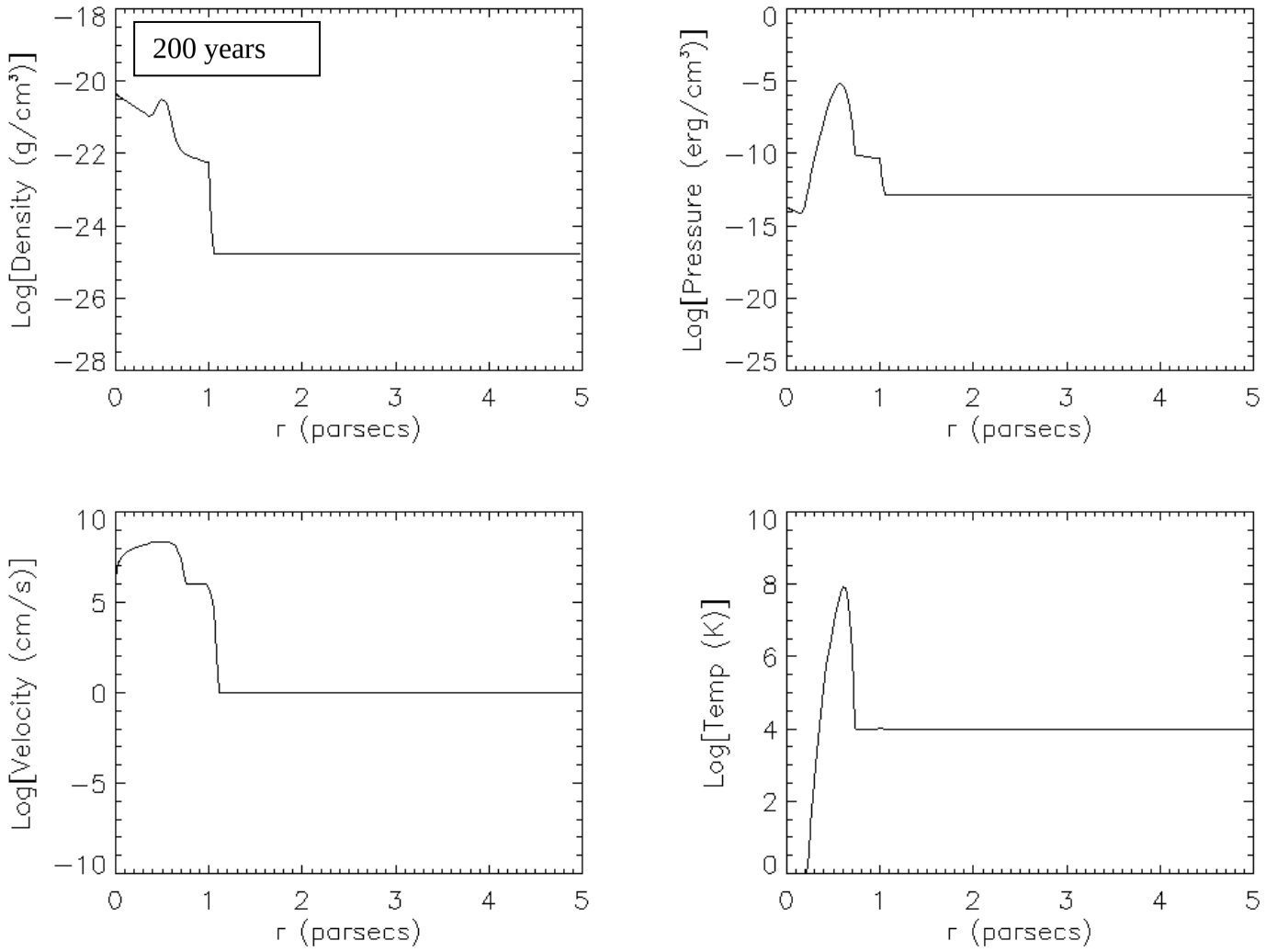

Figure 14: Single supernova at 200 years.
20 solar mass star and 10 solar mass CSM. ISM=0.1/cm^3

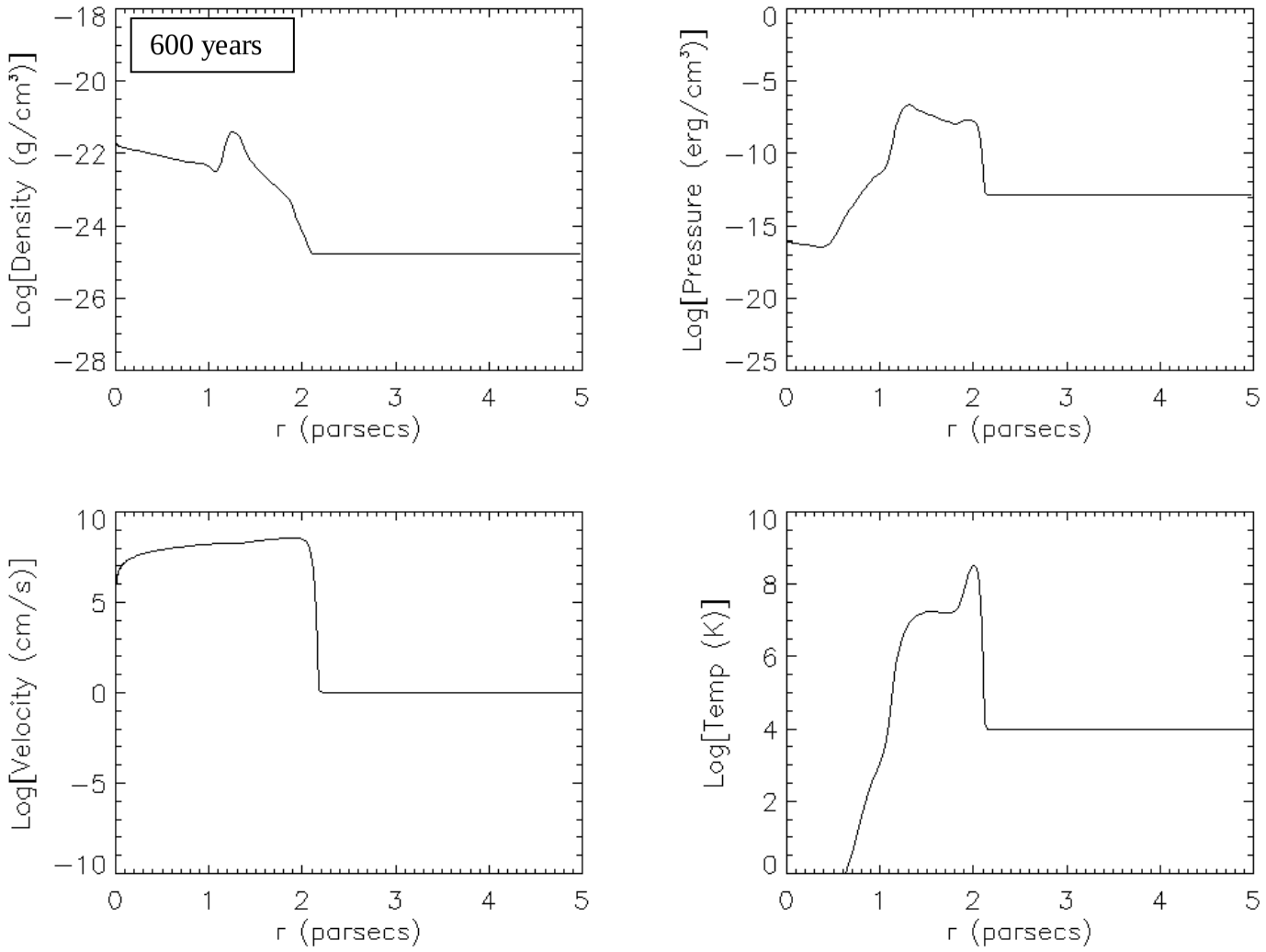

Figure 15: Single supernova at 600 years. ISM=0.1/cm^3

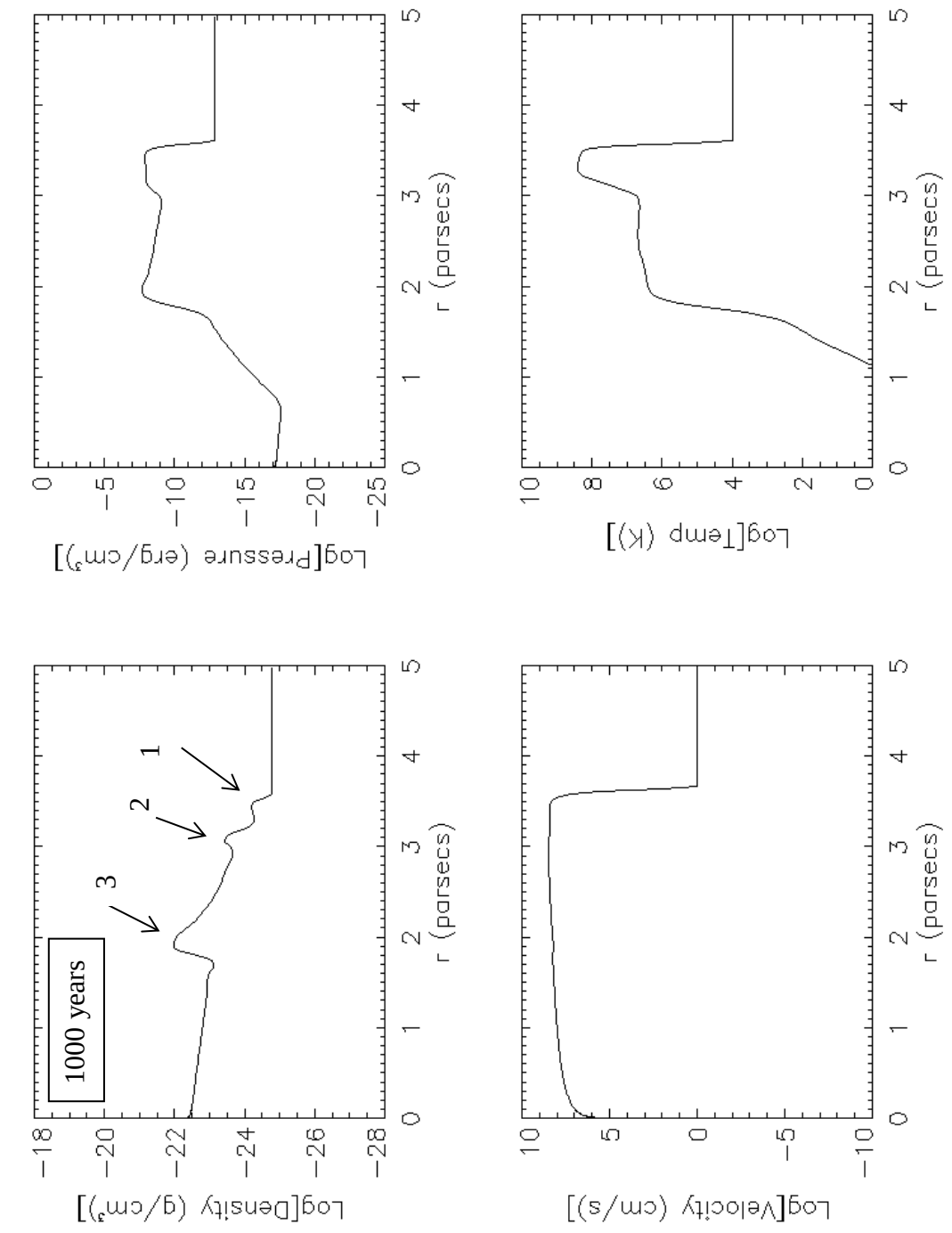

Figure 16: Single supernova at 1000 years. ISM=0.1/cm^3

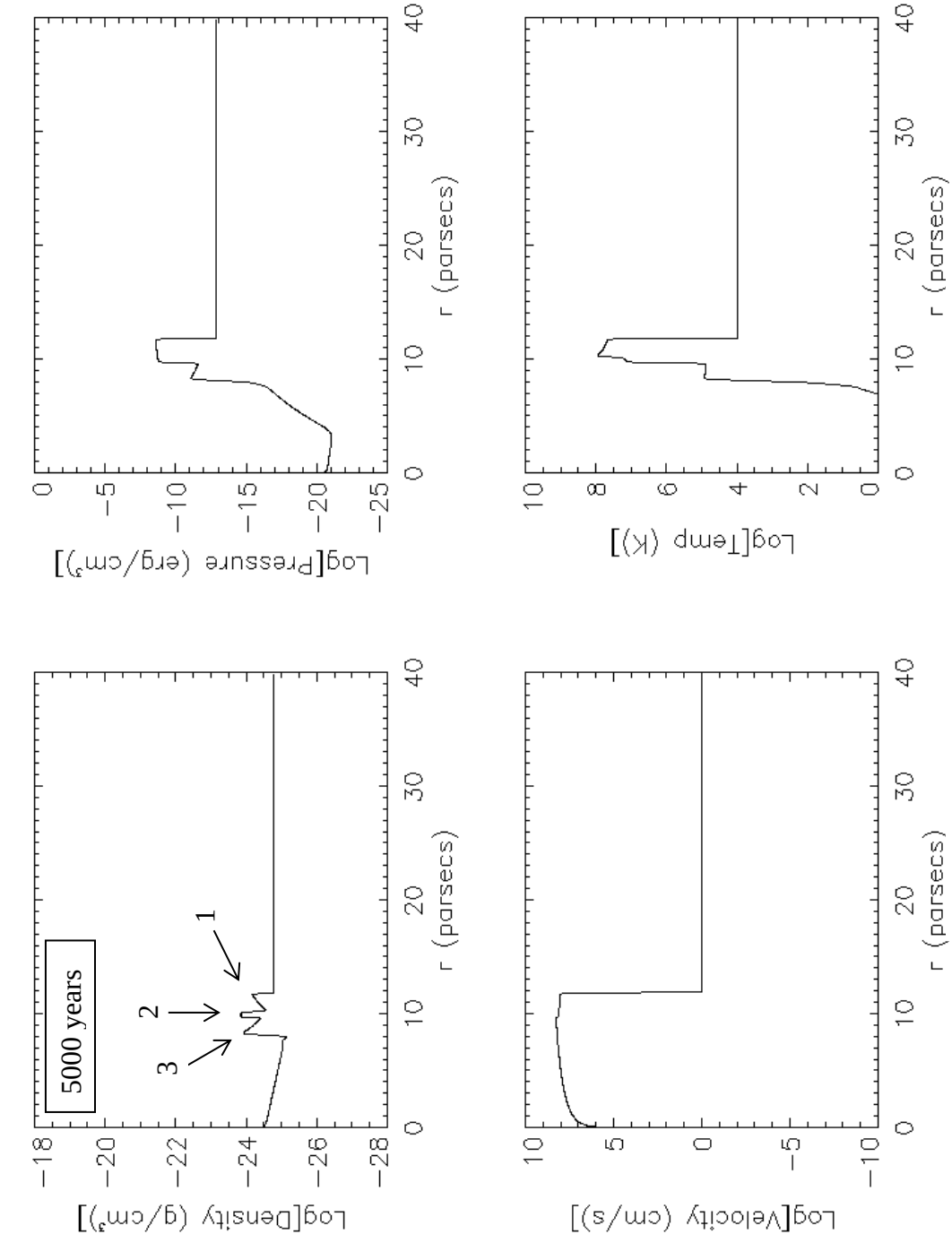

Figure 17: Single supernova at 5000 years. ISM = 0.1/cm^3

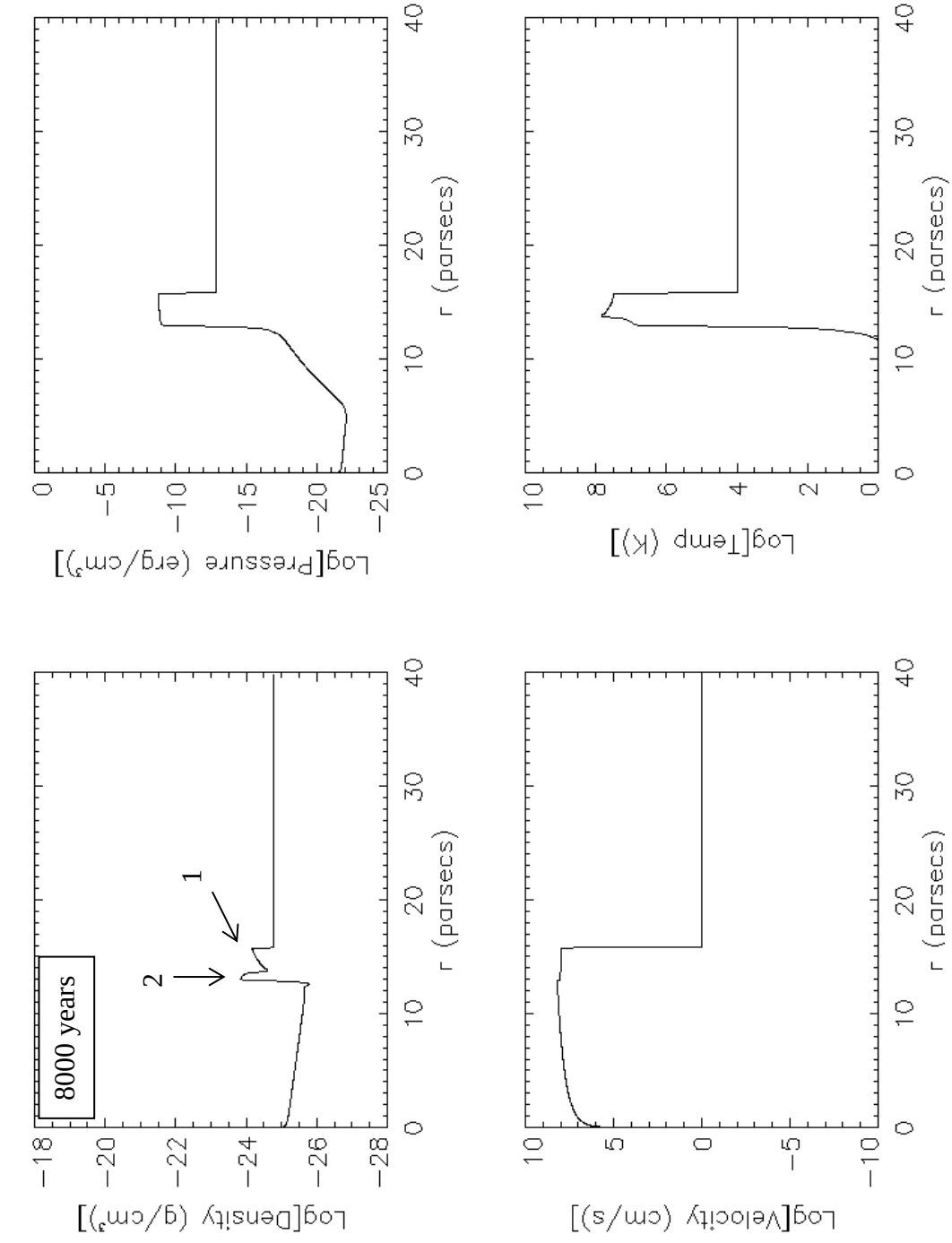

Figure 18: Single supernova at 8000 years. ISM = 0.1/cm^3

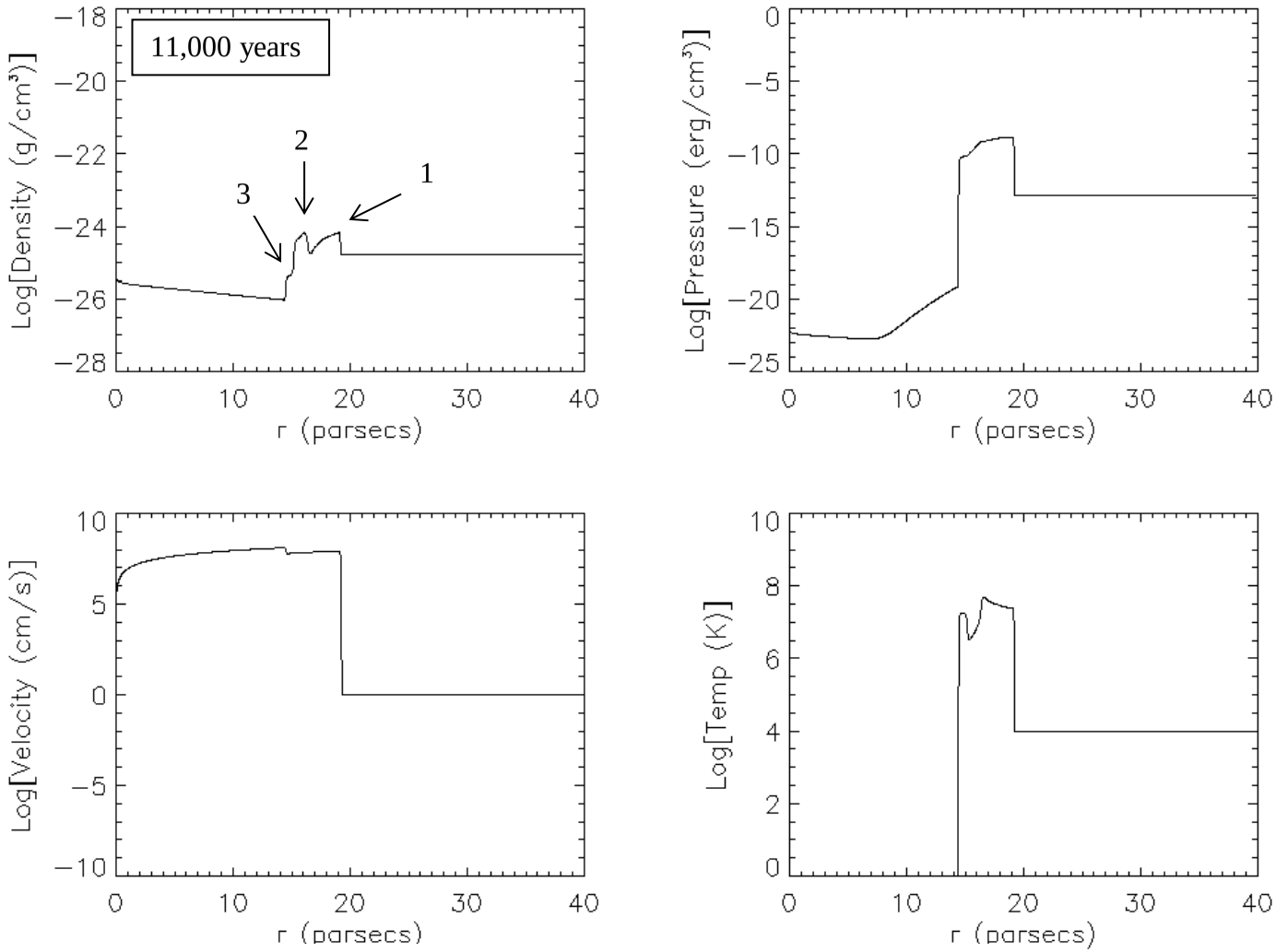

Figure 19: Single supernova at 11,000 years. ISM=0.1/cm^3

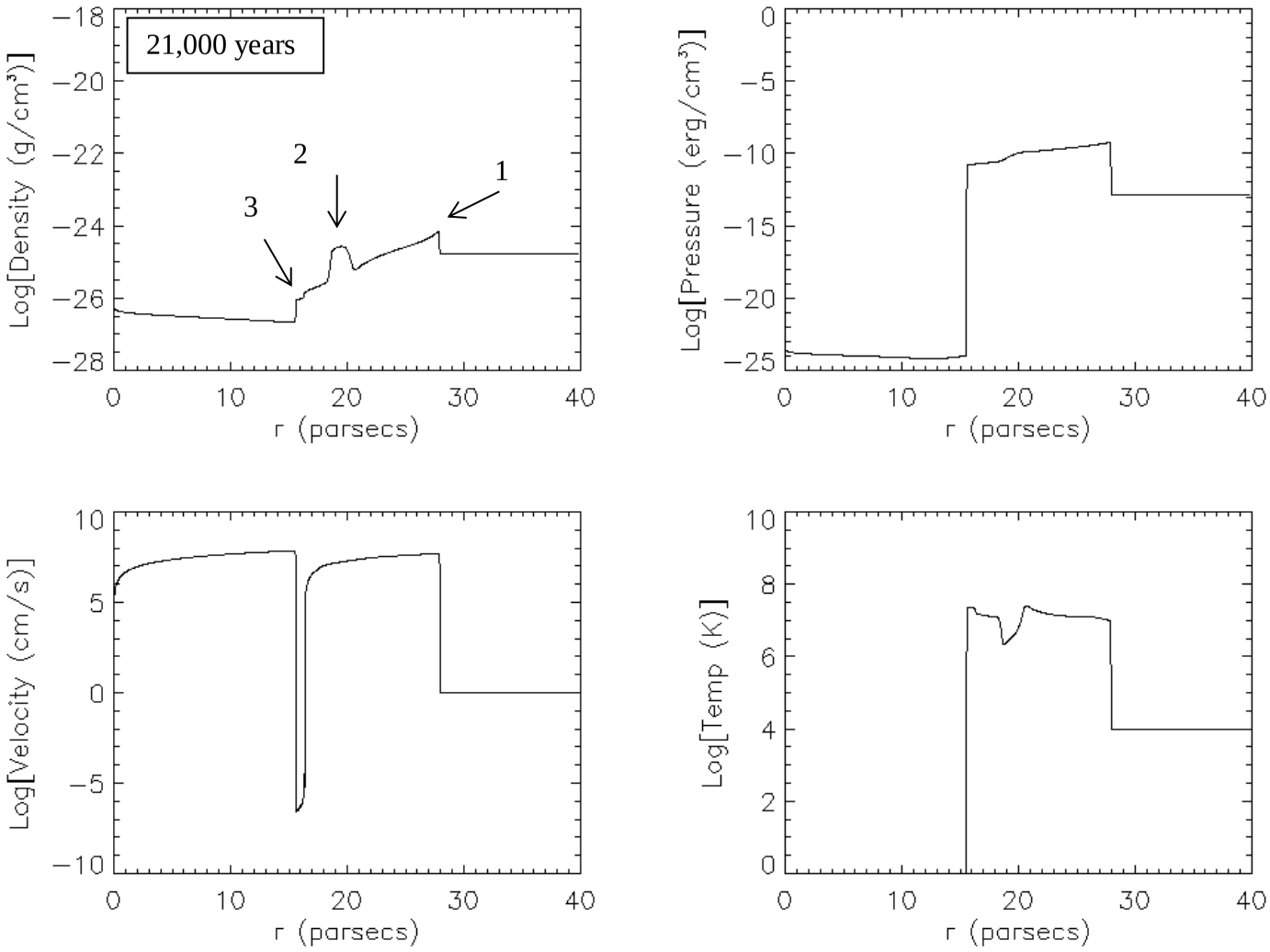

Figure 20: Single supernova at 21,000 years. ISM=0.1/cm^3

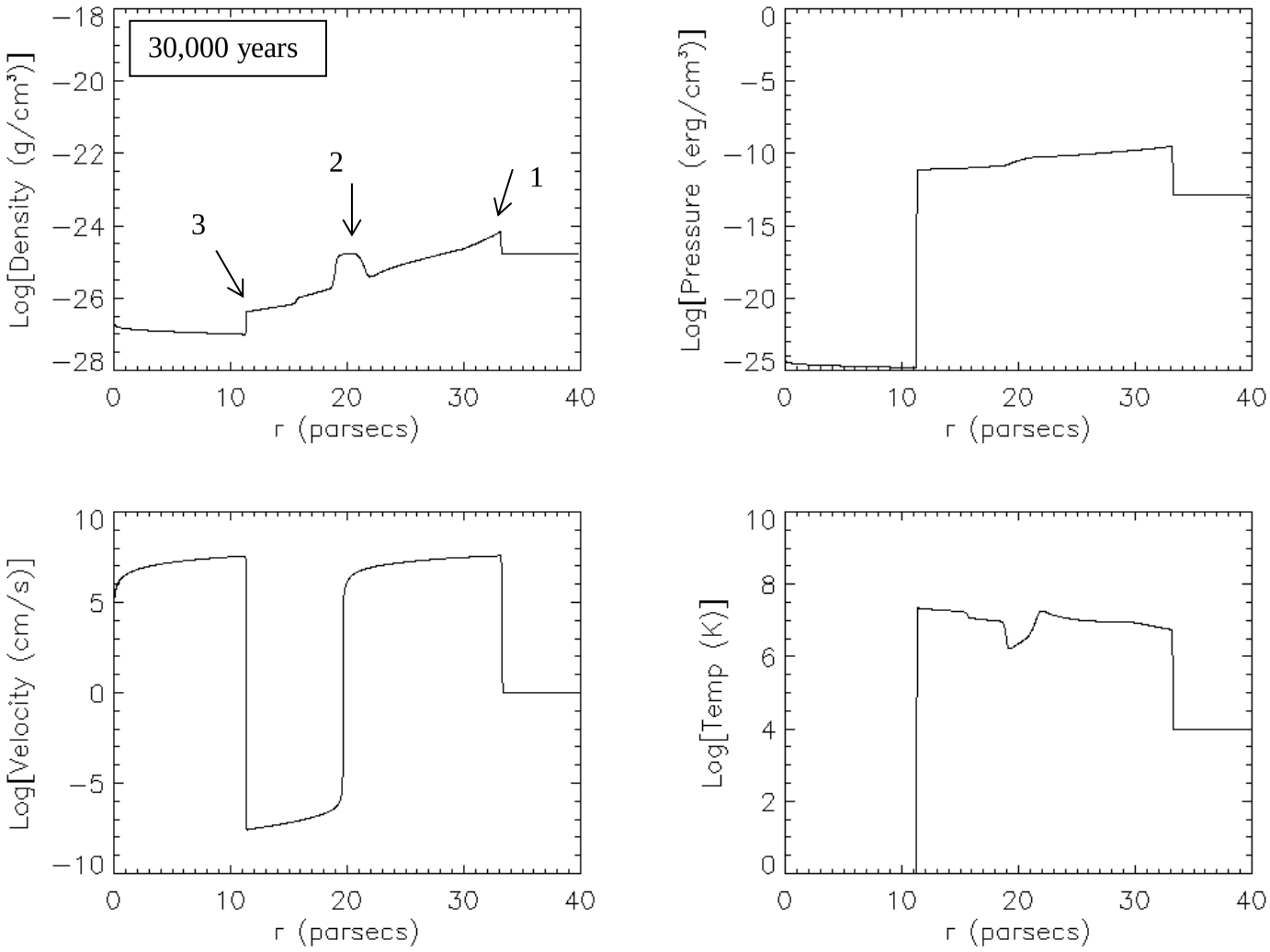

Figure 21: Single supernova at 30,000 years. ISM=0.1/cm^3

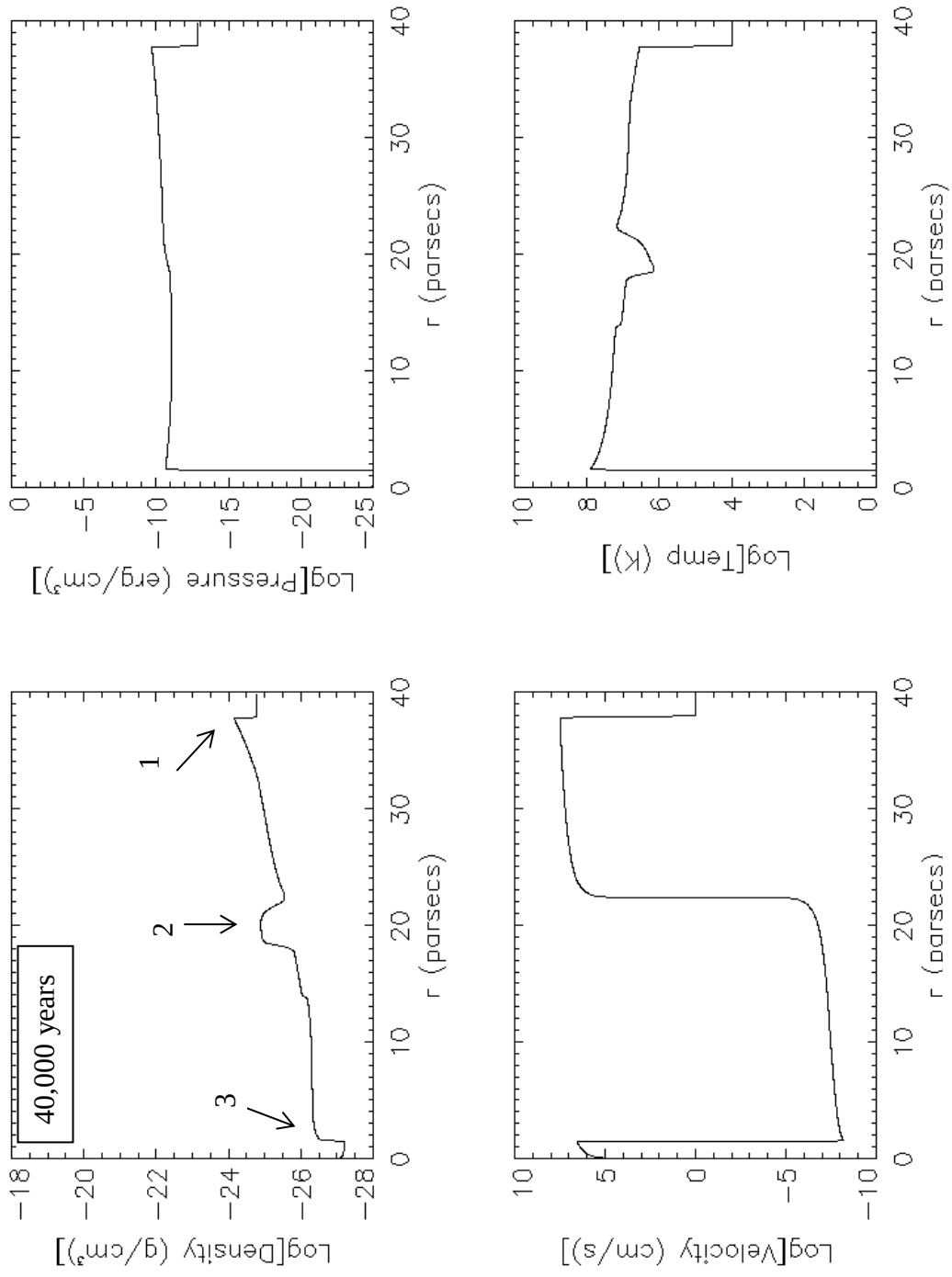

Figure 22: Single supernova at 40,000 years. ISM=0.1/cm3

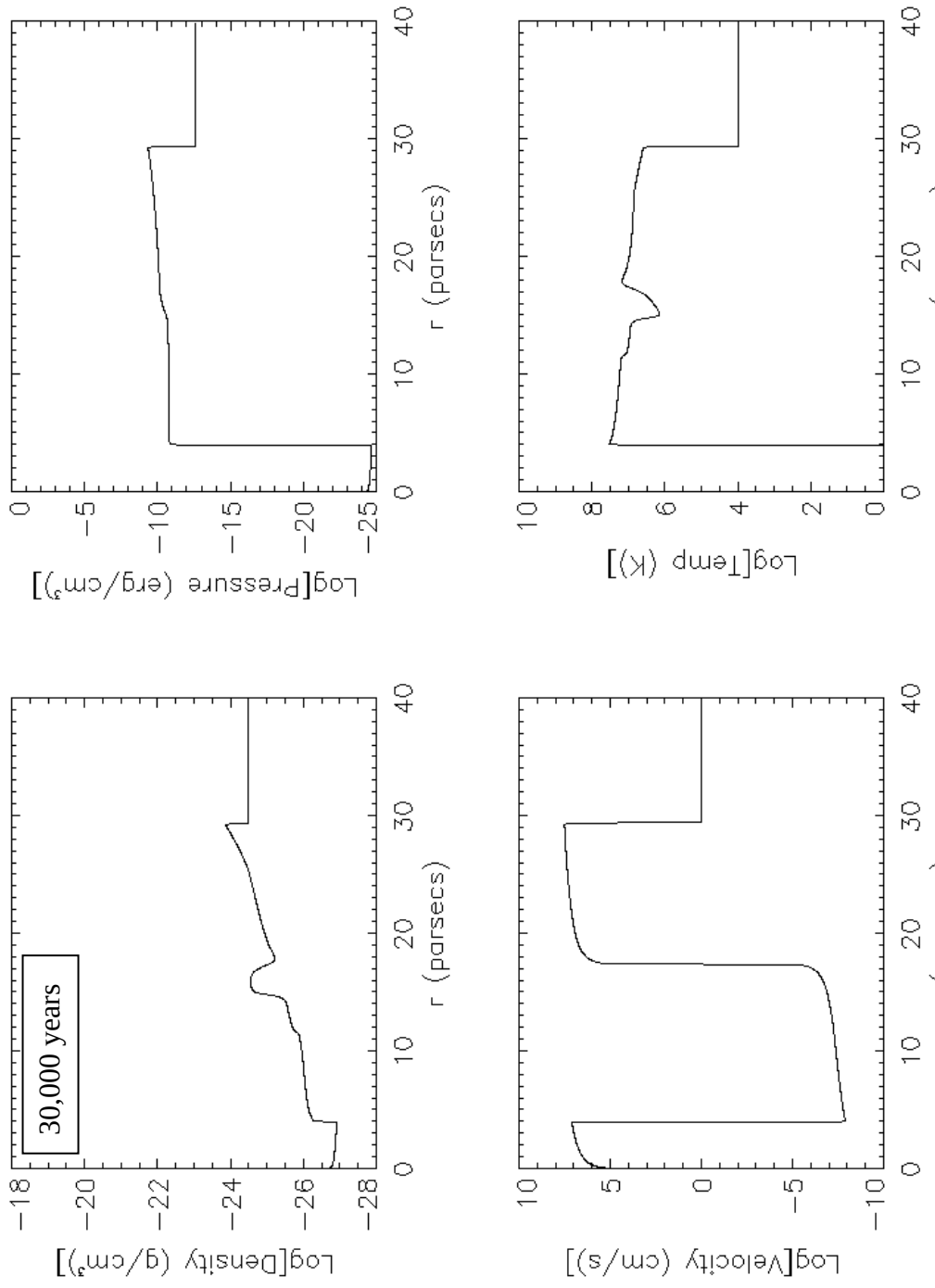

Figure 23: Single supernova at 30,000 years with an ISM density of 0.2/cm^3

Double Supernova Results

The second supernova explosion in the simulation was initiated 10,000 years after the first supernova explosion. The same stellar and CSM masses were used. The results shown here are for a 20 solar mass star with 10 solar masses of circumstellar material. The following description and figures show the remnant after 10,000 years as the time period before this will be the same as for a single supernova.

The resulting profile fourteen thousand years after the first blast (4000 years after the second) shows that the second blast wave has almost caught up to the first shock wave and there are now a total of five features in the density plot. After this, the morphology changes quickly as the shock from the second supernova interacts with the first. Figure 26 shows the remnant after 15,500 years. At this time, the second forward shock (4) has passed the reflected shock from the first blast (3). Sixteen thousand years after the first supernova (Figure 27), feature 3 from the first blast and feature 4 from the second blast appear to have disappeared. At 18,000 years (Figure 30), a reflected shock (3) can again be seen and there are three central density features. After 22,000 years (Figure 31), the reflected shock (3) now has a negative velocity. The forward shock from the second blast wave (4) has almost reached the first. After 27,000 years (Figure 32), the forward shock from the second supernova (4) has reached the first (1). The density profile is similar to that of a single supernova except that it shows two central shells instead of one. After 35,000 years (Figure 33), it appears that the two forward shocks have separated, although the difference is small. One of the forward shocks appears as a small increase in density behind the other. Also, a second reflected shock has formed and is moving back toward the origin.

A scenario that included a longer time between blasts was also simulated. A second blast was initiated 34,000 years after the first and was found to collide with the reflected shock moving toward the origin. This differs from the previous case where the reflected shock was still moving away from the origin. As shown in Figure 34, at 55,000 years after the first blast the same overall morphology as the previous case is observed, with the second forward shock on track to catch up to the first.

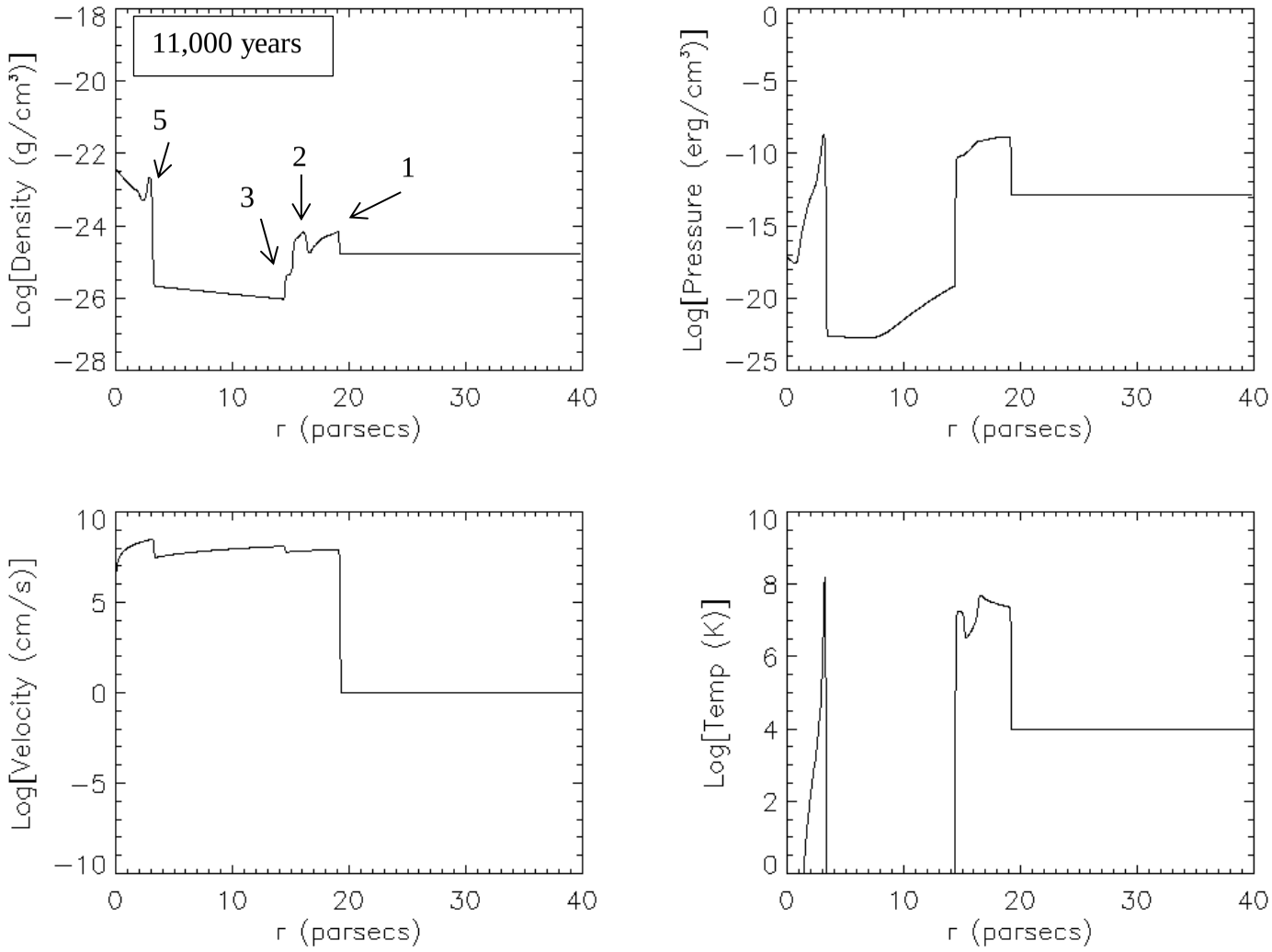

Figure 24: Double supernova at 11,000 years. ISM=0.1/cm^3

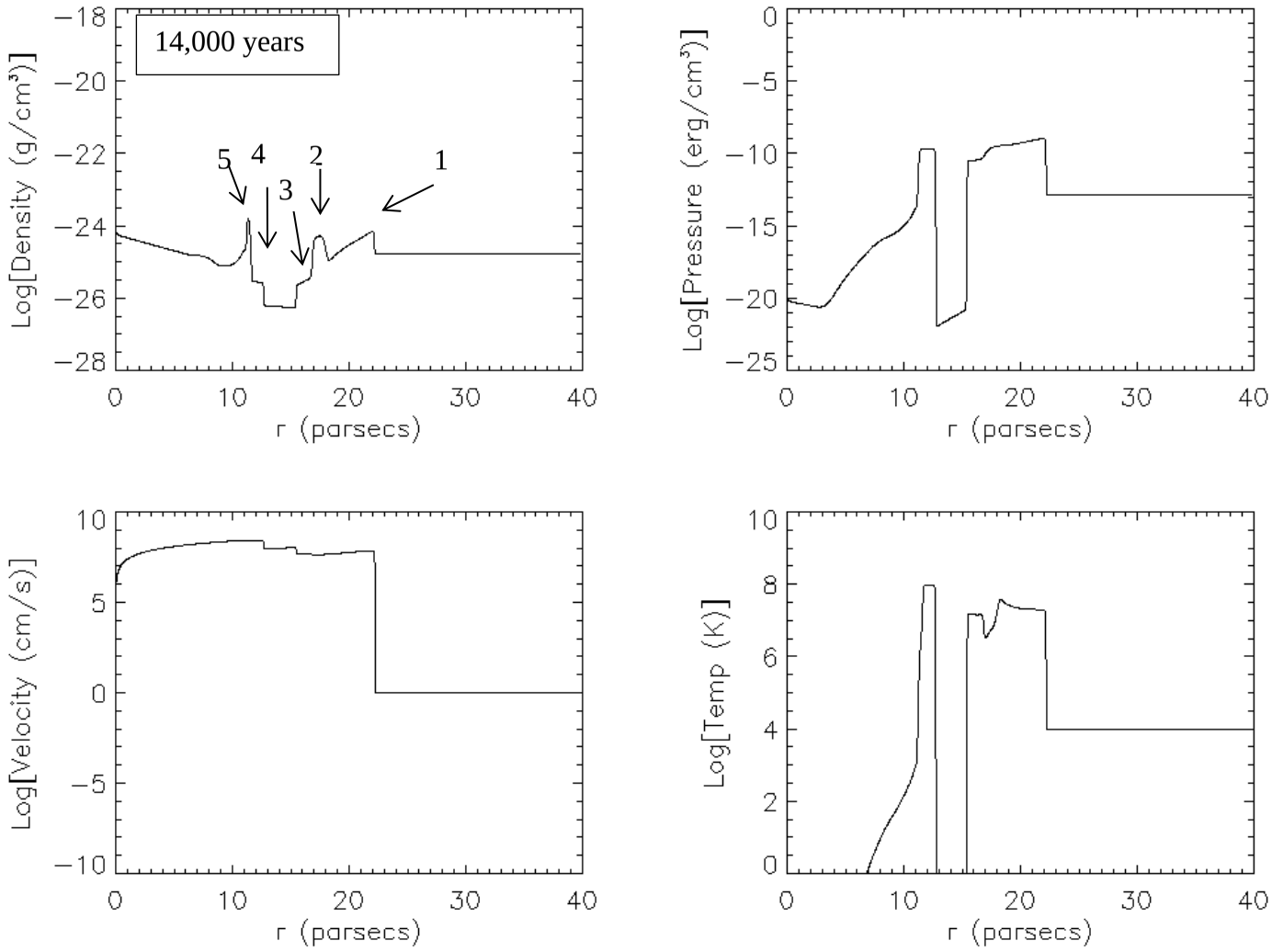

Figure 25: Double supernova at 14,000 years. ISM=0.1/cm^3

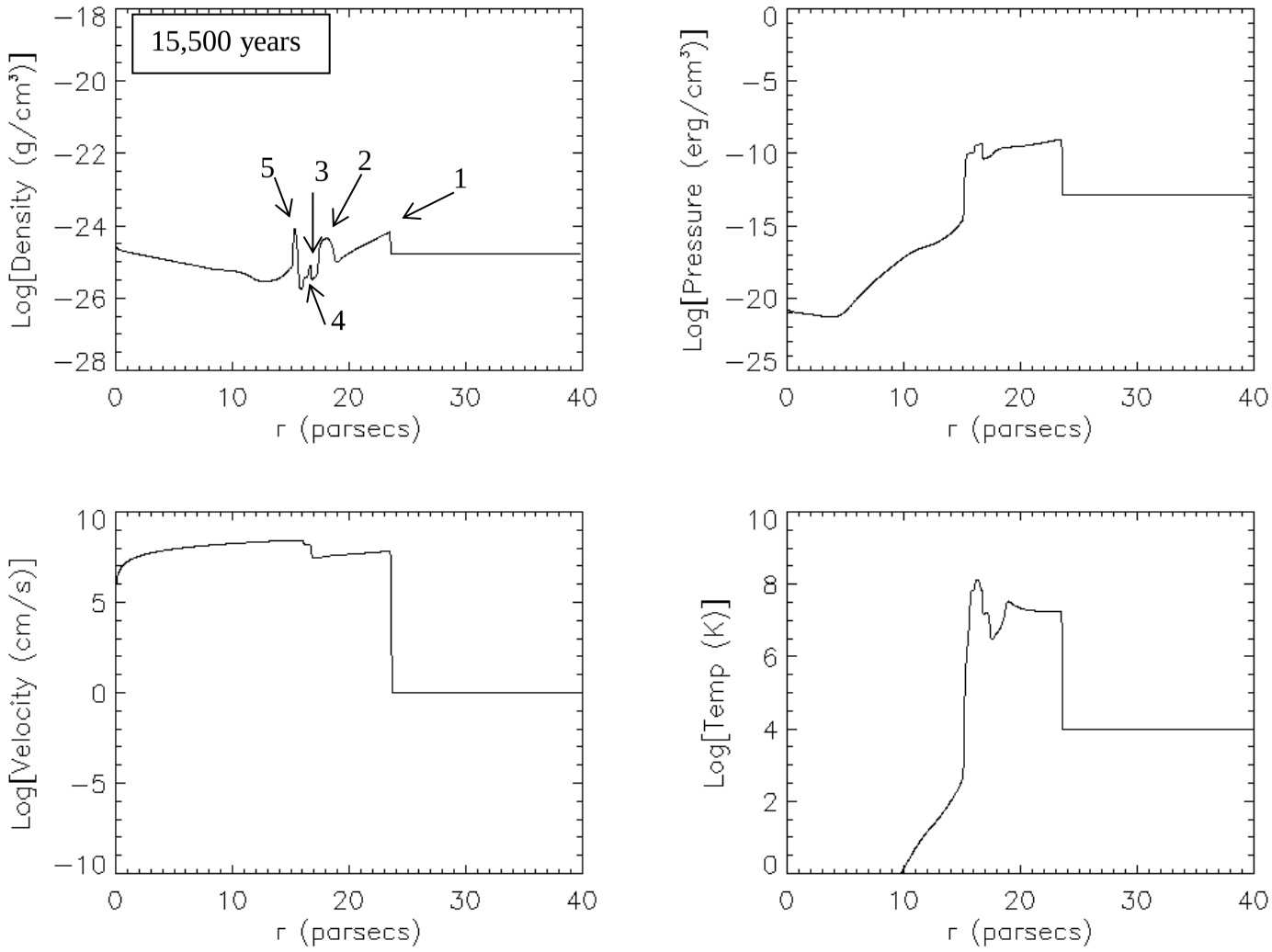

Figure 26: Double supernova at 15,500 years. ISM=0.1/cm^3

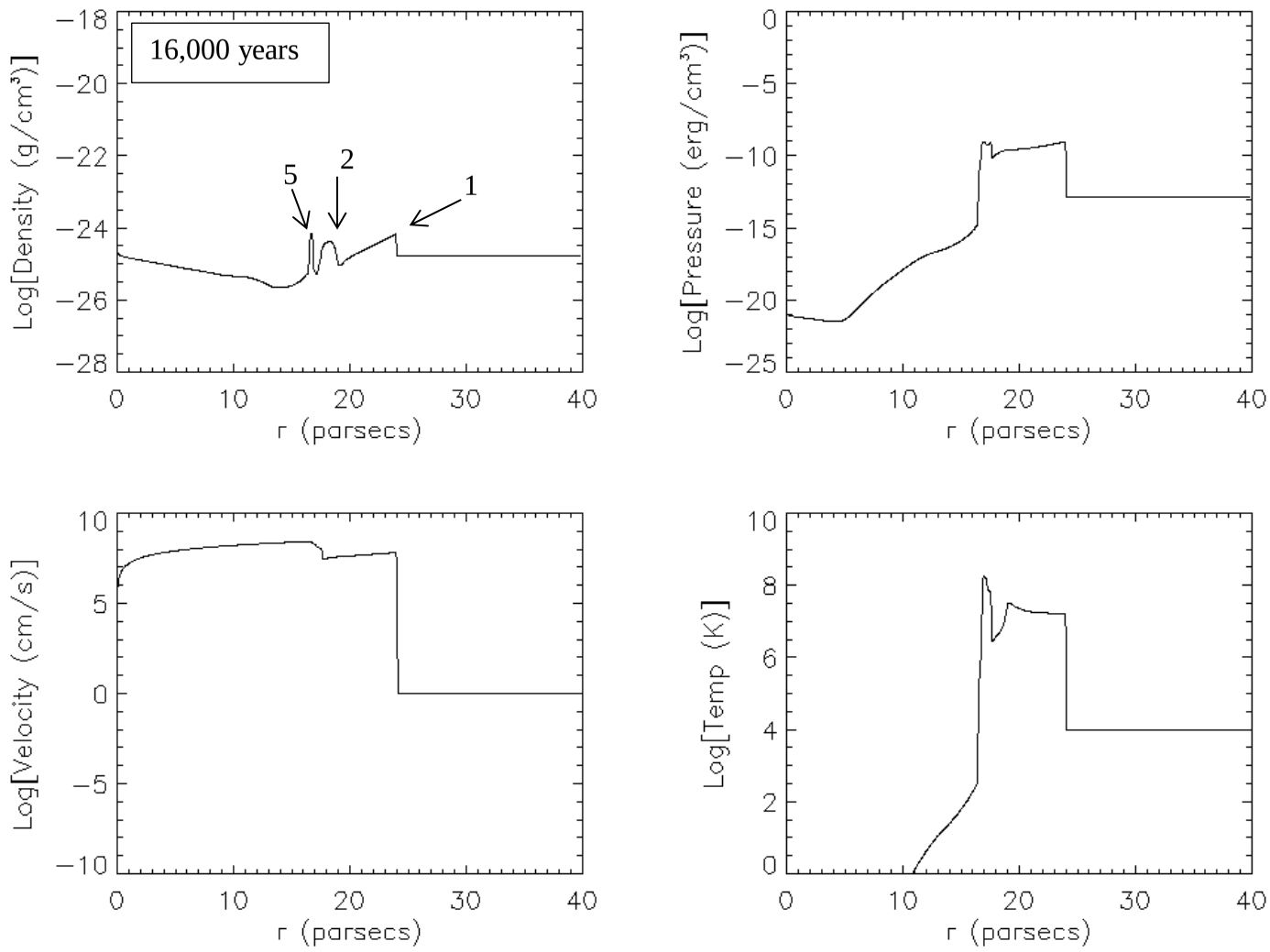

Figure 27: Double supernova at 16,000 years. ISM=0.1/cm^3

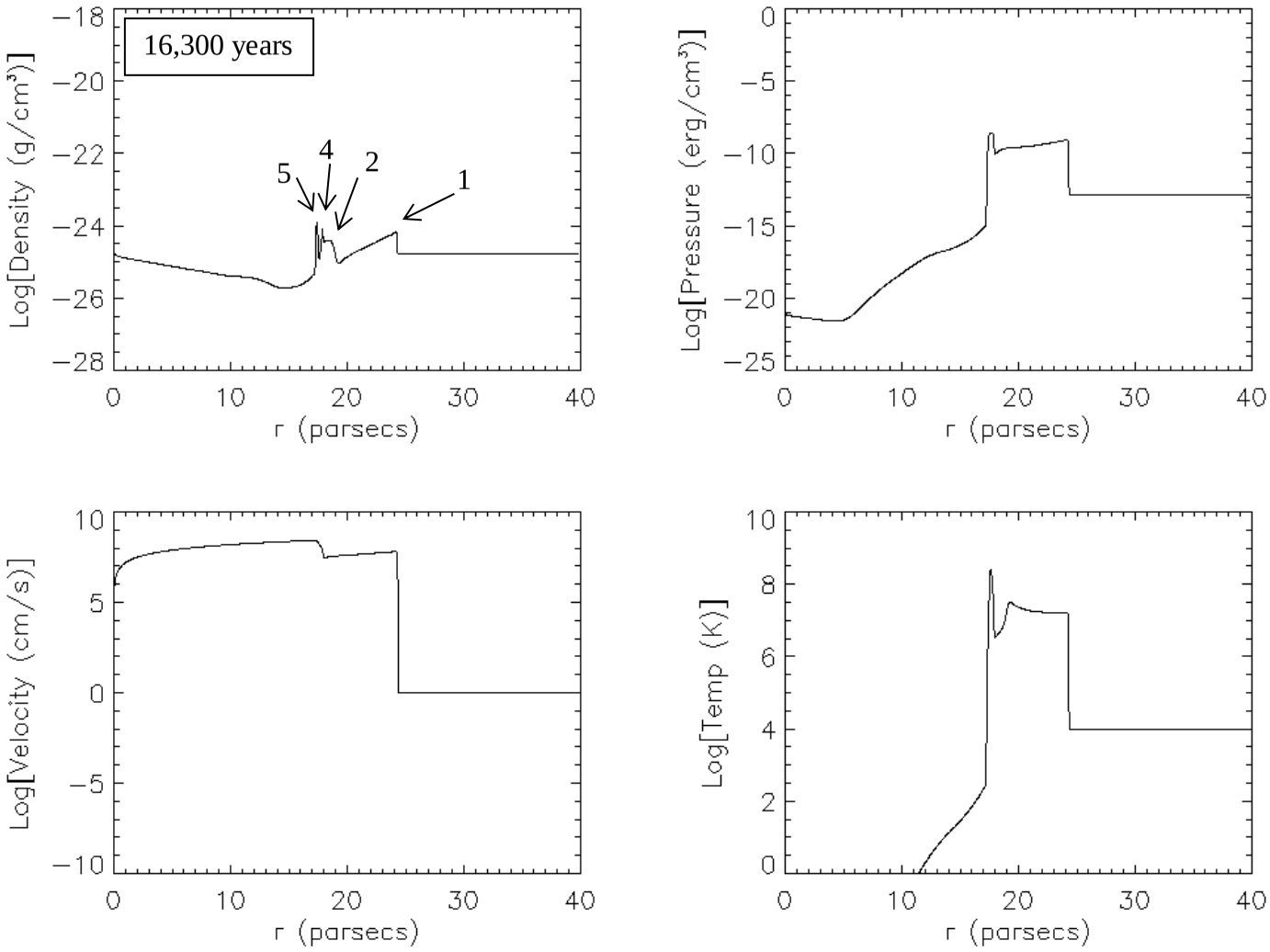

Figure 28: Double supernova at 16,300 years. ISM=0.1/cm^3

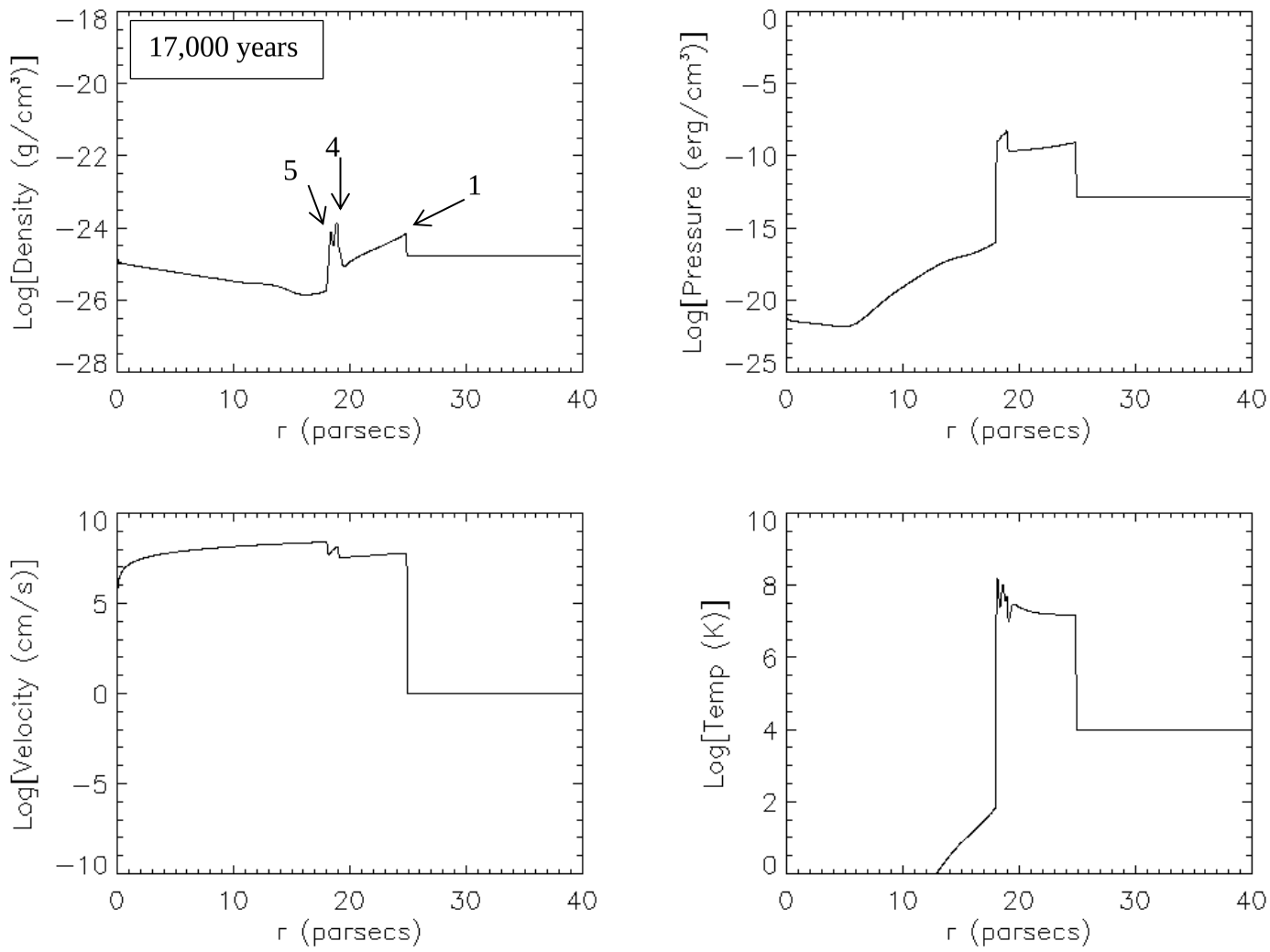

Figure 29: Double supernova at 17,000 years. ISM=0.1/cm^3

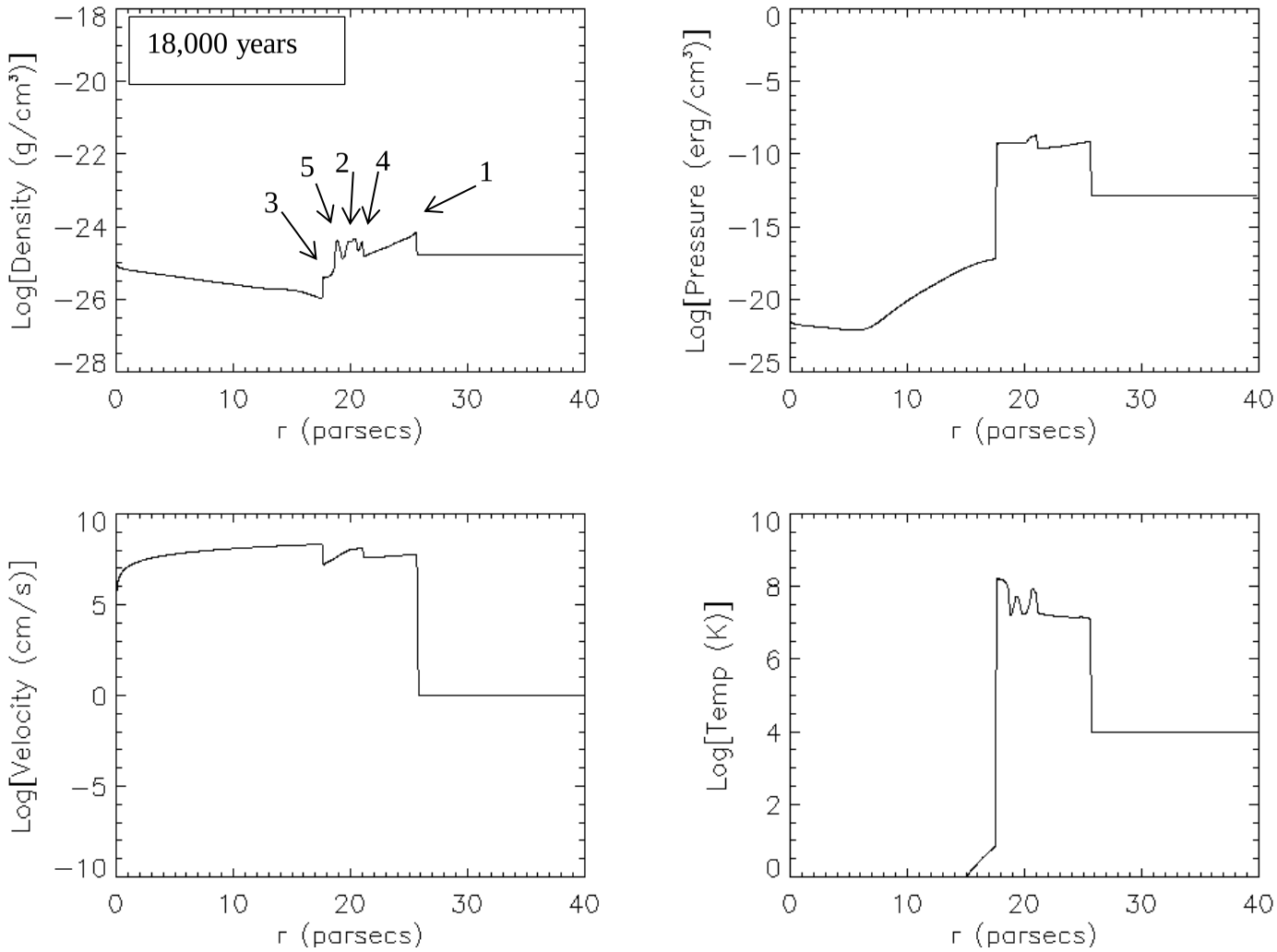

Figure 30: Double supernova at 18,000 years. ISM=0.1/cm^3

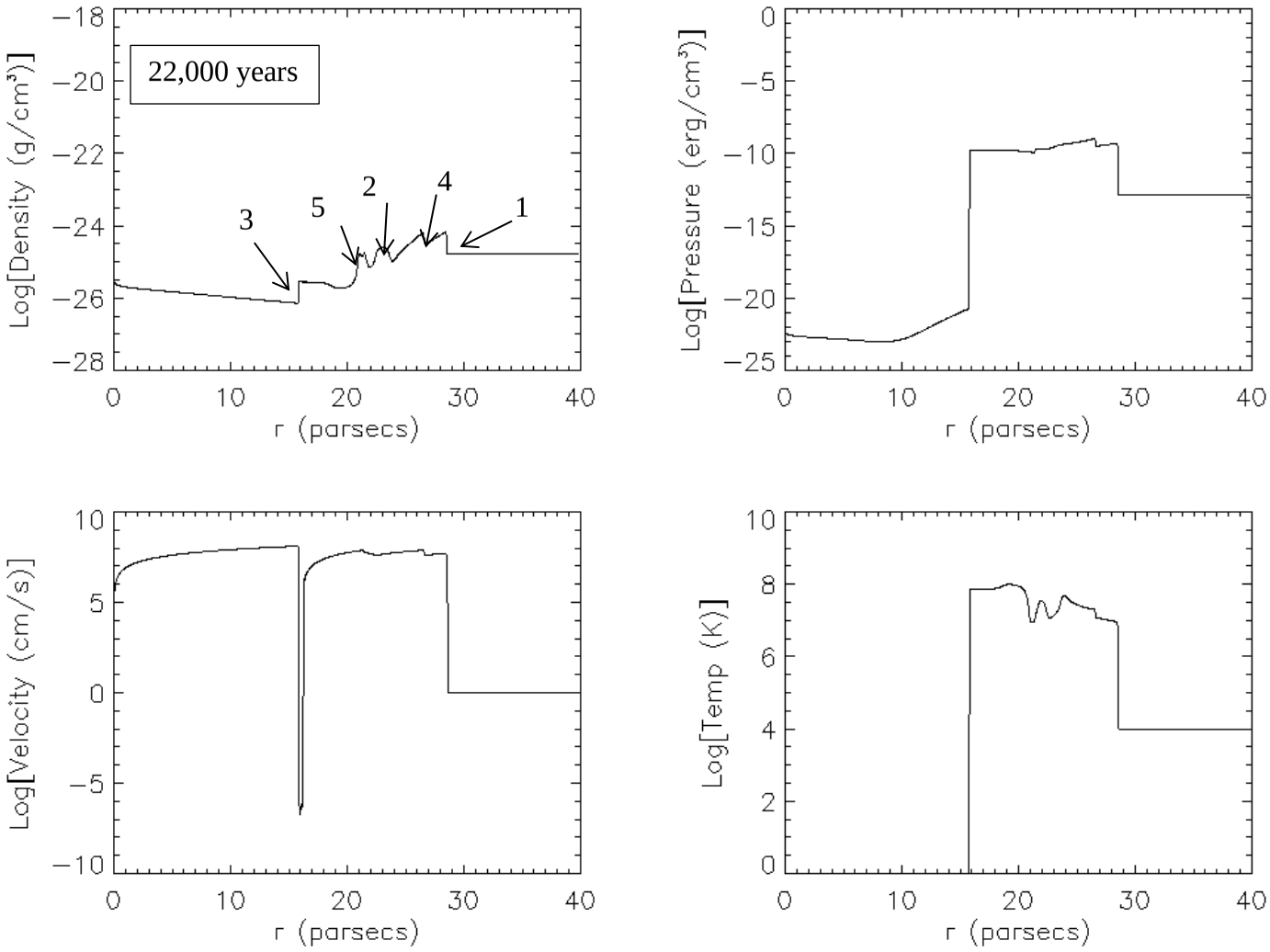

Figure 31: Double supernova at 22,000 years. ISM=0.1/cm^3

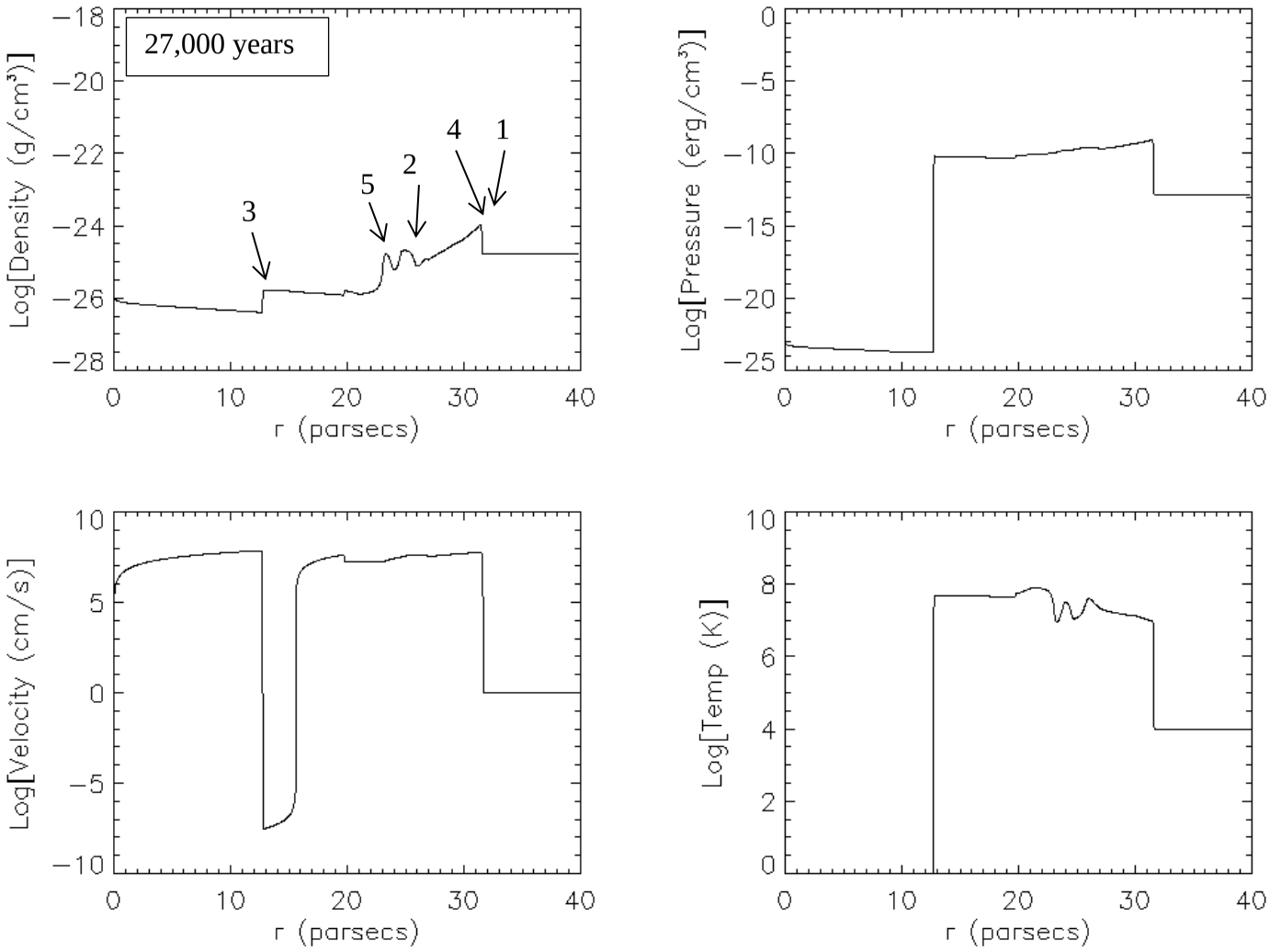

Figure 32: Double supernova at 27,000 years. ISM=0.1/cm^3

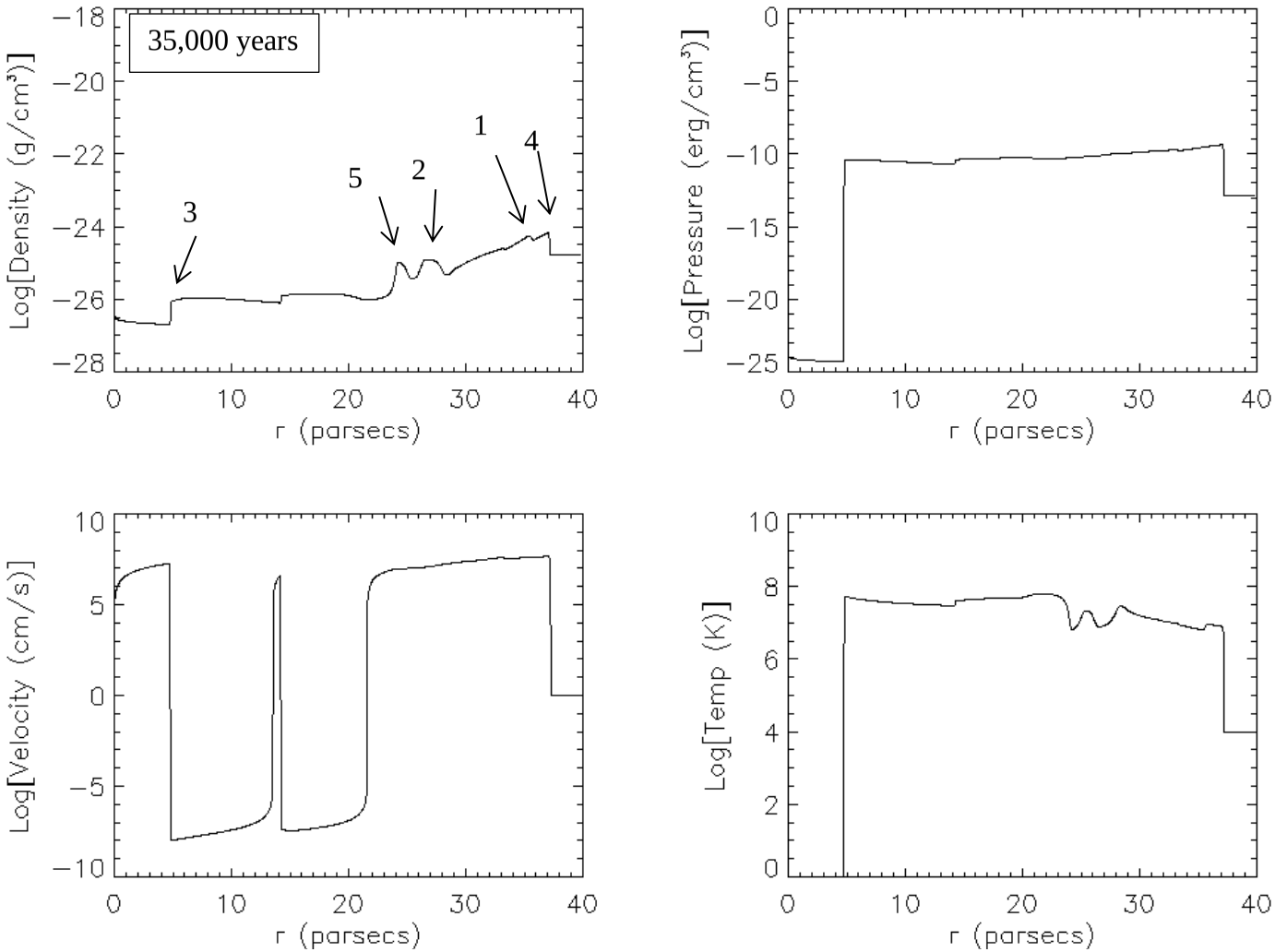

Figure 33: Double supernova at 35,000 years. ISM=0.1/cm^3

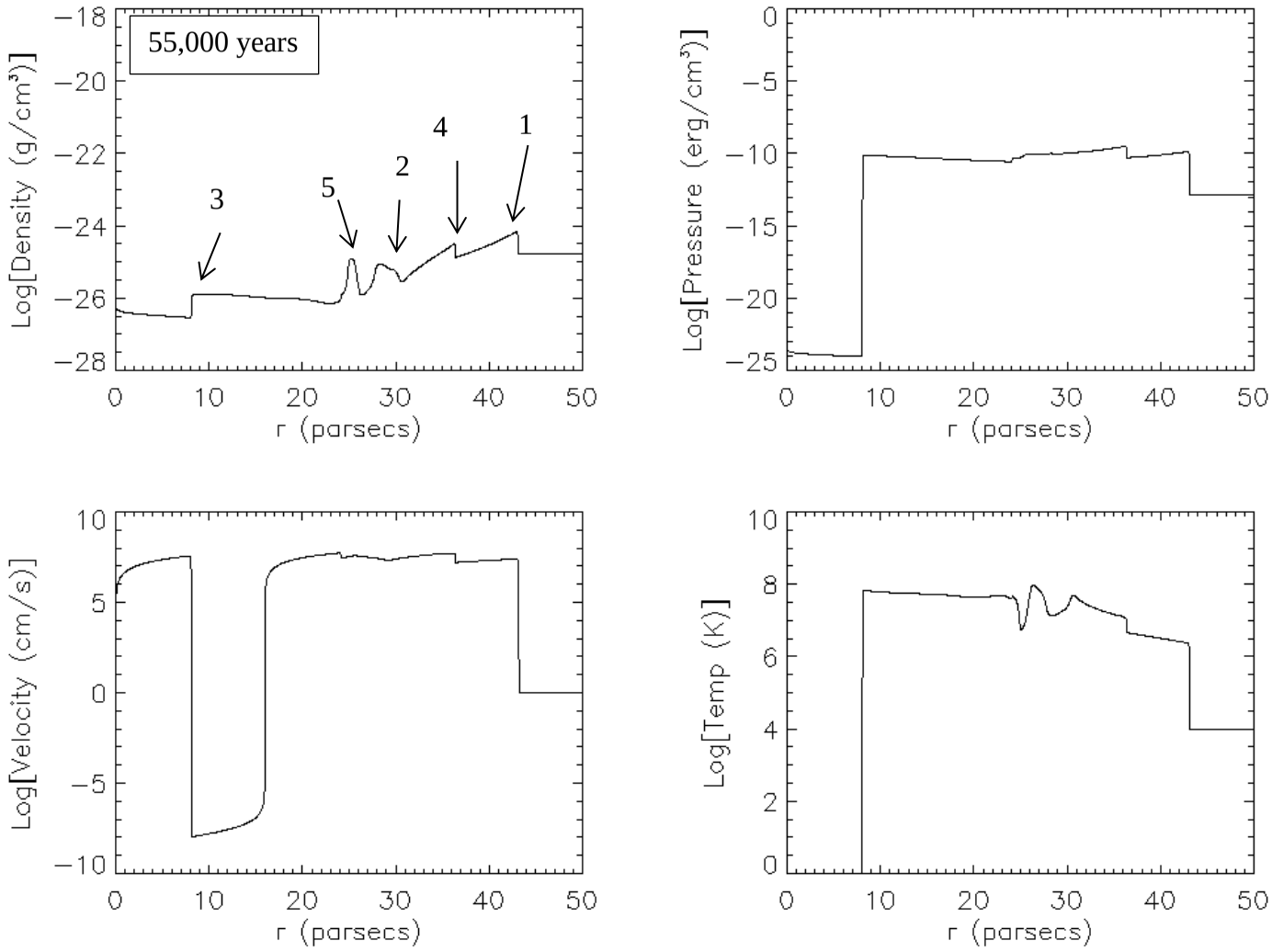

Figure 34: Double Supernova. The 2nd supernova blast occurs 34,000 years after the first.

Parameter Study

Simulations were run for a variety of combinations of final stellar masses and circumstellar mass. The initial mass of the star is sum of the final mass and the circumstellar mass. This study included initial masses of 20, 30, and 40 solar masses. The overall morphology is similar for each with distances and times varying. This section summarizes positions of key features at early and late times as well as times of key events. For a single supernova, positions of the forward shock, central shell, and rear/reflected shock were measured at 2,000 years and 30,000 years. Positions were measured at maximum density except for the reflected shock, which was measured where the density sharply increased. Two thousand years was chosen because that is the earliest time at which the features were prominent in all cases. Thirty-thousand years was chosen to avoid cases where the reflected shock had reached the origin. Simulations were unable to continue past that point. Also, the time at which the reflected shock attained a negative velocity was also measured.

For a double supernova, the positions of the forward shock, reflected shock, and the two central density shells were measured at 30,000 years. The time when the front of the second forward shock reached the rear of the first is listed as "first contact". The time when the second forward shock front reached the first forward shock front is given as well as both times when a reverse shock reached a negative velocity.

Simulations were also run for a higher interstellar number density of $0.2/cm^3$. At this density, reverse shocks formed and reached the origin more quickly. For a fifteen solar mass star, the reverse shock reached the origin in 25,000 years and this case was handled separately with features measured at 24,000 years.

All supernovae started with the same amount of kinetic energy. The Sedov-Taylor relation only depends on initial energy and the density of the environment so under those assumptions, it predicts that the radius of a remnant at a given time is the same for all starting masses. This is mostly true but there are small differences depending on the expanding mass, even if the circumstellar material is the same. As seen in Table 3, there was a large variation in times for the reflected shock. Larger mass stars resulted in longer times for the reflected shock to reach the origin. Increasing the interstellar medium density caused the reflected shock to form faster and reach the origin more quickly, with the exception of the single case of a 20 solar mass star expanding into 20 solar masses of circumstellar material.

Table 3: Single Supernova structure with ISM density of 0.1/cm^3

Single Supernova ISM = 0.1/cm^3		15sm star 5sm csm	15sm star 15sm csm	20sm star 10sm csm	25sm star 5sm csm	20sm star 20sm csm	30sm star 10sm csm
2000 years	forward shock (1)	6.6 pc	6.5 pc	6.2 pc	5.6 pc	5.9 pc	5.8 pc
	central shell (2)	5.8 pc	5.7 pc	5.4 pc	5.0 pc	5.2 pc	5.1 pc
	rear shock (3)	4.5 pc	3.3 pc	3.5 pc	3.9 pc	3.3 pc	3.2 pc
30,000 years	forward shock (1)	33.7 pc	35.8	33.1 pc	33.0 pc	32.4 pc	35.3 pc
	central shell (2)	17.5 pc	24.0 pc	20.3 pc	20.5 pc	22.4 pc	24.8 pc
	reflected shock (3)	1.7 pc	14.4 pc	11.4 pc	12.9 pc	11.0 pc	20.1 pc
reflected shock time		15,000 years	23,000 years	21,000 years	24,000 years	19,000 years	34,000 years
time to reach origin		31,000 years	46,000 years	41,000 years	45,000 years	40,000 years	65,000 years

Table 4: Double Supernova structure with ISM density of 0.1/cm^3

Double Supernova ISM = 0.1/cm^3		15sm star 5sm csm	15sm star 15sm csm	20sm star 10sm csm	25sm star 5sm csm	20sm star 20sm csm	30sm star 10sm csm
30,000 years	forward shock (1)	37.6 pc	37.6 pc	33.1 pc	33.4 pc	34.0 pc	35.2 pc
	front central shell (2)	28.7 pc	29.4 pc	26.0 pc	26.2 pc	26.3 pc	29.0 pc
	rear central shell (5)	25.8 pc	26.2 pc	23.8 pc	24.5 pc	23.0 pc	27.7 pc
	reflected shock (3)	9.0 pc	10.7 pc	10.4 pc	13.5 pc	3.5 pc	20.3 pc
reflected shock time		20,000 years	22,000 years	22,000 years	24,000 years	20,000 years	33,000 years
second reflected shock		29,000 years	29,000 years	30,000 years	33,000 years	27,000 years	40,000 years
time to reach origin		35,000 years	36,000 years	38,000 years	44,000 years	32,000 years	64,000 years
first contact		15,000 years	15,000 years	15,000 years	16,000 years	14,000 years	18,000 years
shock merge time		27,000 years	24,000 years	27,000 years	29,000 years	23,000 years	30,000 years

Table 5: Single Supernova structure with ISM density of 0.2/cm^3

Single Supernova ISM = 0.2/cm^3		15sm star 5sm csm	15sm star 15sm csm	20sm star 10sm csm	25sm star 5sm csm	20sm star 20sm csm	30sm star 10sm csm
2000 years	forward shock (1)	6.16 pc	5.9 pc	5.77 pc	5.35 pc	5.27 pc	5.02 pc
	central shell (2)	5.38 pc	5.12 pc	5.01 pc	4.7 pc	4.63 pc	4.53 pc
	rear shock (3)	4.44 pc	3.31 pc	3.52 pc	3.92 pc	3.16 pc	3.25 pc
30,000 years	forward shock (1)	See Table 7	29.13 pc	29.20 pc	29.1 pc 3	28.58 pc	28.78 pc
	central shell (2)		15.91 pc	15.88 pc	16.52 pc	17.56 pc	17.69 pc
	reflected shock (3)		2.84 pc	4.02 pc	6.58 pc	9.37 pc	10.92 pc
reflected shock time		13,000 years	16,000 years	17,000 years	19,000 years	21,000 years	23,000 years
time to reach origin		25,000 years	32,000 years	33,000 years	36,000 years	41,000 years	44,000 years

Table 6: Double Supernova Structure with ISM density of 0.2/cm^3

Double Supernova ISM = 0.2/cm^3		15sm star 5sm csm	15sm star 15sm csm	20sm star 10sm csm	25sm star 5sm csm	20sm star 20sm csm	30sm star 10sm csm
30,000 years	forward shock (1)	See Table 7		29.88 pc	29.65 pc	29.77 pc	29.17 pc
	front central shell (2)			22.22 pc	22.55 pc	22.73 pc	22.85 pc
	rear central shell (5)			19.69 pc	20.41 pc	19.87 pc	21.06 pc
	reflected shock (3)			2.00 pc	7.48 pc	2.48 pc	10.79 pc
reflected shock time		17,000 years	18,000 years	19,000 years	21,000 years	19,000 years	23,000 years
second reflected shock		25,000 years	25,000 years	27,000 years	30,000 years	27,000 years	32,000 years
time to reach origin		26,000 years	26,000 years	31,000 years	36,000 years	31,000 years	42,000 years
first contact		13,000 years	14,000 years	15,000 years	15,000 years	15,000 years	16,000 years
shock merge time		26,000 years	24,000 years	26,000 years	27,000 years	24,000 years	28,000 years

Table 7: Structure of 15 solar mass supernovae at 24,000 years

		15sm star 5 sm csm	15sm star 15 sm csm
Single supernova 24,000 years ISM = 0.1	forward shock (1)	30.46 pc	31.94 pc
	front central shell (2)	17.76	23.98
	reflected shock (3)	8.62	16.84
Double Supernova 24,000 years ISM = 0.1	forward shock (1)	33.37	31.89
	front central shell (2)	26.15	26.77
	rear central shell (5)	24.50	24.96
	reflected shock (3)	14.94	16.54
Single supernova 24,000 years ISM = 0.2	forward shock (1)	26.83	26.24
	front central shell (2)	14.00	16.10
	reflected shock (3)	1.65	8.00
Double supernova 24,000 years ISM = 0.2	forward shock (1)	26.80	26.18
	front central shell (2)	20.16	20.87
	rear central shell (5)	17.99	18.41
	reflected shock (3)	3.92	5.38

2-D with Instabilities

For comparison, a simulation was also run using a different hydrodynamic code by Toshikazu Shigeyama from Tokyo University. This code was written specifically for simulating supernovae. In the initial setup, the interstellar medium is not homogeneous and Rayleigh-Taylor instabilities result. Rayleigh-Taylor instabilities tend to occur when a dense shell is decelerated by a lower density gas. Fingers of low-density gas protrude into the higher density region, resulting in mixing of the material. This is prominent when a reverse shock occurs (Chevalier R. , 1977). Comparing ZEUS to this code allowed me to compare the results of two codes as well as the impact of instabilities on large scale structure.

Introducing instabilities results in 2-dimensional structures. Both one-dimensional and two-dimensional plots are presented below. The example discussed here was set up with a 20 solar mass star and 10 solar mass circumstellar material as before. The ISM is low density ~0.1/cm^3. The 1-dimensional line profiles below were created with IDL software and only represent the properties along a line at 45°. The structures seen above are smeared out but some general features are still visible. A reverse shock still forms and travels toward the center. Comparing Figure 20and Figure 36, the remnant in the ZEUS code has traveled 28pc while the remnant in the 2-d reference code has traveled 25pc. Both have temperatures near 10^7K.

One goal of this project was to compare the impact of instabilities on features. Another goal was to compare the general purpose ZEUS code to one written specifically for supernova remnants. The greater flexibility of ZEUS allows for a greater variety of environments. For this project, ZEUS was run in 2-d but the homogenous environment

resulted in essentially 1-d results. However, ZEUS is not restricted to this and can be extended to more complex problems. Future work could extend ZEUS to allow examination of supernovae in a variety of environments, including those that result in 2-d structures. Full 3-d simulations are also possible.

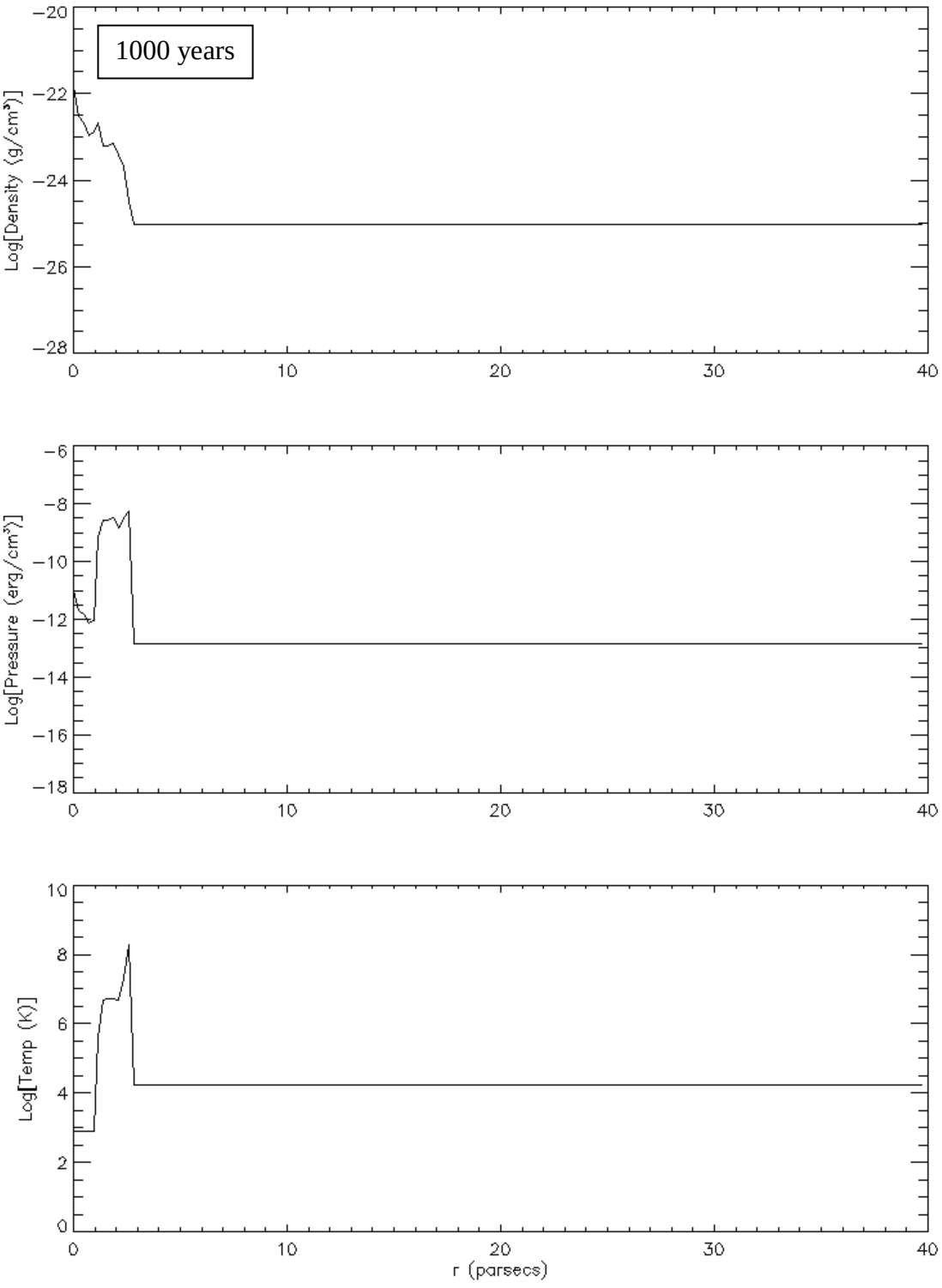

Figure 35: Single 2-d supernova at 1000 years

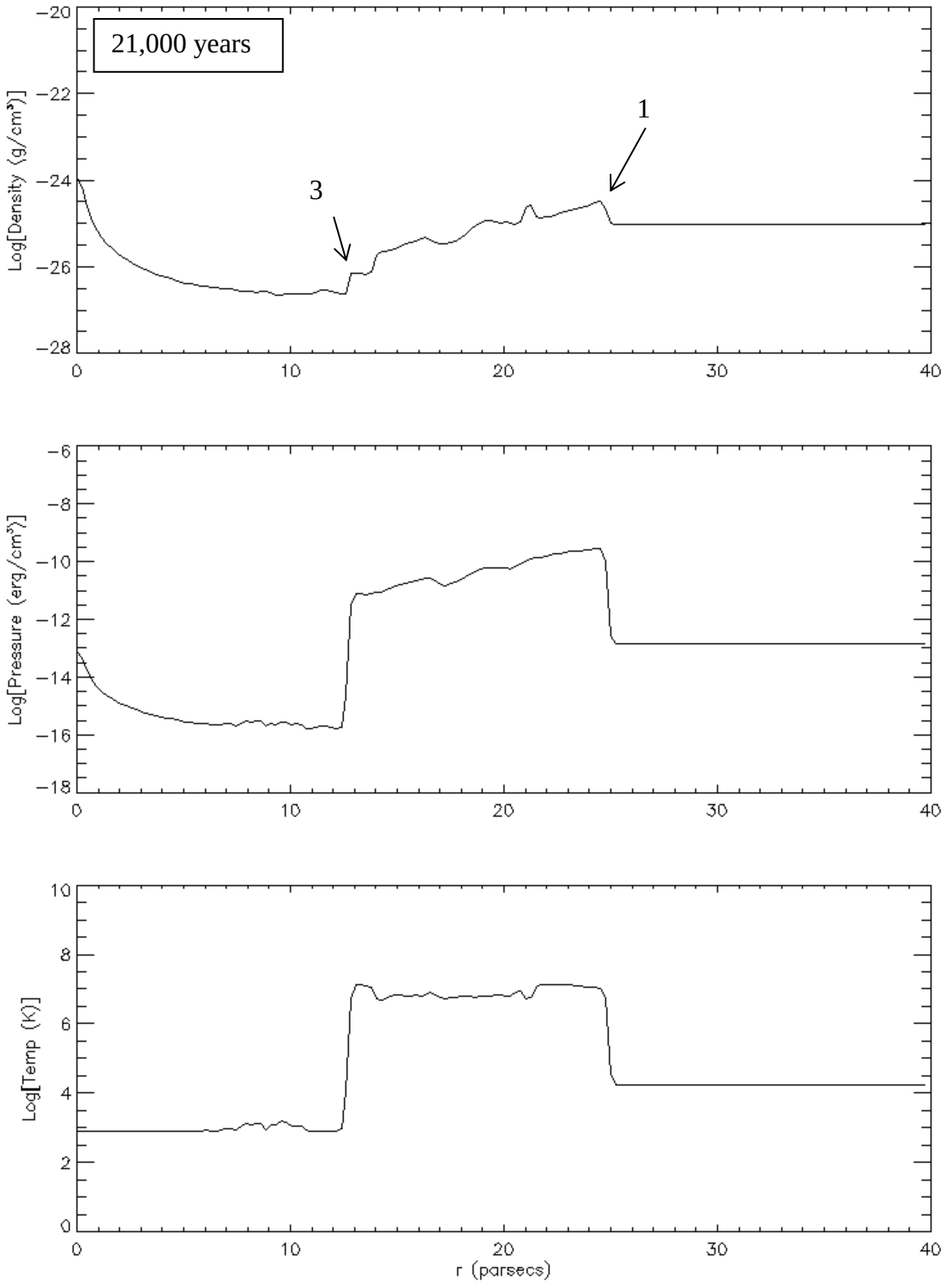

Figure 36: Single 2-d supernova at 21,000 years

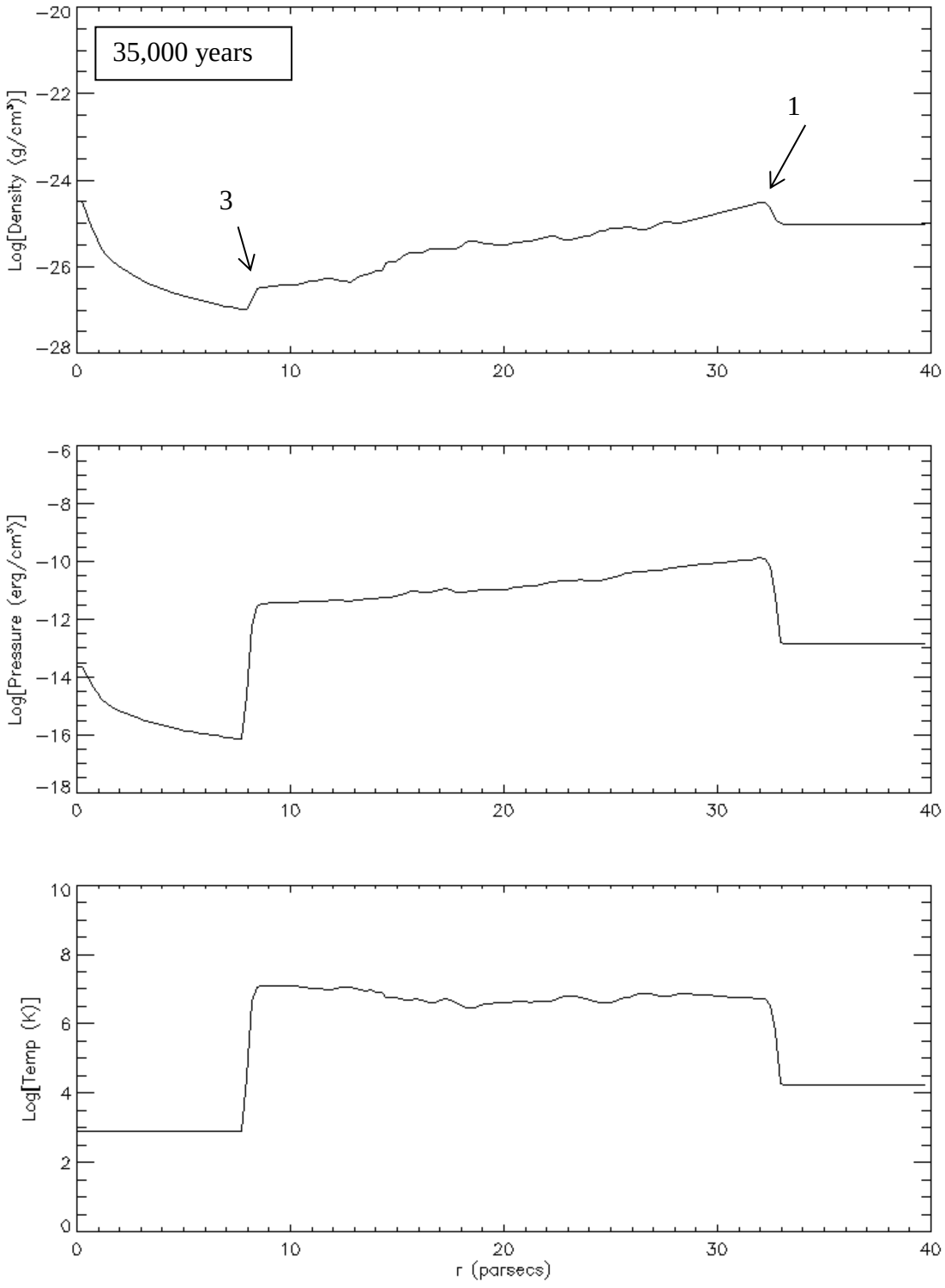

Figure 37: Single 2-d supernova at 35,000 years

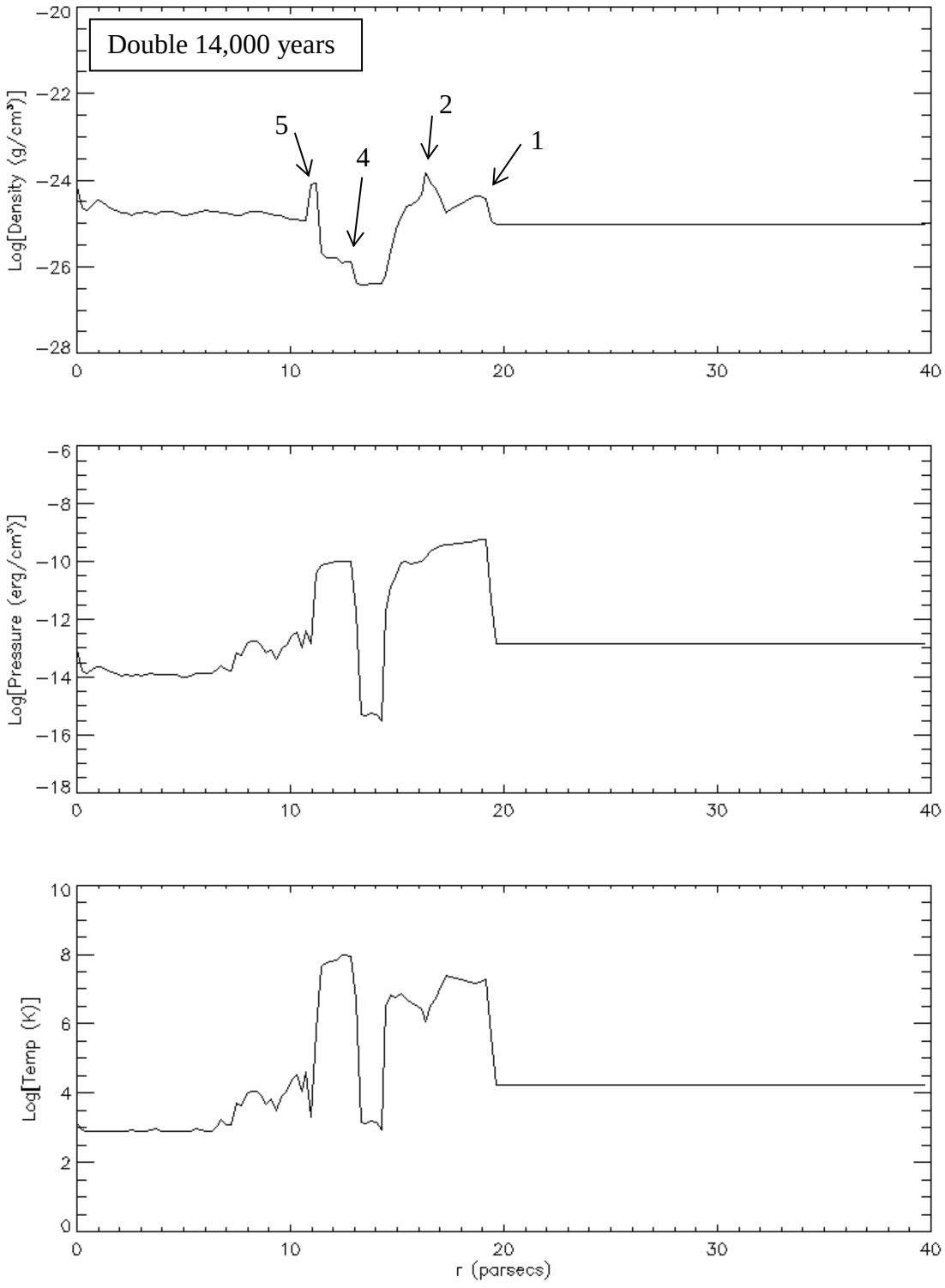

Figure 38: Double Supernova at 14,000 years

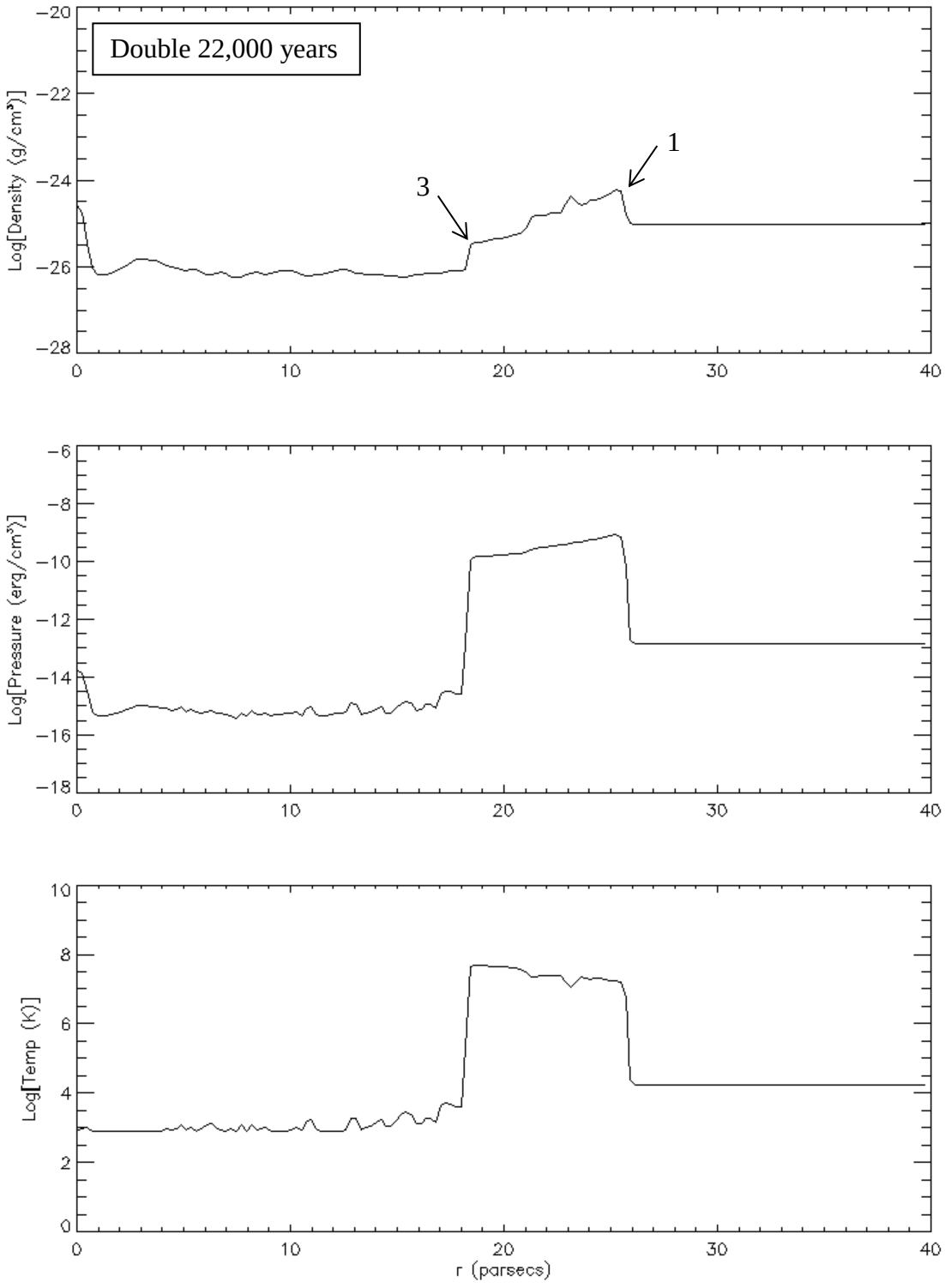

Figure 39: Double Supernova at 22,000 years. The second shock has caught up to the first.

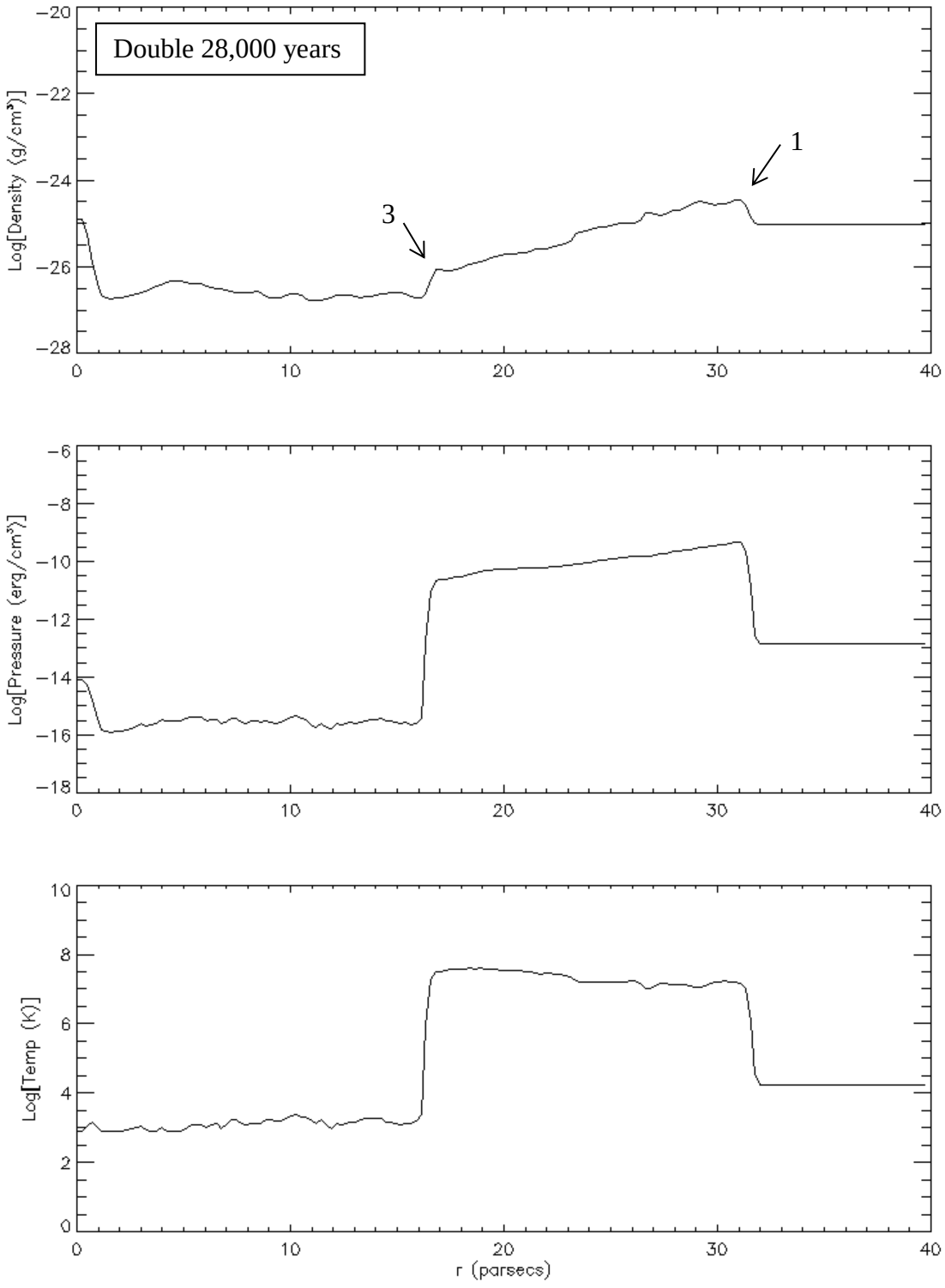

Figure 40: Double Supernova at 28,000 years

2-D Plots

In this section, the density is plotted in 2-D so the full structure can be seen. While ZEUS was essentially 1-d, the simulation was run in 2-d so comparison plots can be made. ZEUS output is in polar coordinates while the reference code was in Cartesian. Color is used to represent density. Red represents 10^{-24} g/cm^3 and blue represents 10^{-27} g/cm^3. Densities higher than this range are white. The results from both codes show similar large scale features. One exception is the high density shell visible in the ZEUS output. This region is unstable and breaks apart when instabilities are introduced. By 30,000 years, the high density shell has disappeared.

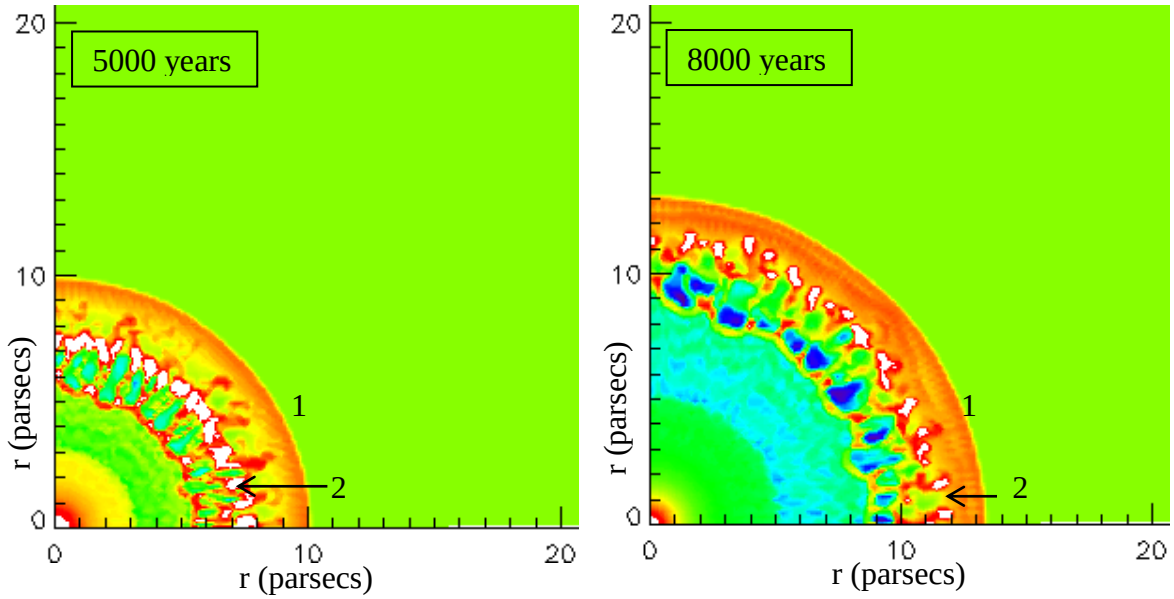

Figure 41: SNR with instabilities. The high density shell breaks up due to instabilities.

An early attempt at simulating a 30 solar mass explosion resulted in a surprising outcome (Figure 42). Despite symmetric initial conditions and a smooth ISM, instabilities were seen. These occurred at the leading edge of the high density shell that separated the forward and reflected shocks. What was different here was that I had tried

an angular resolution four times higher. Apparently, small numerical errors were enough to produce instabilities in the leading edge of the shell.

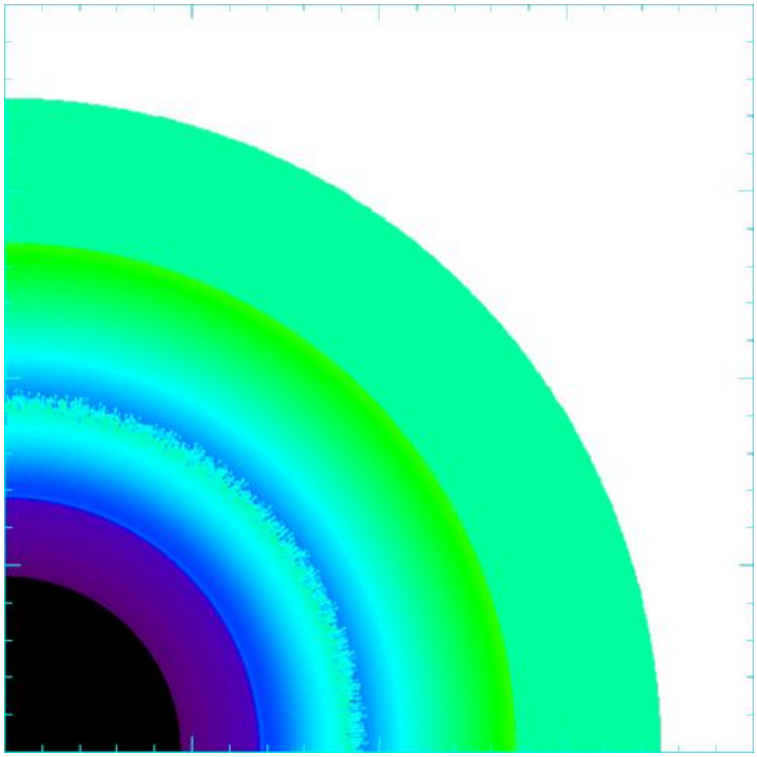

Figure 42: Early attempt at modeling a 30 solar mass supernova with high angular resolution. Unexpected instabilities are noticeable at 50,000 years.

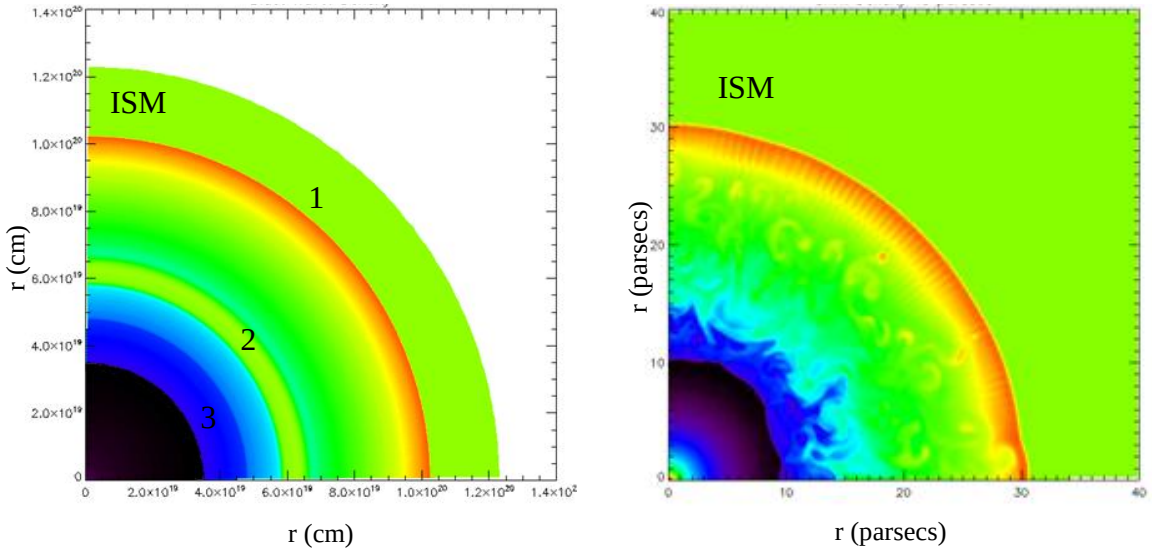

Figure 43: Single Supernova from 20 sm star and 10sm CSM at t = 30,000 years ZEUS output (left) and reference code including instabilities (right)

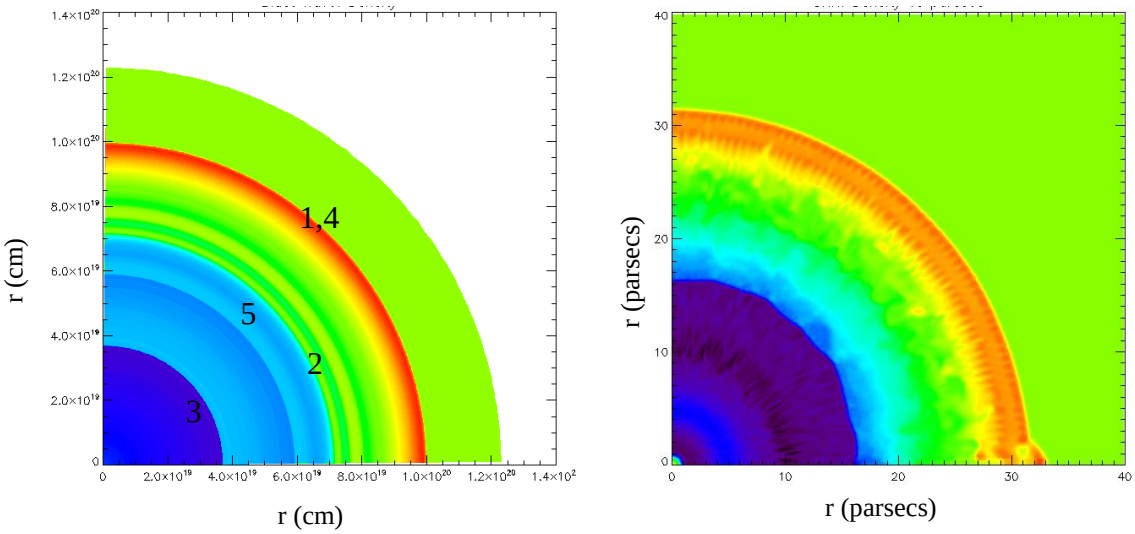

Figure 44: Double Supernova at 28,000 years
ZEUS output (left) and reference code with instabilities (right)

One notable result is the similarity of the remnants when comparing the double supernova to a single one. Comparing Figure 43 and Figure 44, both show a shell with a radius of about 30 pc. When the second shock has caught up to the first, the double remnant simulation appears similar to one produced by a single blast. There is a period of time when a double supernova does not necessarily show a double-ring structure and there appears to be a single forward shock. In the simulation, the second shock moved through the first forward shock. As the distance between the shocks increases, the remnant should again show a double ring. However, the outer ring after this time will be due to the second supernova rather than the first. As with a single supernova, the central shells don't appear when instabilities are allowed.

CHAPTER IV

CONCLUSION

Two research projects relating to supernovae have been presented in this dissertation. I have shown that the light curves of a class of supernova, known as Bright Type II Linears, can be explained using the collapsar model used to explain gamma-ray bursts. This extends the idea that jets may occur in Type II supernova with hydrogen envelopes, rather than just type Ic supernovae that have been identified as the sources of gamma ray bursts. The presence of a jet should be considered when attempting to explain these types of supernovae. The jets in these types of supernovae are not powerful enough to produce a gamma ray burst but they do collide with circumstellar material with enough energy such that an afterglow can form that overpowers the light from the actual supernova at early times. The best fits suggest a Lorentz factor of 2.1 and opening angle of 27°. The jet model required to produce the bright part of the light curve leads to a prediction that a black hole had formed in order to produce it. The observational evidence of a black hole at the core of SN 1979c lends credibility to the model.

The second project followed the blast wave of one or two supernovae remnants for tens of thousands of years. The main features that develop are a forward shock, a reverse shock traveling back toward the origin, and a cooler, denser, almost stationary shell. This shell is unstable and disappears in simulations that include Rayleigh-Taylor instabilities. In the event that a second supernova occurs, the second shock travels with a

faster velocity through the post-shock environment created by the first and it eventually catches up to and passes the first shock. There exists a period of time when the overall density morphology is similar to that of a single supernova. For most of the simulation outside of this time, there are two sets of forward and reverse shocks and two high density shells indicating that the single and double models can be uniquely separated. This leads to an observational prediction that with detailed observations, it should be possible to detect double SNR. It is puzzling that almost none have been found at present. This may be due to the subtle distinction and the noise in SNR observations.

Much future work can be done in this area. Comparison with observations should be carried out. Other parameters that could be varied include the time between supernova blasts and the masses of each star in a binary system. The stars could also be offset. Not only are the stars in different physical locations, but proper motion may significantly move the system before the second blast. ZEUS is flexible enough to include an inhomogeneous ambient medium to study 2-d structure. More complicated environments could be studied to try to replicate known remnants. Extending the simulation into three dimensions would allow examination of even more complex structures. Results from other hydrodynamic codes, such as ENZO and Athena, could also be compared.

APPENDICES

APPENDIX I
Light Curve Fitting

The following Mathematica code was used to create an interpolated function of SN 1969L. The data file consists of two columns, Julian date and B-band apparent magnitude, with a header. Output is suppressed for clarity except for the final graph showing the interpolated function with the data. The distance modulus is the difference between apparent (measured) magnitude and absolute magnitude which is used to compare supernovae at different distances. The data are chopped up into linear segments. Lines are then fit to each segment and an interpolated function, msn(t), is created. This function can then be used as a template Type II-P supernova in the fitting programs for Type II-L supernovae.

```
sn1969 = Delete[Import["D:\\1969l-b.txt", "table"], 1];

μ = 29.84; (*distance modulus*)

(*change date to start on day 10 and convert apparent
 magnitude to absolute*)

Do[{sn1969[[i, 1]] = sn1969[[i, 1]] - 548.23;
   sn1969[[i, 2]] = sn1969[[i, 2]] - μ}, {i, 1, Length[sn1969]}];

(*split data into linear sections*)

sn1969line0 = Take[sn1969, 4];

sn1969line1 = Drop[Take[sn1969, 20], 3];

sn1969line2 = Drop[Take[sn1969, 29], 17];

sn1969line3 = Drop[Drop[sn1969, 29], -15];

sn1969line4 = Take[sn1969, -15];
```

```
(*Fit lines to each segment*)

fitline0 = Fit[sn1969line0, {1, t}, t];

fitline1 = Fit[sn1969line1, {1, t}, t];

fitline2 = Fit[sn1969line2, {1, t}, t];

fitline3 = Fit[sn1969line3, {1, t}, t];

fitline4 = Fit[sn1969line4, {1, t}, t];

(*Find intersection between neigboring lines*)

t01 = Root[fitline0 - fitline1, 1];

t12 = Root[fitline1 - fitline2, 1];

t23 = Root[fitline2 - fitline3, 1];

t34 = Root[fitline3 - fitline4, 1];

(*Create new data consisting of day and intersections*)

{{10, fitline0 /. t → 10}, {t01, fitline1 /. t → t01},
  {t12, fitline2 /. t → t12}, {t23, fitline3 /. t → t23},
  {t34, fitline4 /. t → t34}, {420, fitline4 /. t → 420}};

(*draw lines between these points and save as interpolated
 function*)

msn = Interpolation[%, InterpolationOrder → 1];
```

The following program attempts to fit data from a light curve to a function combining afterglow emission from a jet and the Type II Plateau template represented by the function *msn* found above.

```
(*This program attempts to fit a two-
 component model to a supernova light curve.
   One component is a type II plateau light curve given by the
  function 'msn' which is defined elsewhere.  The notebook defining
  msn should be run before this one.
   The other is a power law decay similar to a GRB afterglow.  This
  is given by 'm'.  mt is the sum of these two components*)
```

$$m = -2.5 * \text{Log}\left[10, 10^{-.4*m1}\left(\left(\frac{t-d}{tb}\right)^{a1*n} + \left(\frac{t-d}{tb}\right)^{a2*n}\right)^{-1/n}\right];$$

mt =

$$-2.5 * \text{Log}\left[10, 10^{-.4*m1}\left(\left(\frac{t-d}{tb}\right)^{a1*n} + \left(\frac{t-d}{tb}\right)^{a2*n}\right)^{-1/n} + k * 10^{-.4\,msn[(t-\tau)/s]}\right];$$

```
(*read in data for the light curve in form (day,abs magnitude)*)

sn1979 = Delete[Import["D:\\1979c-b.txt", "table"], 1];

(*Here you can adjust the start time of the supernova light curve*)

Do[sn1979[[i, 1]] = sn1979[[i, 1]] - 15, {i, 1, Length[sn1979]}];
sn1979;

(*fit total emission including non-sn and sn*)

$RecursionLimit = 2048;

(*Try to fit 'mt' to the data
  d shifts the powerlaw in time.  usually leave it 0
  n relates to how severe the break is
  k shifts the underlying supernova up and down in magnitude.  k=
 1 leaves it alone
  τ shifts the underlying supernova in time.  usually leave it at 0
  m1 is the magnitude of the supernova when the break occurs
  s stretches the underlying supernova, s=1 leaves it alone
  a1 and a2 are 'slopes' of power law
  tb is time of break in power law.  It will be used to find opening angle *)
```

```
fit = FindFit[sn1979, mt /. d → 0 /. n → 10 /. k → 1 /. τ → 0,
  {{m1, -19}, s, {a1, 1}, {a2, 2}, {tb, 20}}, t]
```

```
{m1 → -17.8071, s → 1.04993, a1 → 0.785247, a2 → 3.41016, tb → 31.0351}
```

```
(*NonlinearModelFit can be used to find confidence intervals*)
```

```
model = NonlinearModelFit[sn1979, mt /. d → 0 /. n → 10 /. k → 1 /. τ → 0,
   {{m1, -19}, {s, 1}, {a1, 1}, {a2, 2}, {tb, 20}}, t];
```

$$\text{FittedModel}\left[-1.08574\,\text{Log}\left[10^{-0.4\,\text{InterpolatingFunction}[\{\{10.,420.\}\},<>][\ll 1\gg]}+\frac{1.32692\times 10^{7}}{(\ll 1\gg)^{1/10}}\right]\right]$$

```
model["ParameterConfidenceIntervals"]
```

```
{{-17.9907, -17.6235}, {1.00661, 1.09325},
 {0.662504, 0.907991}, {3.01371, 3.80661}, {28.7603, 33.3099}}
```

```
(*non-sn emission*)
```

```
sn1969 = Plot[2.5 Log[10, k] - msn[(t - τ) / s] /. fit /. k → 1 /. τ → 0, {t, 1, 350}];
```

```
(*power law (afterglow) emission*)
```

```
sn1979data = ListPlot[Abs[sn1979], PlotRange → All,
   Ticks → {Automatic, Table[{y, -y}, {y, 12, 22}]}];
```

```
afterglow = Plot[-m /. fit /. d → 0 /. n → 10, {t, 1, 350}]
```

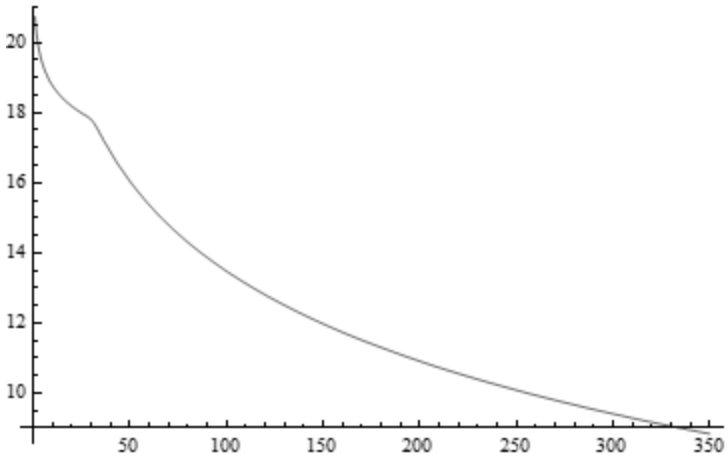

```
(*sum of above two*)

total = Plot[-mt /. fit /. d → 0 /. k → 1 /. n → 10 /. τ → 0, {t, 1, 350}]
```

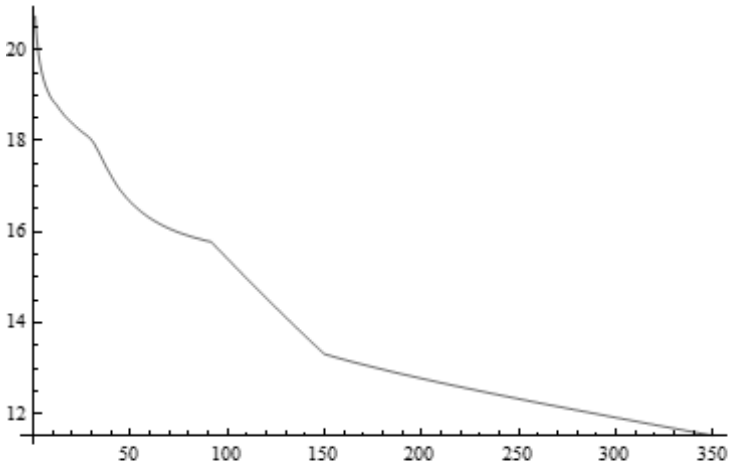


```
Show[sn1979data, total, afterglow, sn1969, AspectRatio → .8, Axes → None,
 Frame → True,
 FrameTicks → {Automatic, Table[{y, -y}, {y, 10, 22}], Automatic,
   Table[{y, ""}, {y, 10, 22}]}]
```

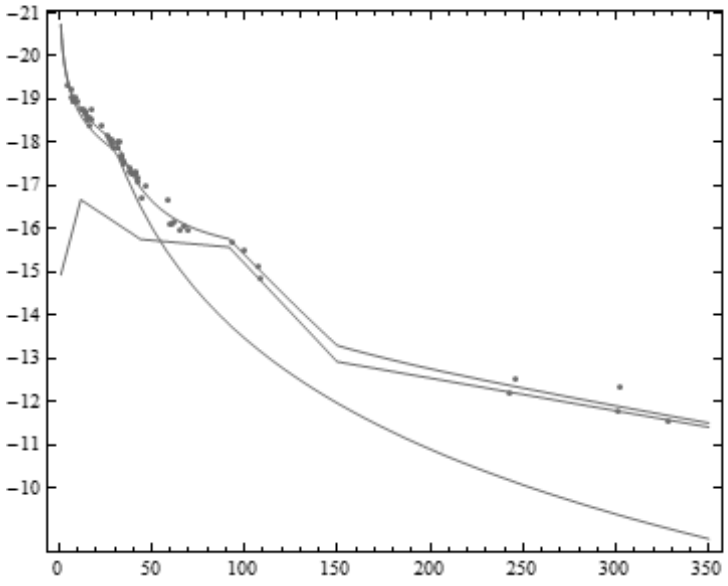

APPENDIX II
IDL and HDF Files

IDL software was used to extract data from HDF (version 4) files and create both 1-d line profiles and 2-d colored contours of supernova remnants. It is my hope that printing the scripts here will be helpful to anyone new to IDL and HDF files. An HDF file is composed of multiple arrays that can be accessed with IDL using a number. Using software such as HDFView, one can view these arrays and data and count from top to bottom to find the numeric label of each array. IDL counts the first array as zero. Each data array is accompanied by coordinate arrays. These latter arrays correlate an array index to coordinates and allow IDL to plot data from a grid that may not be uniform. This was the case in this research since grid blocks close to zero were smaller than those further out.

```
;********************dataselect*************************
; this function provided by LCA
Function dataselect,FileID, nn
      sds= HDF_SD_SELECT(FileID, nn)
      HDF_SD_GETDATA, SDS, newData
      return,  newData
end
;*****************************************************
pro hdfline

;set high and low ranges for density,pressure, and temp
dlow=-28
dhigh=-15
plow=-23
phigh=-3
tlow=0
thigh=9
vlow=-9
vhigh=10
r=1500; number of zones to plot

infile = FindFile('hdfaa.*', Count=numfiles)

;output are images
```

```
thisDevice = !D.NAME
Set_Plot, 'Z', /COPY
Device, Set_Resolution=[1024,768], Z_Buffer=0
Erase

jstart = 0
jend   = numfiles-1
jskip  = 1

for j=jstart,jend,jskip do begin

 filename = infile(j)
 FileID   = HDF_SD_START(filename, /READ)

; The first array in an HDF file is zero
 angle   = dataselect(FileID, 10)
 angle = n_elements(angle)/2 ;choose data along a single angle
 radius  = dataselect(FileID, 11)
 radius = radius/3.08568d18 ;convert cm to pc
 radius  = radius[0: r]

 density = dataselect(FileID, 12)
 density = alog10(density[*,angle])
 density = density[0: r,*]

 energy=dataselect(FileID, 16)

 pressure=alog10(2./3.*energy[*,angle])

 ;since pressure and density are already logs, use log rules to construct temp
 ;t = (m/k)*pressure/density
 temp=alog10(1.66d-24/1.38065d-16)+pressure-density

 velocity=dataselect(FileID, 0)
 velocity=velocity[*,angle]+1
 velocity=(velocity)/(abs(velocity))*alog10(abs(velocity))

 hdf_sd_end, FileID

!P.Multi=[0,2,2,0,1]; puts multiple plots on a page
 plot,radius,density,yrange=[dlow,dhigh],ytitle='Density (g/cm!E3!N)', $
 BACKGROUND = 255, COLOR = 0

 plot,radius,velocity,yrange=[vlow,vhigh],ytitle='Velocity (cm/s)', $
 BACKGROUND = 255, COLOR = 0
```

```
 plot,radius,pressure,yrange=[plow,phigh],ytitle='Pressure (erg/cm!E3!N)', $
 BACKGROUND = 255, COLOR = 0

 plot,radius,temp,yrange=[tlow,thigh],ytitle='Temp (K)',xtitle='parsecs', $
 BACKGROUND = 255, COLOR = 0

 image = tvrd()
 outfile = 'HDlines' + String(j, Format='(I3.3)') + '.png'
 write_png, outfile, image

endfor

end
```

APPENDIX III
Circumstellar Model

The following code is part of the problem generator for ZEUS and placed the circumstellar material around the star. This model assumes a constant wind velocity and mass loss rate. The total amount of mass lost was read in from an input file and could be changed for each simulation.

```
c ***add circumstellar material***
c rwind is the radius of the csm
c v12=wind velocity in cm/s; dMdt=mass loss in g/s
c Mlost=total circumstellar mass read from input file
c distances rwind (radius of csm) and rsq (radius of star) are squared
c rin is the square of the distance of the current grid square.  Rout is the square of the
c distance of the next grid square
c e is the energy density; e0 and d0 are properties of the ISM read from input file
      v12=1000000
      dMdt=.0001*1.989d33/3.1557d7
      rwind=(Mlost*v12/dMdt)**2
      if((rin.gt.rsq).and.(rout.le.rwind))then
         d (i,j,k) = dMdt/(4*3.14159*v12*rin)
         e(i,j,k) = e0*d(i,j,k)/d0
         v1(i,j,k) = v12
         v2(i,j,k) = 0
         v3(i,j,k) = 0
      end if
c ***end circumstellar***
```

REFERENCES

Arnett, D. (1996). *Supernovae and Nucleosynthesis.* Princeton: Princeton University Press.

Arroyo-Torres, B. (2013). The atmospheric structure and fundamental parameters of the red supergiants AH Scorpii, UY Scuti, and KW Sagittarii. *Astronomy and Astrophysics, 554*, A76.

Baade, W., & Zwicky, F. (1934). On super-novae. *Proceedings of the National Academy of Sciences, 20*, 254-259.

Baade, W., & Zwicky, F. (1934). Remarks on super-novae and cosmic rays. *Physical Review, 46*, 76-77.

Barbon, R. (1979). Photometric properties of type II supernovae. *Astronomy and Astrophysics*, 287-292.

Barbon, R., Ciatti, F., & Rosino, L. (1979). Photometric Properties of Type II Supernovae. *Astronomy and Astrophysics*, 287-292.

Bietenholz, M. (1991). The Expansion of the Crab Nebula. *The Astrophysical Journal*, L59-L62.

Blinnikov, S., & Bartunov, O. (1993). Non-equilibrium radiative transfer in supernova theory: models of linear type II supernovae. *Astronomy & Astrophysics, 273*, 106-122.

Blondin, J. (1998). Transition to the radiative phase in supernova remnants. *The Astrophysical Journal, 500*, 342-354.

Bloom, J. S. (1999). The unusual afterglow of the gamma-ray burst of 26 March 1998 as evidence for a supernova connection. *Nature, 401*, 453-456.

Carroll, B. (1996). *Modern Astrophysics.* Addison-Wesley.

Chevalier, R. (1977). The interaction of supernovae with the interstellar medium. *Annual Review of Astronomy and Astrophysics, 15*, 175-196.

Chevalier, R. (1982). Are young supernova remnants interacting with circumstellar gas? *The Astrophysical Journal*, L85-L89.

Chevalier, R. (1982). The radio and X-ray emission from type II supernovae. *The Astrophysical Journal*, 302-310.

Chevalier, R., & Oishi, J. (2003). Cassiopeia A and its clumpy presupernova wind. *The Astrophysical Journal Letters, 593*, 23-26.

Chevalier, R., Kirshner, R., & Raymond, J. (1980). The optical emission from a fast shock wave with application to supernova remnants. *The Astrophysical Journal, 235*, 186-195.

Decin, L. (2012). The enigmatic nature of the circumstellar envelope and bow shock surrounding Betelgeuse as revealed by Herschel. *Astronomy and Astrophysics, 548*, A113.

Dopita, M. A., & Sutherland, R. (2004). *Astrophysics of the Diffuse Universe.* Springer.

Frail, D. A. (2001). Beaming in Gamma-Ray Bursts: Evidence for a Standard Energy Reservoir. *The Astrophysical Journal*, L55-L58.

Galama, T. (1998). An unusual supernova in the error box of the γ-ray burst of 25 April 1998. *Nature, 395*, 670-672.

Gaskell, C. M. (1992). Type II-L Supernovae-Standard Bombs. *The Astrophysical Journal*, L17-L20.

Green, D. (2009). A Revised Galactic Supernova Remnant Catalogue. *Bulletin of the Astronomical Society of India*, 1-18.

Guetta, D. (2001). Efficiency and Spectrum of Internal Gamma-Ray Burst Shocks. *The Astrophysical Journal*, 399-407.

Heger, A. (2003). How Massive Single Stars End Their Life. *The Astrophysical Journal*, 288-300.

Iwamoto, K. (1998). A hypernova model for the supernova associated with the γ-ray burst of 25 April 1998. *Nature, 395*, 672-674.

Kervella, P. (2011). The Close Circumstellar Environment of Betelgeuse. *Astronomy and Astrophysics, 531*, A117.

Klebesadel, R. W., Strong, I. B., & Olson, R. A. (1973). Observations of Gamma-Ray Bursts of Cosmic Origin. *The Astrophysical Journal*, L85-L88.

Levenson, N. (2002). Shell Shock and Cloud Shock: Results from Spatially Resolved X-Ray Spectroscopy with Chandra in the Cygnus Loop. *The Astrophysical Journal, 576*, 798-805.

Lu, F. (2011). The Single-Degenerate Binary Origin of Tycho'S Supernova As Traced By the Stripped Envelope of the Companion. *The Astrophysical Journal*, 11.

Macfadyen, A., Woosley, S., & Heger, A. (2001). Supernovae, Jets, and Collapsars. *The Astrophysical Journal*, 410-425.

Maund, J. (2004). The Massive Binary Companion Star to the Progenitor of Supernova 1993J. *Nature*, 129-31.

McKee, C. (1974). X-ray emission from an inward-propagating shock in young supernova remnants. *The Astrophysical Journal*, 335-339.

McKee, C., & Ostriker, J. (1977). A theory of the interstellar medium - Three components regulated by supernova explosions in an inhomogeneous substrate. *The Astrophysical Journal, 218*, 148.

Metzger, M., Djorgovski, S., & Kulkarni, S. (1997). Spectral Constraints on the Redshift of the Optical Counterpart to the Gamma-Ray Burst of 8 May 1997. *Nature*, 878-880.

NASA/IPAC Extragalactic Database. (n.d.). Retrieved from http://ned.ipac.caltech.edu/.

Nomoto, K. (1990). Supernova 1987a: From Progenitor to Remnant. *Les Houches, Session LIV: Supernovae* (pp. 489-568). Les Houches: Elsevier Science.

Norman, M. L. (2000). Introducing ZEUS-MP: a 3d, parallel, multiphysics code for astrophysical fluid dynamics. *arXiv:astro-ph/0005109*.

Patat, F. (1994). Light curves of type II supernovae. 2: The analysis. *Astronomy and Astrophysics, 282*, 731-741.

Patnaude, D. (2011). Evidence for a possible black hole remnant in the Type IIL Supernova 1979C. *New Astronomy*, 187-190.

Preibisch, T. (2000). Multiplicity of massive stars. *IAU Symposium 200: The Formation Of Binary Stars*, (pp. 1-10).

Pskovskii, Y. (1978). Photometric classification and observed characteristics of type II supernovae. *Soviet Astronomy*, 201-205.

Reynolds, S. P. (2008). Supernova Remnants at High Energy. *Annual Review of Astronomy and Astrophysics, 46*, 89-126.

Rhoads, J. E. (1999). The Dynamics and Light Curves of Beamed Gamma-Ray Burst Afterglows. *The Astrophysical Journal, 525*, 737-749.

Sari, R., Piran, T., & Halpern, J. (1999). Jets in Gamma-Ray Bursts. *The Astrophysical Journal*, L17-L20.

Sedov, L. (1959). *Similarity and Dimensional Methods in Mechanics.* New York: Academic Press.

Slavin, J., & Cox, D. (1992). Completing the evolution of supernova remnants and their bubbles. *The Astrophysical Journal*, 131.

Smartt, S. J. (2009). Progenitors of Core-Collapse Supernovae. *Annual Review of Astronomy and Astrophysics*, 63-106.

Smith, N. (2001). The asymmetric nebula surrounding the extreme red supergiant VY Canis Majoris. *The Astronomical Journal, 121*, 1111-1125.

Stone, J., & Norman, M. (1992). ZEUS-2D: A radiation magnetohydrodynamics code for astrophysical flows in two space dimensions. I - The hydrodynamic algorithms and tests. *The Astrophysical Journal Supplement Series*, 753.

Swartz, D. (1991). Model light curves of linear Type II supernovae. *The Astrophysical Journal, 374*, 266-280.

Taylor, J., Fowler, L., & McCulloch, P. (1979). Measurements of general relativistic effects in the binary pulsar PSR1913 + 16. *Nature, 277*, 437-440.

Trimble, V. (1973). The Distance to the Crab Nebula and NP 0532. *Publications of the Astronomical Society of the Pacific, 85*, 579.

Truelove, J., & McKee, C. (1999). Evolution of Nonradiative Supernova Remnants. *The Astrophysical Journal Supplement Series*, 299-326.

Woosley, S. (2005). The Physics of Core-Collapse Supernovae. *Nature Physics*, 147-154.

Woosley, S. E., Eastman, R. G., & Schmidt, B. P. (1999). Gamma Ray Bursts and Type Ic Supernova SN 1998bw. *The Astrophysical Journal*, 788-796.

Woosley, S., Zhang, W., & Heger, A. (2002). Gamma-Ray Bursts and Jet-Powered Supernovae. *"From Twilight to Highlight - The Physics of Supernovae" ESO/MPA/MPE Workshop* (pp. 87-96). Garching: arXiv:astro-ph/0211063. Retrieved from http://arxiv.org/abs/astro-ph/0211063.

Young, T. R. (2004). A Parameter Study of Type II Supernova Light Curves Using 6 Solar Mass He Cores. *The Astrophysical Journal*, 1233-1250.

Young, T. R., & Branch, D. (1989). Absolute light curves of type II supernovae. *The Astrophysical Journal*, L79.

Young, T. R., Smith, D., & Johnson, T. A. (2005). An Optical Afterglow Model for Bright Linear Type II Supernovae. *The Astrophysical Journal*, L87-L90.

Young, T., Shigeyama, T., & Suzuki, T. (1996). A Double Supernova Model for the VELA Supernova Remnant. *X-Ray Imaging and Spectroscopy of Cosmic Hot Plasmas, Proceedings of an International Symposium on X-ray Astronomy ASCA Third Anniversary*, (p. 405). Waseda University, Tokyo.

Zeh, A., Klose, S., & Hartmann, D. H. (2004). A Systematic Analysis of Supernova Light in Gamma-Ray Burst Afterglows. *The Astrophysical Journal, 609*, 952-961.